Photocatalytic Reduction of Nitroaromatics initiated by Bare/Metal-TiO_2 Nanostructures

Thesis submitted in fulfillment of the

requirement of the degree of

Doctor of Philosophy

by

Jaspreet Kaur

(Regd. No. 901109005)

Under the supervision of

Dr. Bonamali Pal

(Professor and Head)

School of Chemistry and Biochemistry

Thapar University

Patiala – 147004

Punjab, India

November – 2015

Certificate

This is to certify that thesis entitled "**Photocatalytic Reduction of Nitroaromatics initiated by Bare/Metal-TiO_2 Nanostructures**", being submitted by Jaspreet Kaur in the fulfillment of the requirement for the award of Degree of Doctor of Philosophy to the School of Chemistry and Biochemistry, Thapar University, Patiala, is a record of candidate's own work carried out by her under my supervision and guidance. The matter presented in this thesis has not been submitted in part or full for the award of any degree in any other University or Institute.

30/10/15

(Supervisor and Head)

Dr. Bonamali Pal
Professor and Head
School of Chemistry and Biochemistry
Thapar University, Patiala - 147 004
Punjab (India)

Candidate's Declaration

I, hereby declare that the work presented in the thesis entitled "**Photocatalytic Reduction of Nitroaromatics initiated by Bare/Metal-TiO_2 Nanostructures**" in fulfillment of the requirement for the award of the Degree of Doctor of Philosophy, School of Chemistry and Biochemistry, Thapar University, Patiala, is an authentic record of my own work carried out under the supervision of Dr. Bonamali Pal, Professor, School of Chemistry and Biochemistry, Thapar University, Patiala, India. The matter embodied in this thesis has not been submitted in part or full to any other university or institute for the award of any degree in India or Abroad.

Jaspreet Kaur
30/10/15

Jaspreet Kaur

30/10/15

(Supervisor)

Dr. Bonamali Pal
Professor and Head
School of Chemistry and Biochemistry
Thapar University, Patiala - 147 004
Punjab (India)

Dedicated to
My
Parents and Teachers

Acknowledgements

I wholeheartedly thank my mighty God for giving me the vision, power, spirit and endurance to complete this interesting research.

Completion of this doctoral dissertation was possible with the support of several people. I would like to express my sincere gratitude to all of them.

First of all, I am extremely grateful to my research guide, Dr. Bonamali Pal, Professor and Head, School of Chemistry and Biochemistry, for his valuable guidance, scholarly inputs and consistent encouragement I received throughout the research work. He has always made himself available to clarify my doubts despite his busy schedules and I consider it as a great opportunity to do my doctoral programme under his guidance and to learn from his research expertise. His mentorship was paramount in providing a well rounded experience consistent my long-term career goals.

I am also very grateful to my doctoral committee members Dr. Vijay Luxmi, Dr. Amjad Ali and Dr. S.D. Tiwari for their encouragement, constructive criticism and inspirations.

My sincere thanks also go to Dr. S.K. Pandey and Dr. Kamaldeep Paul for their motivation, scientific advice and many insightful discussions and suggestions.

Special thanks to my senior labmates Mr. Rohit Singh, Mrs. Rupinder Kaur, Mr. Inderpreet Singh Grover, Mrs. Nidhi Gupta who all have extended their support in a very special way. I gained a lot from them, through their personal and scholarly interactions, their suggestions at various points of my research programme.

I am also thankful to my batchmates and friends Miss Anila, Mr. Bhupender Pal, Mr. Rayees Ahmad, Mr. Roopchand Prajapati, Miss Tanushree Basu, Miss Prinka, Mrs. Sakshi Gupta for always standing by my side and sharing a great relationship as compassionate friends. I will forever cherish the warmth shown by them, whose smiling face always made me refreshing.

I am especially thankful to my father Mr. Mohinder Pal Singh, mother Mrs. Pritpal Kaur and younger brothers Mr. Bhartinder Singh and Mr. Simarpreet Singh who have always showered unconditional love on me, encouraged and supported me in every aspect. My mother has been my best friend all my life and I love her dearly and thank her for all her advice and support.

My gratitude to my father-in-law Mr. Baldev Singh, mother-in-law Mrs. Jasbir Kaur, brother-in-law Mr. Sukhdeep Singh, sister-in-law Mrs. Ravneet Kaur and nephew Nirvair for courage to go ahead and consistent moral support in the life, along with their cordial endeavours, sustained encouragement, throughout and always.

Saving the most important for last, I wish to give my heartfelt thanks to my husband, Mr. Jagdeep Singh, whose unwavering love, patience and continual support of my academic endeavours over the past several years enabled me to complete this thesis.

Jaspreet Kaur
30/10/15
Jaspreet Kaur

Table of Contents

Chapter	Section	Contents	Page No.
		List of Abbreviations	1-2
		List of Symbols	3
		Abstract	4-6
1		**Introduction, Preparation and Characterization Techniques**	**7-26**
	1	Introduction	7-12
	2	Literature review	12-14
	3	Research Gap	14-15
	4	Objectives	14
	5	Preparation and Characterization Techniques	15
	5.1	Materials used	15-16
	5.2	Methods for the preparation of bare TiO_2 and metal-TiO_2 nanostructures	16
	5.2.1	Preparation of sintered TiO_2 nanoparticles	16
	5.2.2	Synthesis of metal-TiO_2 nanoparticles	16
	5.2.3	Synthesis of R-TiO_2 nanorods	16
	5.2.4	Synthesis of anatase nanorods	17
	5.2.5	Synthesis of anatase nanoparticles	17
	5.3	Characterization	17
	5.3.1	UV-Vis diffuse reflectance spectrophotometer	17-18
	5.3.2	X-ray diffraction analysis	18
	5.3.3	Surface area analysis	18
	5.3.4	Photoluminescence measurement	18-19
	5.3.5	Transmission electron microscopy	19

	5.3.6	Time resolved spectroscopy	19
	5.4	Photocatalytic activity	19
	5.4.1	Photoreduction studies	19-20
	5.4.2	High Performance Liquid Chromatography	20-21
	5.4.3	Gas chromatography-mass spectroscopy	21
	5.4.4	Nuclear Magnetic Resonance Spectroscopy	21
	5.4.5	Gas chromatography	21-22
	5.5	Photocatalytic reactor with Hg (UV) light source	22
	5.6	References	23-26
2		**100% selective yield of *m*-nitroaniline by rutile TiO_2 and *m*-phenylenediamine by P25-TiO_2 during *m*-dinitrobenzene photoreduction**	**27-37**
	2.1	Introduction	28
	2.2	Experimental section	29
	2.2.1	Preparation of sintered TiO_2 samples	29
	2.2.2	Characterization	29
	2.2.3	Photocatalytic study	29
	2.3	Results and discussion	29
	2.3.1.	Structural analysis of catalysts	29
	2.3.2.	Photocatalytic activity of sintered P25-TiO_2 catalysts	29-35
	2.4	Conclusions	35
	2.5	References	35-37
3		**Influence of coinage and platinum group metal co-catalysis for the photocatalytic reduction of *m*-dinitrobenzene by P25 and rutile TiO_2**	**38-53**
	3.1	Introduction	39-40
	3.2	Experimental section	40
	3.2.1	Preparation of R-TiO_2 nanoparticles	40

	3.2.2	Metal (Au, Ag, Cu, Pt, Pd, Rh) photodeposition	40
	3.2.3	Characterization techniques	40
	3.2.4	Photocatalytic activity for *m*-DNB reduction	40
	3.3	Results and discussion	41
	3.3.1	Optical, structural and morphological analysis of M/TiO_2 composites	41-46
	3.3.2	Photocatalytic study	47-51
	3.4	Conclusion	51
	3.5	References	51-53
4		**Selective formation of benzo[c]cinnoline by photocatalytic reduction of 2,2′-dinitrobiphenyl using TiO_2 and under UV light irradiation**	**54-64**
	4.1	Introduction	55
	4.2	Experimental section	55
	4.2.1	Photoreduction studies	56-57
	4.3	Results and discussion	57-62
	4.4	Conclusion	62
	4.5	References	63-64
5		**Crystal phase and shape dependent photoactivity of titania for nitroaromatics reduction under UV light irradiation**	**65-76**
	5.1	Introduction	66-67
	5.2	Experimental section	67
	5.2.1	Synthesis of titania nanostructures of different crystal phase, size and shape	67
	5.2.2	Characterization techniques	67
	5.2.3	Photocatalytic activity for nitroaromatics reduction	67
	5.3	Results and discussion	67-72
	5.3.1	Structural analysis	67
	5.3.2	Morphological analysis	68

5.3.3	Optical properties	68-72
5.3.4	Photocatalytic study	72-73
5.4	Conclusion	74
5.5	References	74-76
	Conclusions	77-79
	List of publications	80
	List of papers/posters presented in conferences	80-81

List of Abbreviations

UV	Ultraviolet
Vis	Visible
DRS	Diffuse reflectance spectroscopy
HPLC	High pressure liquid chromatography
GC	Gas chromatography
GC-MS	Gas chromatography - mass spectrometry
TEM	Transmission electron microscopy
XRD	X-ray diffraction
BET	Brunauer Emmett Teller
JCPDS	Joint committee on powder diffraction standards
TNT	Titania nanotubes
TNR	Titania nanorods
m-DNB	*meta*-dinitrobenzene
m-NA	*meta*-nitroaniline
m-PDA	*meta*-phenylenediamine
m-CNB	*meta*-chloronitrobenzene
m-CA	*meta*-chloroaniline
m-NBA	*meta*-nitrobenzoic acid
m-ABA	*meta*-aminobenzoic acid
m-NT	*meta*-nitrotoluene
p-DNB	*para*-dinitrobenzene
p-NA	*para*-nitroaniilne
p-PDA	*para*-phenylenediamine
BC	Benzo[c]cinnoline
BPD	1,1’ Biphenyl 2,2’-diamine
BPO	Benzo[c]cinnoline 5,6-dioxide
VB	Valence band
CB	Conduction band
SC	Semiconductor

M	Metal
P25-TiO_2	Commercially available P25-TiO_2
RNP	Rutile nanospheres
RNR	Rutile nanorods
ANP	Anatase nanospheres
ANR	Anatase nanorods
NC	Nanocrystals
1D	One dimensional
SP	Surface Plasmon
SPR	Surface plasmon resonance
vol%	Volume percentage
wt%	Weight percentage
L	Length
W	Width
mL	Milli-litre
µL	Micro-litre
min	Minute
mol	Mole
mM	Milli molar
nm	Nanometre
AR	Aspect ratio
µM	Micro moles
PCA	Photocatalytic activity
a.u.	Arbitrary unit
c.a.	Calculated amount
vol%	Volume percentage

List of Symbols

e^-	Electron
h^+	Hole
$OH^\cdot$	Hydroxyl radical
E_g	Band gap
Å	Angstrom
α	Absorption coefficient
A	Absorbance
°	Degree
λ	Wavelength
%	Percentage
μ	Micro
θ	Theta
τ_{av}	Average lifetime
h	Hour
ϕ	Work function
E_o	Reduction potential
m	Meter
g	Gram
mg	Milligram
E_f	Fermi energy
V	Volt
d	Distance
s	Second
C	Concentration
υ	Frequency

Abstract

This thesis presents a fine approach into many aspects of Titanium dioxide (TiO_2) nanomaterials and their applications for photocatalytic reduction of nitroaromatics. Bare and metal loaded TiO_2 nanostructures viz., nanospheres and nanorods of different crystal phases viz., anatase and rutile have been synthesized to investigate the effect of size, shape, phase, nature of co-catalyst onto the change in absorbance, photoluminescence, relaxation lifetime and photocatalytic activity for the reduction of nitroaromatics. The present thesis is divided into **five** chapters:

Chapter 1: Introduction, Preparation and Characterization Techniques

The first chapter introduces the brief mechanism of TiO_2 semiconductor photocatalysis, effect of metal loading onto TiO_2, crystal phase, morphology, photoreduction of nitroaromatics with TiO_2 and literature survey on TiO_2 nanostructures with photocatalysis as an application point of view. Further, various techniques used for synthesis and characterization of bare and metal loaded TiO_2 nanocomposites are discussed. TiO_2 nanostructures of different morphologies viz.; nanospheres and nanorods as well different phase viz.; anatase and rutile have been synthesized by calcinations at temperature 400-800 ºC, hydrothermal, solvothermal and sol gel methods. Coinage and platinum group metals were deposited onto TiO_2 surface by photodeposition techniques.

The as synthesized materials have been characterized by diffused reflectance spectroscopy, photoluminescence; time resolved spectroscopy, transmission electron microscope, BET surface area analyzer and X-ray diffraction study. Photoreduction of nitroaromatics were conducted under UV light irradiations. Products and intermediates have been identified by high performance liquid chromatography, gas chromatography-mass spectroscopy, nuclear magnetic resonance spectroscopy and gas chromatography techniques.

Chapter 2: 100% selective yield of *m*-nitroaniline by rutile TiO_2 and *m*-phenylenediamine by P25-TiO_2 during *m*-dinitrobenzene photoreduction

The effect of rutile content, solvent, catalyst amount, irradiation time, crystallinity, surface area and electron withdrawing groups for selective photoreduction of *m*-dinitrobenzene have been discussed here. Photoreduction of *m*-dinitrobenzene (25 μmol) in the deaerated aqueous iso-propanol exhibits 100% selective yield of *m*-nitroaniline (25 μmol) by rutile TiO_2 (50 mg) or *m*-phenylenediamine (25 μmol) by P25-TiO_2 separately under 8 and 4 h of UV light irradiation (125 W Hg arc, 10.4 mW/cm^2), respectively. It revealed that insertion of a second –NO_2 group in

nitrobenzene ring has an important role in expediting $–NO_2$ reduction to $–NH_2$ as compared to a negligible reduction of nitrobenzene under similar conditions, indicating that electron withdrawing groups lower the electron density on $–NO_2$ present on meta position and favor quick reduction of the $–NO_2$ group.

Chapter 3: Influence of coinage and platinum group metal co-catalysis for the photocatalytic reduction of *m*-dinitrobenzene by P25 and rutile TiO_2

In this chapter, the co-catalytic activity of 1 wt% coinage (Au, Ag and Cu) metals and platinum group (Pt, Pd and Rh) metals deposited P25 and rutile TiO_2 (R-TiO_2) have been relatively investigated for the optical absorption, emission, surface structural morphology and photocatalytic activity for the selective reduction of *m*-dinitrobenzene under UV light irradiation. An average particle size ~122 nm of R-TiO_2 is increased after calcinations of P25-TiO_2 (25-30 nm) at 800 $^{\circ}$C and Au and Pt deposits of size ~4.0–6.5 nm were found to be uniformly distributed over TiO_2 surface. Although the optical band gap does not alter much, but intense photoluminescence having several characteristic bands between 400-550 nm are significantly quenched depending on the nature of metal loading. Photoirradiation (125 W Hg arc, 10.4 $mWcm^{-2}$) of bare P25-TiO_2 suspended in isopropanol (50 vol%) containing *m*-dinitrobenzene selectively produces 100% *m*-phenylenediamine, while metal deposited P25-TiO_2 produces *m*-nitroaniline as a major product after 4 h of UV light irradiation. However, bare R-TiO_2 produces 100% *m*-nitroaniline and metal loading does not alter the selectivity except the decrease in reduction efficiency of R-TiO_2. The decrease in active Ti^{3+} sites available on the surface after metal loading might be responsible for the decrease in photocatalytic activity.

Chapter 4: **Selective formation of benzo[c]cinnoline by photocatalytic reduction of 2,2′-dinitrobiphenyl using TiO_2 and under UV light irradiation**

This chapter demonstrates that the photocatalytic reduction of 2,2′-dinitrobiphenyl (DNBP, 25 μmol) in aqueous iso-propanol (50 vol%) and P25-TiO_2 (50 mg) under argon atmosphere and 20 h of UV light irradiation selectively produced 23.8 μmol of benzo[c]cinnoline (BC, 95%), and 2,2′-biphenyldiamine (BPD, 5%) whose amount is gradually increased with irradiation time beyond 20-24 h due to further reduction of BC. It is also observed that the reduction process is accompanied by the simultaneous oxidation of iso-propanol (hole scavenger) to acetone whose amount is increased with (20 to 24 h) irradiation time, and no H_2 production is detected by

photoexcited holes (h^+) in the valence band under UV irradiation. Furthermore, over oxidation of acetone into CO_2 was not observed. It is evident that DNBP undergoes intramolecular reductive cyclization reactions by TiO_2 because of the close spatial proximity of the interacting NO_2 groups that lie in two different benzene rings separately relative to their location in a same benzene moiety in various dintirobenzene.

Chapter 5: Crystal phase and shape dependent photoactivity of titania for nitroaromatics reduction under UV light irradiation

This chapter describes importance of different shapes and crystal phases of TiO_2 nanostructures such as RNP, RNR, ANP, ANR and P25-TiO_2 (70:30 anatase and rutile) for the PCA for *m*-nitrotoluene (*m*-NT) and *m*-nitrobenzoic (*m*-NBA) photoreduction under UV light irradiation. RNR (L×W = 28-30 nm × 3.5-3.8 nm) showed superior photoactivity (~3 times) as compared to RNP of size 122 nm for the photoreduction of *m*-NT into *m*-toluidine (*m*-TD) and *m*-NBA into *m*-aminobenzoic acid (*m*-ABA) under 8 h UV irradiation. The obtained results show that the long distance electron transport along longitudinal length, larger surface area (69 m^2g^{-1}), quenched PL emission, increased lifetime of charge carriers (1.8 ns) of RNR as compare to RNP having lower surface area (18 m^2g^{-1}) and charge carrier lifetime (1.1 ns) collectively contribute to its enhanced PCA. Furthermore, ANP of size 8-10 nm having surface area 89 m^2g^{-1} also shows higher PCA than anatase nanorods of size (L×W = 80-132 nm × 8-13 nm and surface area = 71 m^2g^{-1}) and P25-TiO_2 (25-30 nm) for *m*-NBA and *m*-NT photoreduction under 6 h UV light irradiation. The overall rate of reduction/hour for *m*-NBA and *m*-NT photoreduction with all of these catalysts has been found to vary in the following order ANP> P25-TiO_2> RNR> ANR> RNP.

Chapter 1: Introduction, Preparation and Characterization Techniques

1. Introduction

TiO_2 with remarkable optical and physicochemical properties is the most extensively used standard photocatalyst in the field of energy and environmental applications [1-4]. It is used in light-induced redox processes due to its electronic structure. Upon photo irradiation with light energy greater than or equal to the band gap energy of TiO_2, electrons (e^-) get excited from valence band (VB) to conduction band (CB) by leaving positively charged holes (h^+) in the VB as shown in **Fig. 1**.

When photogenerated e^-/h^+ pair comes in contact [5-8] with the absorbed H_2O, it gets oxidized by positive holes and forms hydroxyl radicals ($OH^{\cdot}$) in the process, which are highly oxidizing and oxidize organic compounds completely. In the presence of oxygen, the intermediate radicals in the organic compounds and oxygen molecules undergo radical chain reactions and consume oxygen to finally give carbon dioxide and water as shown below:

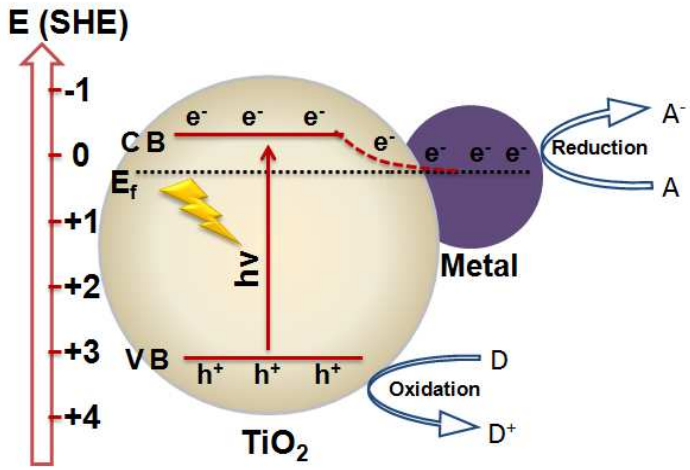

Fig. 1 Mechanism of TiO_2 photocatalysis

$$TiO_2 \xrightarrow{h\nu} (e^-/h^+)$$

$$e^- + h^+ \longrightarrow \text{heat}$$

$$TiO_2\,(h^+) + H_2O_{ads} \longrightarrow TiO_2 + OH_{ads}^{\cdot} + H^+$$

$$TiO_2\,(h^+) + OH_{ads}^- \longrightarrow TiO_2 + OH_{ads}^{\cdot}$$

$$OH_{ads}^{\cdot} + \text{organics} \longrightarrow CO_2 + H_2O$$

Under certain circumstances, organic substrates directly react with the positive holes (h^+) and results in oxidative decomposition. On the other hand, in the existence of air, reduction of oxygen takes place in place of hydrogen generation and forms superoxide anions ($O_2^{\cdot -}$). $O_2^{\cdot -}$

anions attach to the intermediate products in the oxidation reaction and form peroxide or convert to hydrogen peroxide and then to water as shown below:

$$TiO_2\,(e^-) + O_{2,ads} \longrightarrow TiO_2 + O_2^{\cdot -}$$

$$TiO_2\,(e^-) + H_2O_{2,ads} \longrightarrow TiO_2 + OH^- + OH_{ads}^{\cdot}$$

On the other hand, when charge traps or scavengers are absent, CB electrons and VB holes recombine to dissipate energy as heat and no chemical transformation takes place.

TiO_2 exhibits three distinct polymorphs- anatase, rutile and brookite. Among these, anatase has proven to be more prominent for various environmental processes such as deodorization, water purification, air purification, sterilization, solar-energy conversion and photocatalytic reactions [4-9], whereas the use of rutile form is limited due to its poor photocatalytic activity. The structures of anatase and rutile are shown in **Figure 2** and some of the structural and physical and properties of them are shown in **Table 1**.

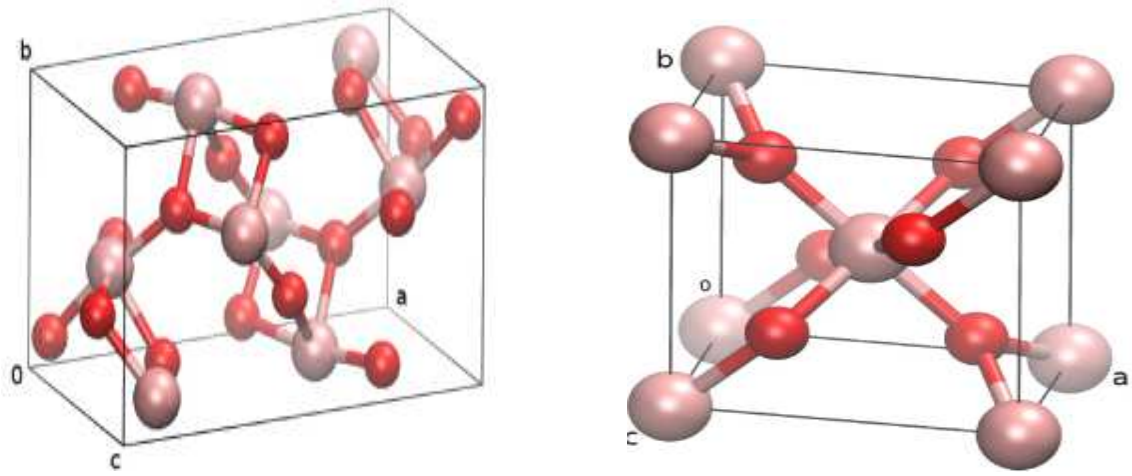

Anatase **Rutile**

Fig. 2 Stuctures of anatase and rutile.

The difference in the behavior of rutile and anatase is attributed to the difference in the band gap of anatase (3.2 eV) and rutile (3.02 eV) which is due to the difference in the position of the conduction band (higher in anatase than that of rutile) and to the higher rate of e^--h^+ pairs recombination in rutile as compared to anatase. Rutile TiO_2, generally obtained at higher temperatures, has very low density of superficial hydroxyl groups, which leads to poorer O_2

Table 1 Structural and physical properties of Anatase and Rutile structure of TiO_2

Property	**Rutile**	**Anatase**
Crystal structure	Tetragonal	Tetragonal
TiO_2 Formula units per unit cell	2	4
Band gap	3.0 eV	3.21 eV
Lattice Constants(Aº)	a = 4.5936	a = 3.784
	c = 2.9587	c = 9.515
Ti-O bond length (Aº)	1.949 (4)	1.937 (4)
	1.980 (2)	1.965 (2)
Density (g/cm^3)	4.13	3.79
Dielectric constant	114	31
Refractive index	2.75	2.55
Specific gravity	4.0	3.9
Molecular weight (g/mol)	79.88	79.88
Boiling point (ºC)	2500~3000	2500~3000

adsorption and such performance of rutile TiO_2 could be ascribed to a better crystallized bulk [10-15] and surface state, which is not as much of favorable for a potential photocatalytic activity. However, recently rutile TiO_2 (R-TiO_2) has drawn considerable attention that is reflected in selective oxidation [16] of benzyl alcohol to benzaldehyde, reduction of *m*-nitrotoluene [17] to *m*-aminotoluene, and other nitroorganics reduction [18,19] to aromatic amines and the experiments pointed the primary influence of crystallinity of rutile titania on the selectivity. Thus, photoactivity and product selectivity of TiO_2 can also be influenced with the change of phase from anatase to rutile. The photocatalytic activity of TiO_2 nanoparticles for selective reduction could further be enhanced by loading metals like Au, Ag, Cu, Pt, Pd, and Rh etc. In general the metal (M) deposited on the surface of TiO_2 forms a metal-semiconductor Schottky barrier that act as a trap for photoexcited electrons [20−22], and thus improve the efficiency of charge separation for improved oxidation and reduction rate of the organic substrates adsorbed on the surface. It is reported that the charge separation and Fermi level [23-25] equilibration (**Fig. 1**) in M/TiO_2 composites are further affected by the amount, nature, size of distribution, Fermi energy/work function, reduction potential, [26,27] and electronegativity of the metal deposited onto TiO_2. This creates future scope of research interest to load different

metals on TiO_2 for organic functional group transformation based on oxidation-reduction reaction.

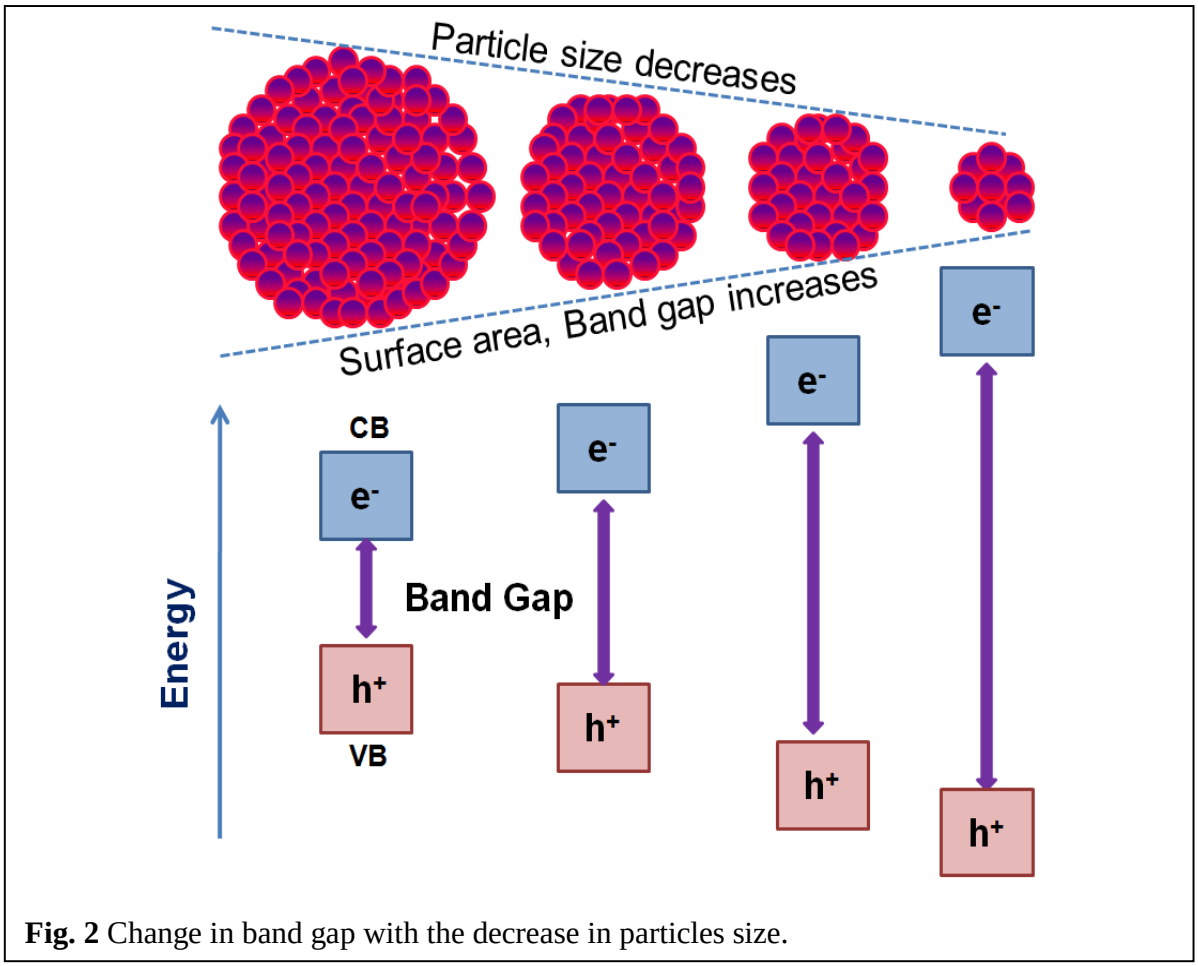

Fig. 2 Change in band gap with the decrease in particles size.

Other factors on which photocatalytic activity of TiO_2 depends are particle shape, size and specific surface area. Altering the size and shape of the particle, alters the extent of confinement of the electrons, and affects the electronic structure of the solid, in particular 'band edges, which are tunable with particle size. When the size of particle is decreased to the extent that the relative proportions of the surface and bulk regions of the particle are comparable, the energy band becomes discrete and will exhibit chemical and optical properties different from those of the bulk material. This phenomenon is known as quantum size effect. Size quantization of particles [28,29] will lead to the change in the position of CB and VB to higher and lower respectively, resulting in the larger energy gap **(Fig. 2)** between them. Therefore, it would be possible to control the redox ability of photocatalyst nanoparticles by changing their size. Titania

nanotubes (TNT) and nanorods (TNR) are gaining importance due to their exceptional features which also includes larger specific surface area and higher photocatalytic ability. These titania nanostructures showed their potential in photocatalysis [30,31] hydrogen sensing, and solar cells.

TiO_2 photocatalyst has also been used for the selective photoreduction and photooxidation of the functional groups in many organic compounds because of its many positive advantages over conventional synthetic routes. Out of various organics, nitroaromatics and its reduction products aminoaromatics have wide-range applications in the synthesis of fine chemicals, agrochemicals, pharmaceutical products, food additives and dye products. Typically, amino aromatic compounds are synthesized [32-34] by reduction of nitro aromatic compounds using Fe, Sn, Zn, Au–Ni alloy, Au/Pt-Al_2O_3, Pt/TiO_2, Fe_2O_3 and ZrO_2 [35-40] etc. under harsh conditions such as high temperature and pressure, toxic solvents and strong reducing agents like $NaBH_4$. The direct reduction of nitroaromatic compounds to their corresponding amino compounds can be appreciated by a photocatalytic route that is much more controlled, simplified, single step and a greener process by using TiO_2. The reduction of nitroaromatics is performed by irradiating TiO_2 suspended in alcohol under UV light in inert atmosphere. Photoexcited TiO_2 produces the electron (e^-) and positive hole (h^+) pairs. The alcohol get oxidized by h^+ and ketone and proton is produced. The photoreduction of nitroaromatics [18] by e^- produces the corresponding aminoaromatics, via a formation of nitrosobenzene (Ar−NO) and N-phenylhydroxylamine (Ar−NHOH) intermediates as shown below:

$$TiO_2 + h\nu \longrightarrow (e^-/h^+)$$

$$(CH_3)_2CHOH \xrightarrow{2h^+} (CH_3)_2CO + 2H^+$$

$$Ar\text{-}NO_2 \xrightarrow{2e^-,\,2H^+} Ar\text{-}NO + H_2O$$

$$Ar\text{-}NO \xrightarrow{e^-,\,H^+} [Ar\text{-}NOH^{\bullet}] \xrightarrow{e^-,\,H^+} Ar\text{-}NHOH$$

$$Ar\text{-}NHOH \xrightarrow{e^-,\,H^+} [Ar\text{-}NH^{\bullet}] + H_2O \xrightarrow{e^-,\,H^+} Ar\text{-}NH_2$$

The overall reaction is expressed as follows:

$$Ar\text{-}NO_2 + 3(CH_3)_2CHOH \longrightarrow Ar\text{-}NH_2 + 3(CH_3)_2CO + 2H_2O$$

The selective reduction of nitroaromatic compounds using TiO_2 catalyst is practically feasible because the reduction potential of the nitro group is below the conduction band energy of TiO_2. For example, the reduction potential [41-45] of nitrobenzene (-0.5 V versus SCE) is lower than that of the TiO_2 (-0.85 V versus SCE) and easily reduced to aniline and other

photoproducts. Also, nitro group can be selectively reduced over other functional groups (e.g. aceto (RCO-), ester (RCOOR'), cyano (CN) and aldehyde (-CHO) etc.) as their reduction potential [26] are high in comparison to the nitro group. Nitro group is selectively reduced in 4-nitrobenzaldehyde using Au/TiO_2 to obtain 4-aminobenzaldehyde [4] with 99.05% conversion and 96.8% selectivity. V. Brezova studied the effect of various solvents (methanol, ethanol, 1-propanol, 2-propanol, 1-butanol, *i*-butanol) for the photoreduction of 4-nitrophenol [46] in TiO_2 suspensions and found that 4-aminophenol was selectively formed up to 92% in methanol suspension. The solvent properties like viscosity, solvent polarity, and solvent polarity/polarisibility can substantially affect the electron transfer kinetics in TiO_2 mediated photocatalytic processes.

Thus, there is a possibility to change the product selectivity and yield by changing the nature of TiO_2 phase-anatase to rutile, surface morphology, size, shape, heat treatment and solvent. Moreover, the substitution of aromatic ring in nitroaromatics by electron withdrawing groups (EWG) and electron donating group (EDG) also affects the yield of a particular product. EWG lowers the electron density on a nitro group and facilitates the conversion of the nitro group into an amino group. Fernando Cardenas-Lizana group [47] examined the photocatalytic activity of 1 mol% Ag/TiO_2 and Au/TiO_2 in the gas phase hydrogenation of various para-substituted (–H, –Cl, $–OCH_3$, –OH $–CH_3$ and $–NO_2$) nitroaromatics. The selective $–NO_2$ group reduction was achieved with both of these catalysts and resulted into the only production of the corresponding aminoaromatics. The reaction proceeds via a nucleophilic mechanism where the presence of EWG served to elevate the rate of nitro group reduction in nitroarenes and EDG decreases the rate of reduction.

Advantages of photocatalytic technique than conventional organic synthesis:

(i) In photocatalytic reactions, heterogeneous catalysts are used, which are easy to separate from products, whereas in conventional reduction-oxidation processes, homogeneous catalysts are used, which are difficult to separate from the products.

(ii) Photochemical reaction is a single step reaction, but conventional reactions are multi-step reactions.

(iii) Photocatalytic reactions occur at the ambient temperatures [48] and pressure. So, drastic conditions as required in conventional reactions need not to be maintained.

(iv) Both oxidation and reduction occur simultaneously on the photocatalyst particles but in conventional reactions different oxidizing agent and reducing agent is needed.

(v) The redox reactions by e^- and h^+ leave no by-product that originated in the reductant and oxidant; this is contrastive to conventional redox reagents such as permanganate or $LiAlH_4$, which leave manganese ion or aluminum hydroxide [49], respectively, after oxidation and reduction.

(vi) Greener solvent water or in some reactions, alcohol is used whereas in conventional reactions expensive solvents are used, which are difficult to dispose off.

2. Literature review

Functional group transformations using different shapes and sizes of TiO_2 nanoparticles becomes an active area of research. Ohtani et al. [48] studied that in most cases, oxidation steps involve cyclization in amino acids resulting in the dehydrogenation of ethanol or methanol to yield aldehyde and follow the reduction step that induces conversion of nitro and azo compounds into an amino or hydroxyl amino group which contains heterocyclic compounds without generating any byproduct. It is reported that acyclic and cyclic secondary amines can be formed from primary amines [50] bearing α-methylene group by the use of Pt loaded TiO_2. Pan et al. [51] reported graphene-templated CdS−TiO_2 nanosheets for enhanced photocatalytic selective reduction of nitroaromatics. It is reported [52] that aerobic oxidation of amines to nitriles (97%) under visible light irradiation was catalyzed by $RuO_2.xH_2O/TiO_2$. Shiraishi et al. [53] reported high activity of Pt/P25 for selective photocatalytic oxidation of aniline to nitrosobenzene (90%) under visible light irradiation. It is demonstrated [54] that TiO_2 particles with different surface areas shows deoxygenation of styrene oxide into styrene with very high selectivity (84−95%). Photoirradiation of Degussa P25-TiO_2 in alcohols containing nitroaromatics at room temperature produces the corresponding imines with very high yields (80−96%) was reported. Pd nanoparticles supported on TiO_2 with oxygen vacancies demonstrates [55] an excellent thermocatalytic activity toward rapid and efficient reduction of nitroaromatics in water. It is mentioned in one report [56] that Pt−TiO_2 complex has a higher catalytic activity toward nitrobenzene conversion than pure Pt clusters.

Dihydropyrazine (yield-20%) was synthesized [57] using 2 wt% TiO_2/zeolite under UV irradiation in acetonitrile containing ethylenediamine and propylene glycol in oxygen saturated

condition. It is reported that mesoporous Au-TiO_2 nanocomposites [58] exhibit a higher visible-light photocatalytic activity for photocatalytic degradation of Rhodamine B in water, than that of the pristine TiO_2 nanoparticles. The enhanced photocatalytic efficiency of Au/TNT and Pt/TNT is studied for methyl orange degradation [59], which is found to reach 96.1%. Zn ions surface-doped TNT shows an improvement on the photocatalytic activity [60] for degradation of methyl orange in water as compared to Zn ions doped TiO_2 nanoparticles. It was found that photooxidation of acetone with TNTs under thermal treatment (300–700 ºC), showed better photo catalytic activity [61] than P25-TiO_2. Ag/TNR showed better photocatalytic activity for the photocatalytic decomposition of acid red 44 [62] as compared to TiO_2 nanospheres and nanorods.

Photoreduction of nitrobenzene with various catalysts gives the number of products viz. aniline, azoxybenzene, azobenzene, nitrosobenzene, N-(cyclohex-2-enyl) aniline. Nitrobenzene was reduced by using various semiconductors and yield of azoxybenzene by using TiO_2, WO_3, CdS in 11%, 41%, 28% respectively is reported [63]. Pal et al reported [64] the photoreduction of nitrobenzene by coating CdS by silica and by loading Rh metal on it, and the yield of azoxybenzene increased up to 68%. Photocatalytic conversion of nitrobenzene and its derivatives to quinaldines [65] using Ag–TiO_2 in absolute ethanol is reported. Photocatalytic $2e^-$ reduction of azobenzene to hydrazobenzene [66] using TiO_2 is found to occur at $\lambda > 300$ nm while loading of nanometer-sized Pt particles on TiO_2 induces N=N bond cleavage via $4e^-$ reduction. Arylhydroxylamines were prepared by a controlled reduction of nitro compounds using zinc metal and ammonium chloride under ultrasonic activation [67] in very short reaction times. Reduction of m-dinitrobenzene to *m*-phenylenediamine (yield 60%) by using Pt loaded titania catalyst is reported [37]. In one report [68], 1, 2-dinitrobenzene was reduced to 2-Alkylbenzimidazoles by using bare TiO_2. Photoreduction of 4-nitrobenzaldehyde using (VO*x*)*n* /TiO_2 led to the formation [69] of 4-amino-benzaldehyde with 100% selectivity. Sedat Yurdakal et al. reported [70] rutile TiO_2 nanoparticles for the selective oxidation of aromatic alcohols to aromatic aldehydes in water suspensions. Selective photocatalytic oxidation of benzyl alcohol into benzaldehyde under visible-light irradiation over single crystalline rutile TiO_2 nanorods [16] was done and about 99% product selectivity was achieved. Nitrobenzene photoreduction [71,72] by using TiO_2 and Ag/TiO_2 yields aniline with 88.5 and 84.3% respectively, was reported.

Finding from various research papers suggests that the photocatalytic conversion of many nitroaromatic compounds into useful products are carried out by TiO_2 photocatalysis, and our concern is to convert these aromatic nitro compounds to its commercially important products photocatalyticaly with 90-100% conversion factor in comparison to conventional synthesis techniques.

3. Research Gap:

1. In past, many researchers have been able to transform many functional groups by using bare TiO_2. However, to the best of our knowledge, the use of metal loaded TiO_2 in organic synthesis has not been studied widely despite its many positive effects.
2. PCA of TiO_2 nanoparticles for the selective photoreduction can be enhanced by changing shape and size (nanospheres, nanorods) or by metal loading onto them, where metal acts as a thermal catalyst and co-catalyst for functional group transformation.
3. Till now most of the studies have been done using anatase/rutile TiO_2 mixture and very few reports are present for selective photoreductions using bare or metal loaded R-TiO_2 of different shapes and sizes. Rutile nanoparticles and nanorods have been recently found to be active for selective photoreductions and photooxidations.
4. Nitroaromatics having one nitro group were studied by photocatalytic process but the influence of another nitro group present on same moiety has not been studied much.

   So, it is very interesting to study the effect of bare or M-TiO_2 nanocomposites, thermal treatment, surface area and rutile content for the selective reduction of industrially important nitroaromatics into aminoaromatics.

Keeping in view the above points, the following objectives have been designed.

4. Objectives:

(i) Preparation and characterization of bare and Metal -TiO_2 nanocomposites.

(ii) To study photocatalytic activity of as synthesized nanoparticles.

(iii) To study the effect of rutile content of TiO_2 and surface area on reduction of nitroaromatics.

5. Preparation and Characterization Techniques: The various materials and methods used for preparation of bare and metal-loaded titania nanoparticles of different size and shape,

detailed instrumental techniques used for characterization and analyzing the photoreduced samples of the studied compounds.

5.1 Materials used

Degussa P25-TiO_2, Titanium tetrachloride ($TiCl_4$), titanium (IV) isopropoxide, nitric acid, sodium hydroxide, methanol, ethanol, iso-propanol, n-propanol, silver nitrate ($AgNO_3$), hydrogen tetrachloroaurate (III) hydrate ($HAuCl_4.3H_2O$), copper nitrate ($CuNO_3.4H_2O$), palladium chloride ($PdCl_2$), hexachloroplatinic (IV) acid hexahydrate ($H_2PtCl_6.6H_2O$), rhodium chloride ($RhCl_3$), Nitrobenzene ($C_6H_5NO_2$), aniline (C_6H_7N), *m*-Dinitrobenzene ($C_6H_4N_2O_4$), *m*-Nitroaniline ($C_6H_6N_2O_2$), *m*-Phenylenediamine ($C_6H_8N_2$), *p*-Dinitrobenzene ($C_6H_4N_2O_4$), *p*-Nitroaniline ($C_6H_6N_2O_2$), *p*-Phenylenediamine ($C_6H_8N_2$), *m*-Chloronitrobenzene ($C_6H_4ClNO_2$), *m*-Chloroaniline (C_6H_6ClN), *m*-Nitrobenzoic acid ($C_7H_5NO_4$), *m*-Aminobenzoic acid (C_7H_7N), *m*-Nitrotoluene ($C_7H_7NO_2$), *m*-Toluidine (C_7H_9N) were purchased from Loba Chemicals. 2,2'-dinitrobiphenyl ($C_{12}H_8N_2O_4$) was purchased from sigma Aldrich, Benzo[c]cinnoline ($C_{12}H_8N_2$) was purchased from Alfa Aesar and used without further purification. An ultra filtration system (Milli-Q, Milipore) with conductivity 35 mho cm^{-1} at 25 $^{\circ}C$ was used to obtain deionized water. HPLC grade methanol and water were used for HPLC analysis.

5.2 Methods for the preparation of bare TiO_2 and metal-TiO_2 nanostructures

5.2.1 Preparation of sintered TiO_2 nanoparticles

1.0 g of commercially available Degussa P25-TiO_2 powder was taken in a crucible and subjected to 2 h calcination at 400, 600 and 800 $^{\circ}C$ in a muffle furnace. After this, the as obtained TiO_2 powder was allowed to cool down at room temperature and its phase confirmation was done by X-ray diffraction [73]. Rutile nanoparticles (R-TiO_2) were obtained at 800 $^{\circ}C$.

5.2.2 Synthesis of metal-TiO_2 nanoparticles

As prepared R-TiO_2 or P25-TiO_2 powder (50 mg) was taken in a test tube containing 5 mL of an aqueous isopropanol (50 vol%) solution [74]. An aqueous solution (0.01 M) of metal salts were prepared and subsequently added to above test tube corresponding to its 0.2-1 wt%. For 1 wt%: 256 µL of $HAuCl_4.3H_2O$, 468 µL of $AgNO_3$, 787 µL of $Cu(NO_3)_2.4H_2O$, 256 µL of $H_2PtCl_6.6H_2O$, 465 µL of $PdCl_2$ and 495 µL of $RhCl_3$ was added into the test tube. The test tube was sealed with a rubber septum, purged with argon gas for 15-20 min and irradiated by UV light (125 W Hg arc, 10.4 $mWcm^{-2}$) under constant magnetic stirring for 2 h in a photochemical

reactor. Thus obtained solution was centrifuged, repeatedly washed with distilled water and ethanol, and dried in oven at 50 °C for 30 min.

5.2.3 Synthesis of R-TiO_2 nanorods (RNR)

Pure R-TiO_2 nanorods were synthesized through a seed-mediated growth process [75] by hydrolysing $TiCl_4$ in highly acidic aqueous solution. Typically, 20 mL of aqueous $TiCl_4$ (3 M) was added into 35 mL of nitric acid solution (15 M). The mixture was refluxed for 24 h at 120 ºC. The residue thus obtained was centrifuged, washed three times with dilute nitric acid solution at pH=1. The centrifugated solid was then redispersed in dilute nitric acid solution (6 mL) at pH=1.

Then a growth solution of dilute $TiCl_4$ (0.3 M) was prepared and 20 mL of it was added into above seed solution and refluxed for 24 h at 120 ºC. The residue thus obtained was centrifuged, washed as mentioned above and dried in hot air oven at 70-80 ºC for 3-4 h.

5.2.4. Synthesis of anatase nanorods (ANR)

ANR were synthesized by a hydrothermal method as reported elsewhere [76]. Briefly, 4.73 g of P25-TiO_2 was mixed with 72 mL of NaOH (10 N) and then subjected to hydrothermal treatment at 130 ºC in a Teflon lined autoclave (80 mL capacity) for 20 h. The obtained slurry was washed repeatedly with 0.1 N HNO_3, followed by water and methanol, and dried in a hot air oven at 70-80 ºC for 3 h. 3.2 g of obtained particles were further dissolved in 64 mL of water and the resulted slurry (pH= 5.6) was autoclaved at 175 ºC for 48 h. Thus obtained ANR were filtered, washed with water and ethanol, and dried in hot air oven at 70-80 ºC for 3 h.

5.2.5 Synthesis of anatase nanoparticles (ANP)

ANP were synthesized by sol-gel [77] method. Typically, 0.1M titanium (IV) isopropoxide solution was prepared in 150 mL of iso-propanol. Another solution of measured quantity of water and 150 mL iso-propanol was also prepared. Both solutions were separately sealed and subjected to rapid magnetic stirring so as to obtain homogeneous mixtures. The water solution was then added drop wise to the 0.1M titanium (IV) isopropoxide solution under continuous magnetic stirring for 5 h. This resulted into hydrolysis of titanium (IV) isopropoxide and white colored precipitates were formed. These as obtained precipitates were filtered and washed thrice with deionized water and dried at 80 ºC. The powder thus obtained was calcined at 450 ºC for 2 h and named as ANP catalyst.

***5.3* Characterization:** Sophisticated instrumental techniques had been carried out to characterize titania nanostructures to get an idea of their size, shape, crystal character, defects and surface area etc.

5.3.1 UV-Vis diffuse reflectance Spectrophotometer (DRS)

This technique was used to determine the reflectance/absorption of as prepared bare and metal deposited samples in the UV/visible region, and for determination of their band gap (Eg). The analysis has been on **Avantes Diffuse reflectance spectrophotometer.** Sample (2-5 mg) was taken on a glass slide and the light source probe was placed over the sample to record its reflectance/absorbance spectra by using $BaSO_4$ as a reference.

Bandgap calculations of as prepared samples were done by using Tauc relation [9,10],

$$\alpha h\nu = A(h\nu - E_g)^n$$

where α is the absorption coefficient of the material, h is the Planck constant; ν is the frequency of light, A is a constant and E_g is the band gap of the material, exponent n is the type of the transition (n = ½ for direct, 2 for indirect band gap). The exact value of the band gap is determined by extrapolating the straight-line portion of αhν versus E_g graph to the x-axis.

5.3.2 X-ray diffraction analysis (XRD)

This technique was used to study the phase composition, structural variations and crystallinity of as prepared samples. The studies have been carried out by using X-ray diffractometer by **PANalytical X'Pert PRO** with Cu-Kα (λ = 1.54060˚A) radiation operated at 45 kV within the range of 20-80°. XRD samples were prepared by grinding dried TiO_2 powder in a pestle and mortar to form fine powders.

The fraction of rutile in each sample was calculated by using Spurr equation[28]

$$\% \text{ Rutile} = \frac{1}{1 + 0.8[I_A(101) / I_R(110)]}$$

where I_A is the intensity of (101) peak and I_R is the intensity of (110) peak.

The average size of the particles was calculated using the Scherrer's equation [13];

$$L = k\lambda/\beta \cos\theta,$$

where L is the average particle size, k is a constant of 0.9, λ is the wavelength of X-ray (1.5418 A°), β is the Full-Widths at Half-maximum (FWHM) of the (hkl) diffraction peak and θ is the Bragg angle.

5.3.3 Surface area analysis (BET)

BET surface area analysis was carried out in order to measure the specific surface area of the solids. The analysis of the porous surface was carried out by N_2 adsorption/desorption techniques at 77 K. Adsorption isotherms were determined using a **Smartsorb 92/93** instrument after preheating 100 mg of samples at 150 $^{\circ}$C for 1 h using N_2:He :: 70:30 as calibration gases at cryogenic temperature..

5.3.4 Photoluminescence measurement (PL)

Photoluminescence technique deals with the transitions from the excited state to the ground state, complementary to UV-Vis spectroscopy. **Perkin-Elmer LS55** spectrofluorimeter was used to study the possible defect and emission in as prepared bare and metal deposited titania nanoparticles. For PL analysis, 1mg/mL ethanol suspension of as prepared samples was photoexcited at 320 nm with xenon lamp at room temperature by using a slit width of 2.5: 5 with an average of 4 scans per sample.

5.3.5 Transmission electron microscopy (TEM)

TEM allows the imaging of individual particle and to some extent to evaluate the finest structural details and statistical distribution of sizes and shapes of the particles in sample. The samples were prepared by depositing a drop of a dilute ethanol dispersion of nanoparticles on carbon-coated copper grids and allowing the solvent to evaporate rapidly. The TEM analysis was performed on **Hitachi 7500 model** with resolution 2°A operating at voltage 120 kV.

5.3.6 Time resolved spectroscopy (TCSPC)

The time resolve photoluminescence spectra was measured by time-correlated single photon counting (TCSPC) set up by **Edinburgh FL920 model** at room temperature on excitation with diode lasers at 390 nm in ethanol suspension. The average lifetime (τ_{av}), is related to band edge lifetime τ_1 and trapping or defect's states given by the following equation [5],

$$\tau_{av} = (a_1\tau_1 + a_2\tau_2) / a_1 + a_2$$

where, a_1 and a_2 denote the amplitude of band edge excitonic and trapping state emission, respectively.

5.4 Photocatalytic activity

5.4.1 Photoreduction studies

The photoreduction of various nitroaromatics (Table 2.1) was carried out in a test tube containing bare or M/TiO_2 powder (50 mg) suspended in 5 mL aqueous isopropanol (50 vol%) and nitro compound (25 µmol) using UV light irradiation (125 W Hg arc, 10.4 mW/cm^2) under argon atmosphere and continuous magnetic stirring for different time intervals.

Table 1 Nitroaromatics studied for photoreduction using various titania catalysts

S. No.	Substrate studied	Products analyzed
1	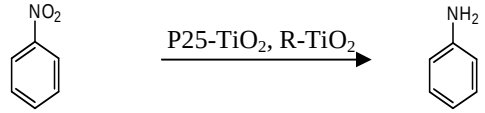	
2	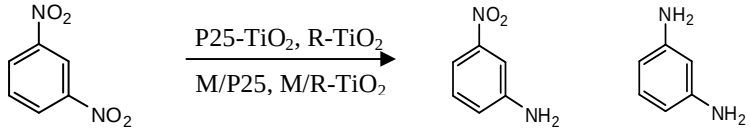	
3	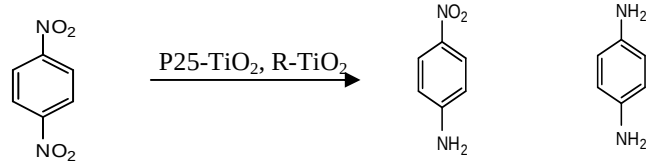	
4	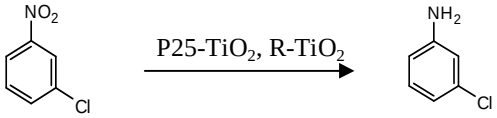	
5	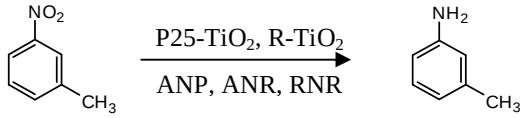	
6	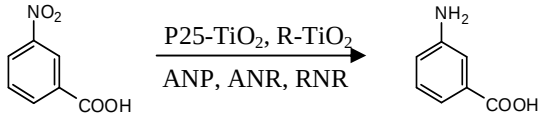	

7	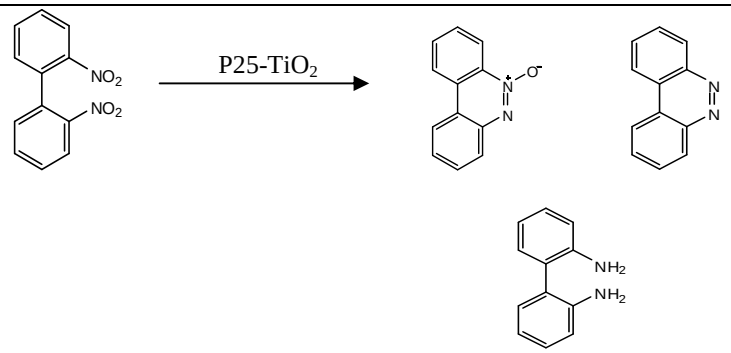

The reaction solutions obtained after photoreduction were analyzed by different techniques described below:

5.4.2 High Performance Liquid chromatography (HPLC): spectra were acquired by **Agilent 1120 Compact LC** equipped with a Qualisil BDS C-18 column (250 mm × 4.6 mm, 5 µm), at λ = 254 nm with flow rate 1 mL/min. The eluent consisted of: 70% methanol, 30% water aqueous solution. The reaction sample was centrifuged and filtered through cellulose filter (0.22 µm) and 20 µL of it was injected into the HPLC. The retention times of the compounds were compared with those of authentic samples.

5.4.3 Gas Chromatography-Mass Spectroscopy (GC-MS): spectra were measured by **Shimadzu GC 2010 and MS QP 2010** Plus equipped with RTX-5 Sil MS column (30 m × 0.25 mm i.d.). Injection temperature was 270 °C, injection mode was split less, injection volume was 1 µL taken by using a 10 µL syringe, electron ionisation detector with temperature 310 °C, oven temperature was 100 °C, and carrier gas was helium with flow rate 1 mL/ min. The reaction solution (5 mL) obtained after photoreduction of DNBP was subjected to centrifugation, filteration (cellulose filter 0.22 µm), and then evaporated to dryness over rota-evaporator. Residue was dissolved in acetonitrile (5 mL) and injected (1 µL) for GC-MS analysis.

5.4.4 Nuclear Magnetic Resonance Spectroscopy (^{1}H NMR): spectra were recorded on **Jeol-400 (^{1}H, 400 MHz)** spectrometer at ambient temperature using $CDCl_3$ as solvent. Chemical shifts are reported in ppm from the solvent resonance. Data are reported as follows: chemical shift, multiplicity (d =doublet, dd =double doublet, m =multiplet, t =triplet, bs =broad spectrum), coupling constants and number of protons. Reaction solution from five test tubes was collected, centrifuged, filtered by cellulose filter (0.22 µm) and evaporated to dryness over rota evaporator.

Residue was dissolved in $CDCl_3$ (0.5 mL) for NMR analysis. The NMR spectra of authentic samples were taken by dissolving authentic DNBP (10 mg) and authentic BC (10 mg), separately in $CDCl_3$ (0.5 mL).

5.4.5 Gas chromatography (GC): The amount of acetone in the liquid phase was determined by Gas chromatograph [**Bruker SCION 436-GC** equipped with a fused-silica capillary column (BR-1, 10 m, 0.53 mm)] and flame ionization detector. The column oven temperature was kept at 50 °C for 1 min, temperature programmed at 10 °C/min up to 250 °C. The injection port was maintained at 230 °C, and the detector was maintained at 230 °C. All the samples were studied by injecting 0.1 μL (using 1 μL syringe) of the sample solution with nitrogen as a carrier gas at a constant flow rate of 1 mL/min. The reaction solution (1 cm^3) was added to a chloroform/water mixture (2:1 v/v, 3 cm^3). After the mixture had been stirred for 10-15 min, acetone in the chloroform phase was analysed.

The detection of CO_2 evolution during the photoreduction of nitroaromatics was determined by injecting 1 mL of gaseous mixture from the reaction vessel (gas tight test tube) into **NUCON-5765 GC** equipped with Thermal Conductivity Detector (TCD) and Porapak-Q column (2 m × 2 mm i.d.) having flow of nitrogen (30 mL/min) as carrier gas. Column oven was maintained at 40 ^oC while injector and detector were isothermally kept at 70 and 80 ^oC, respectively.

5.5 Photocatalytic reaction set up

Photocatalytic reactor with Hg (UV) light source UV light source used here for all photoreduction reactions is made up of a low pressure mercury vapour lamp that emit light at 254 nm wavelength. The Hg lamp (125 W; intensity 10.4 mW/cm^2) was connected to power cords and set inside a quartz tube having a water jacket outside as shown in Fig. 3. A constant flow of cold water was circulated in the outer jacket to make it cool for longer time. A 15 mL capacity test tube containing 5 mL of reaction sample was placed at a distance of 2-3 cm from light source under magnetic stirring. The distance between magnetic stirrer and UV lamp was minimized in order to get optimum flux. This entire set up was placed in a wooden box to prevent the UV exposure as a safety purpose.

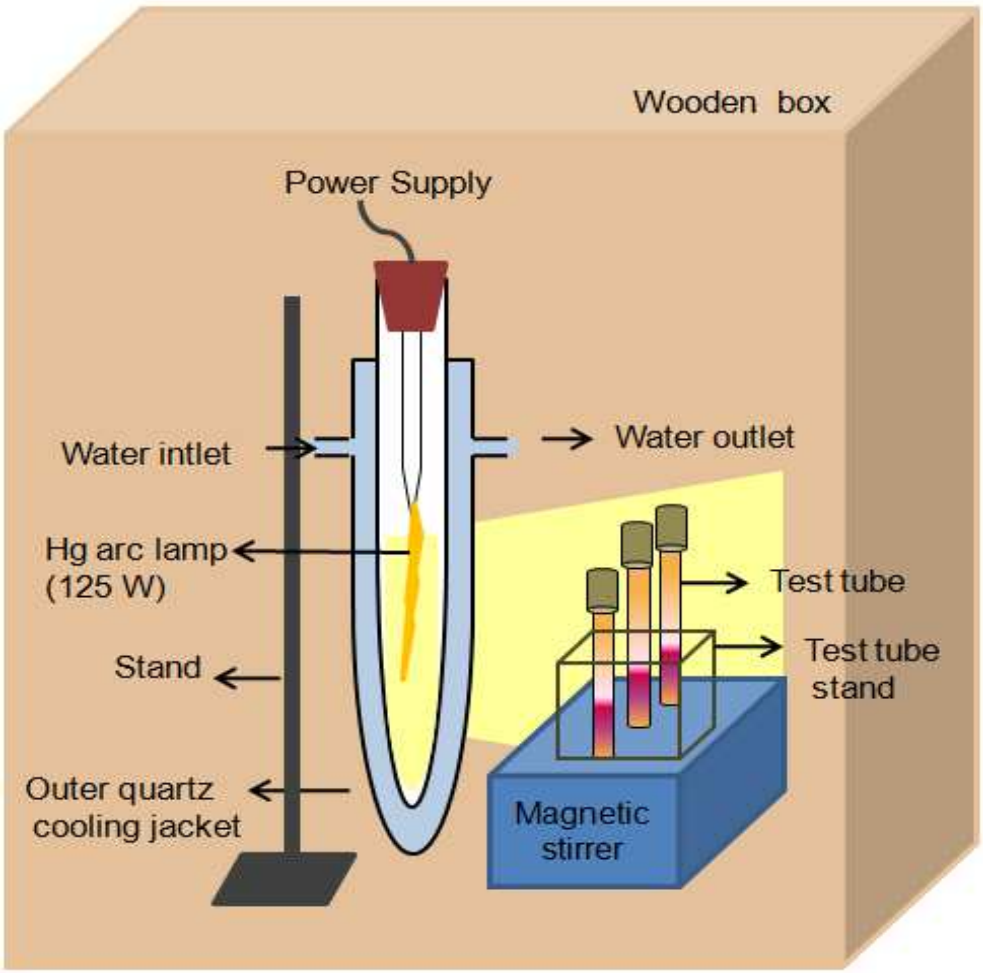

Fig. 3 Photocatalytic UV reactor set up

5.6 References

[1] T.T. Wu, Y.P. Xie, L.C. Yin, G. Liu, H.M. Cheng, J. Phys. Chem. C 119 (2015) 84.

[2] S.G. Kumar, L.G. Devi, J. Phys. Chem. A 115 (2011) 13211.

[3] T. Tachikawa, T. Majima, NPG Asia Mater. 6 (2014) 100.

[4] Y. Zhang, X. Cui, F. Shi, Y. Deng, Chem. Rev. 112 (2012) 2467.

[5] P.V. Kamat, Chem. Rev. 93 (1993) 267.

[6] A. Fujishima, T.N. Rao, D.A. Tryk, J. Photochem. Photobio. C: Photochem. Rev. 1 (2000) 1.

[7] M.A. Fox, M.T. Dulay, Chem. Rev. 93 (1993) 341.

[8] X. Chen, S.S. Mao, Chem. Rev. 107 (2007) 2891.
[9] A. Pearson, H. Jani, K. Kalantar-zadeh, S.K. Bhargava,V. Bansal, Langmuir 27 (2011) 6661.
[10] G. Liu, H.G. Yang, X.W. Wang, L.N. Cheng, H.F. Lu, L.Z. Wang, G.Q. Lu, H.M. Cheng, J. Phys. Chem. C 113 (2009) 21784.
[11] A. Mills, S.L. Hunte, J. Photochem. Photobio A: Chem. 108 (1997) 1.
[12] A. Kudo, Y. Miseki, Chem. Soc. Rev. 38 (2009) 253.
[13] K. Kobayatawa, Y. Nakazawa, M. Ikada, Y. Sato, A. Fujshima, Ber. Bunsen-Ges. Phys. Chem. 94 (1990) 1439.
[14] R. Campostrini, G. Carturan, L. Palmisano, M. Schiavello Sclafani, A. Mater. Chem. Phy. 38 (1994) 277.
[15] C. Morterra, J. Chem. Soc., Faraday Trans. 1 84 (1988) 1617.
[16] C.J. Li, G.R. Xu, B. Zhang, J.R. Gonga, Appl. Catal. B: Environ. 115 (2012) 201.
[17] A. Hakki, R. Dillert, D.W. Bahnemann, Phys. Chem. Chem. Phys. 15 (2013) 2992.
[18] Y. Shiraishi, Y. Togawa, D. Tsukamoto, S. Tanaka, T. Hirai, ACS Catal. 2 (2012) 2475.
[19] S.C. Li, U. Diebold, J. Am. Chem. Soc. 132 (2010) 64.
[20] K. Li, B. Chai, T. Peng, J. Mao, L. Zan, ACS Catal. 3 (2013) 170.
[21] Y. Ma, Q. Xu, X. Zong, D. Wang, G. Wu, X. Wang, C. Li, Energy Environ. Sci. 5 (2012) 6345.
[22] A. Tanaka, S. Sakaguchi, K. Hashimoto, H. Kominami, ACS Catal. 3 (2013) 79.
[23] V. Subramannian, E.E. Wolf, P.V. Kamat, J. Am. Chem. Soc. 126 (2004) 4943.
[24] H. Li, Z. Bian, J. Zhu, Y. Huo, H. Li, Y. Lu, J. Am. Chem. Soc. 129 (2007) 4538.
[25] R. Lv, C. Cao, Y. Guo, H. Zhu, J. Mater. Sci. 39 (2009) 1575.
[26] D. Buso, J. Pacifico, A. Marucci, P. Mulvany, Adv. Func. Mater. 17 (2007) 347.
[27] A. Wood, M. Giersig, P. Mulvaney, J. Phys. Chem. B 105 (2001) 8810.
[28] S. Eustis, A.M. El-Sayeed, Chem. Soc. Rev. 35 (2006) 209.
[29] C. Kormann, D.W. Bahnemann, M.R. Hoffmann, J. Phys. Chem. 92 (1988) 5196.
[30] H.H. Ou, S.L. Lo, Sep. Purif. Technol. 58 (2007) 179.
[31] D.P. Macwan, P.N. Dave, S. Chaturvedi, J. Mater. Sci. 46 (2011) 3669.
[32] P.F. Vogt, J.J. Gerulis, Ullmann's Encyclopedia of Industrial Chemistry. ''Aromatic Amines'', Wiley-VCH, Verlag GmbH & Co. KGaA, Weinheim, 2005, p. 2.

[33] L. Yingxin, C. Jixiang, Z. Jiyan, Chin. J. Chem. Eng. 15 (2007) 63.
[34] E. Killic, S. Aktan, Commun. Fac. Sci. Uni. Ank. Series B 47 (2001) 37.
[35] F.C. Lizana, S.G. Quero, N. Perret, M.A. Keane, Catal. Lett. 127 (2009) 25.
[36] Y. Chen, J. Qiu, X. Wang, J. Xiu, J. Catal. 242 (2006) 227.
[37] H. Rojas, G. Borda, P. Reyes, M. Brijaldo, J. Valencia, J. Chil. Chem. Soc. 56 (2011) 793.
[38] D.P. He, H. Shi, Y. Wu, B.Q. Xu, Green Chem. 9 (2007) 849.
[39] A. Corma, P. Serna, Science 313 (2006) 332.
[40] H. Zhu, X. Ke, X. Yang, S. Sarina, H. Liu, Angew. Chem. 122 (2010) 9851.
[41] M.S. Wrighton, Chem. Eng. News 57 (1979) 29.
[42] M.A. Fox, Nouv. J. Chim. 11 (1987) 129.
[43] T. Kanno, T. Oguchi, H. Sakuragi, K. Tokumm, Tetrahedron Lett. 21 (1980) 467.
[44] J.A. Dean, In Handbook of Organic Chemistry, ed. McGraw Hill, New York, 1987, section 8.
[45] F. Mahdavi, T.C. Bruton, Y. Li, J. Org. Chem. 58 (1993) 744.
[46] V. Brezova, A. Blazkova, I. Surina, B. Havlinova, J. Photochem. Photobio. A 107 (1997) 233.
[47] F.C. Lizanaa, Z.M. Pedrob, S.G. Queroa, M.A. Keanea, J. Mol. Catal. A: Chem. 326 (2010) 48.
[48] M. Kaise, H. Nagai, K. Tokuhashi, S. Kondo, S. Nimura, O. Kikuchi, Langmuir 10 (1994) 1345.
[49] B. Ohtani, B. Pal, S. Ikeda, Catal. Surv. Asia 7 (2003) 165.
[50] S. Nishimoto, B. Ohtani, T. Yoshikawa, T. Kagiya, J. Am. Chem. Soc. 105 (1983) 7180.
[51] X. Pan, Y.J. Xu, J. Phys. Chem. C 119 (2015) 7184.
[52] D.S. Ovoshchnikov, B.G. Donoeva, V.B. Golovko, ACS Catal. 5 (2015) 34.
[53] Y. Shiraishi, H. Sakamoto, K. Fujiwara, S. Ichikawa, T. Hirai, ACS Catal. 4 (2014) 2418.
[54] Y. Shiraishi, H. Hirakawa, Y. Togawa, T. Hirai ACS Catal. 4 (2014) 1642.
[55] X. Pan, Y.J. Xu, ACS Appl. Mater. Interfaces 6 (2014) 1879.
[56] J.J. Chen, W.K. Wang, W.W. Li, D.N. Pei, H.Q. Yu, ACS Appl. Mater. Interfaces 7

(2015) 12671.

[57] K.V.S. Rao, B. Srinivas, A.R. Prasad, M. Subrahmanyam, Chem. Commun. 16 (2000) 1533.

[58] M. Zhou, J. Zhang, B. Cheng, H. Yu, Int. J. Photoenergy 2012 (2012) 1.

[59] Q. Zhao, M. Li, J. Chu, T. Jiang, H. Yin, Appl. Surf. Sci. 255 (2009) 3773.

[60] J.C. Xu, M. Lu, X.Y. Guo, H.L. Lia, J. Mol. Catal. A: Chem. 226 (2005) 123.

[61] J. Yu, H. Yu, B. Cheng, C. Trapails, J. Mol. Catal. A: Chem. 249 (2006) 135.

[62] H.J. Yun, H. Lee, N.D. Kim, J. Yi, Electrochem. Commun. 11 (2009) 363.

[63] A. Maldotti, L. Andreotti, A. Molinari, S. Tollari, A. Penoni, S.J. Cenini, Photochem. Photobiol. A: Chem. 133 (2000) 129.

[64] B. Pal, T. Torimoto, K. Okazak, B. Ohtani, Chem. Commun. 5 (2007) 483.

[65] K. Selvam, M. Swaminathan, J. Mol. Catal. A: Chem. 351 (2011) 52.

[66] H. Tada, M. Kubo, Y. Inubushi, S. Ito, Chem. Commun. 11 (2000) 977.

[67] S. Ung, A. Falguie`res, A. Guy, C. Ferroud, Tetrahedron Lett. 46 (2005) 5913.

[68] H. Wang, R.E. Partch, Y. Li, J. Org. Chem. 62 (1997) 5222.

[69] R. Amadelli, L. Samiolo, A. Maldotti, A. Molinari, D. Gazzoli, Int. J. Photoenergy 2011 (2011) 1.

[70] S. Yurdakal, G. Palmisano, V. Loddo, V. Augugliaro, L. Palmisano, J. Am. Chem. Soc. 130 (2008) 1568.

[71] C. Shifu, Z. Huaye, Y. Xiaoling, L. Wei, Chin. J. Chem. 28 (2010) 21.

[72] H. Tada, T. Ishida, A.Takao, S. Ito, Langmuir 20 (2004) 7898.

[73] J. Kaur, B. Pal, Cat. Comm. 53 (2014) 25.

[74] U. Diebold, Surf. Sci. Rep. 48 (2003) 53.

[75] A. Dessombz, D. Chiche, P. Davidson, P. Panine, C. Chaneac, J.P. Jolivet, J. Am. Chem. Soc. 129 (2007) 5904.

[76] J.N. Nian, H. Teng, J. Phys. Chem. B 110 (2006) 4193.

[77] K.V. Baiju, S. Shukla, K.S. Sandhya, J. James, K.G.K. Warrier, J. Phys. Chem. C 111 (2007) 7612.

Chapter 2: 100% selective yield of *m*-nitroaniline by rutile TiO_2 and *m*-phenylenediamine by P25-TiO_2 during *m*-dinitrobenzene photoreduction

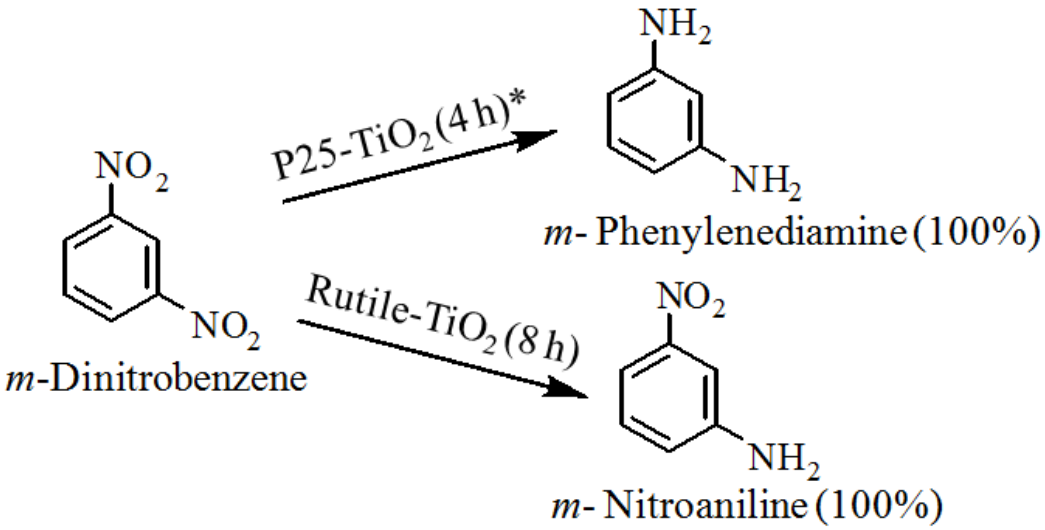

* Reaction conditions: 50 mg TiO_2 in 50% aqueous isopropanol and 125 W Hg arc exposure

2.1 Introduction

Aromatic amino compounds, such as *m*-phenylenediamine (*m*-PDA) and *m*-nitroaniline (*m*-NA) are important intermediates [1,2] for pharmaceuticals, food additives, agrochemicals and dye products. Typically, these are synthesized [3-8] by reduction of nitroaromatics using Fe, Zn, Sn, Au–Ni alloy, Au/Pt-Al_2O_3, Pt/TiO_2, Fe_2O_3 and ZrO_2 etc. under harsh conditions such as high pressure and temperature, toxic solvents and strong reducing agents like $NaBH_4$, where metal nanoparticles transfer the electron [9] from negatively charged BH_4^- to the nitro compound leading to its reduction. Generally, reduction of *m*-dinitrobenzene (*m*-DNB) to *m*-PDA proceeds via formation of *m*-NA, and the main challenge lies in the selective production of *m*-NA where the reduction [10,11] of both $–NO_2$ groups favourably produce *m*-PDA. Therefore, finding an effective technique for the synthesis of *m*-NA or *m*-PDA from *m*-DNB under ambient conditions is of great industrial importance. The direct reduction of nitroaromatic compounds to their corresponding amino compounds can be appreciated by a photocatalytic route that is much more controlled, simplified, and a greener process. Nitroorganics reduction by irradiated TiO_2 is a practically viable [12-16] because of the higher conduction band energy of TiO_2 (-0.85 V) relative to -0.5 V vs SCE of $–NO_2$ group preferably reduced over aceto, cyano, and aldehyde functionality present in the same compound. It has been found in literature that nitrobenzene (NB) was generally reduced [17-21] to aniline, azoxybenzene and azobenzene by CdS, WO_3 and P25-TiO_2 under UV light irradiation, whereas ZnO particles generate hydroxylamine [22], and core-shell SiO_2@Rh-CdS nanocomposites [23] produced 70% azoxybenzene under 436 nm light exposure. Therefore, activity/selectivity of nitroorganics can be controlled by controlling the reaction conditions such as choice of catalyst, material composition and phase and choice of solvent. It is revealed that partial reduction of one $–NO_2$ group of *m*-DNB to *m*-NA, and immediate further reduction of the second $–NO_2$ group to *m*-PDA can limit the selectivity of P25-TiO_2. Recently, rutile TiO_2 (R-TiO_2) has attracted attention because of its superior ability that is reflected in selective oxidation [24] of benzyl alcohol to benzaldehyde, *m*-nitrotoluene reduction [25] to *m*-aminotoluene, and other nitroorganics reduction [26,27] to aromatic amines. Thus, R-TiO_2 possessing low and slow reactivity could be effective for NA yield over PDA formation. Herein, we demonstrated for the first time the photocatalytic reduction of *m*-DNB in iso-propanol suspension by R-TiO_2 that displayed 100% yield of *m*-NA in comparison to negligible activity for NB reduction, whereas, anatase-rutile mixed P25-TiO_2 produced 100% *m*-PDA yield.

2.2 Experimental section

2.2.1 Preparation of sintered TiO_2 samples

The catalysts were obtained by sintering commercial Degussa P25-TiO_2 at 400, 600 and 800 ºC as per discussed in *section-5.2.1* of chapter 1.

2.2.2 Characterization

The characterization of as prepared TiO_2 samples was done by XRD *(section-5.3.2)* and BET *(section-5.3.3)* techniques as mentioned in detailed in *chapter 1*.

2.2.3 Photocatalytic study

Photoreduction of NB or *m/p*-DNB (25 µmol) was carried out with as prepared sintered TiO_2 samples as per procedure given in *section-5.4.1* (chapter-1). Reaction samples were analyzed by HPLC *(section-5.4.2)* and GC-MS *(section-5.4.3)* techniques, amount of acetone in the liquid phase was measured by GC *(section-5.4.5)* technique as given in chapter 1.

2.3 Results and discussion

2.3.1 Structural analysis of catalysts

The rutile phase of sintered P25-TiO_2 was confirmed with XRD spectra as shown in Fig. 1 and the peaks at 2θ = 27.5º, 36.5º, 41º, 54.1º, 56.5º are assigned to its rutile phase. The fraction of rutile in each sample was calculated by using Spurr equation [28]

$$\% \text{ Rutile} = \frac{1}{1 + 0.8[I_A(101) / I_R(110)]}$$

where I_A is the intensity of (101) peak and I_R is the intensity of (110) peak. With the increase in sintering temperature from 400-800 ºC, rutile content increases in P25-TiO_2 and pure (99.4%) R-TiO_2 sample was obtained at 800 ºC. The BET surface area analysis exposed that surface area decreases from 56 m^2g^{-1} of P25-TiO_2 to 18 m^2g^{-1} for pure R-TiO_2 with increased rutile contents.

2.3.2 Photocatalytic activity of sintered P25-TiO_2 catalysts

The various solvents *viz*. methanol, ethanol and n-propanol have been tested for the photoreduction of *m*-DNB by R-TiO_2 using 8 h of UV light irradiation (Fig. 2a). Among various solvents, iso-propanol proved to be the best medium for 100% selective yield of *m*-NA, where 46% *m*-PDA formation took place in ethanol. The higher hole scavenging ability of iso-propanol (secondary alcohol) as compare to other solvents (primary alcohols), avail more and more free

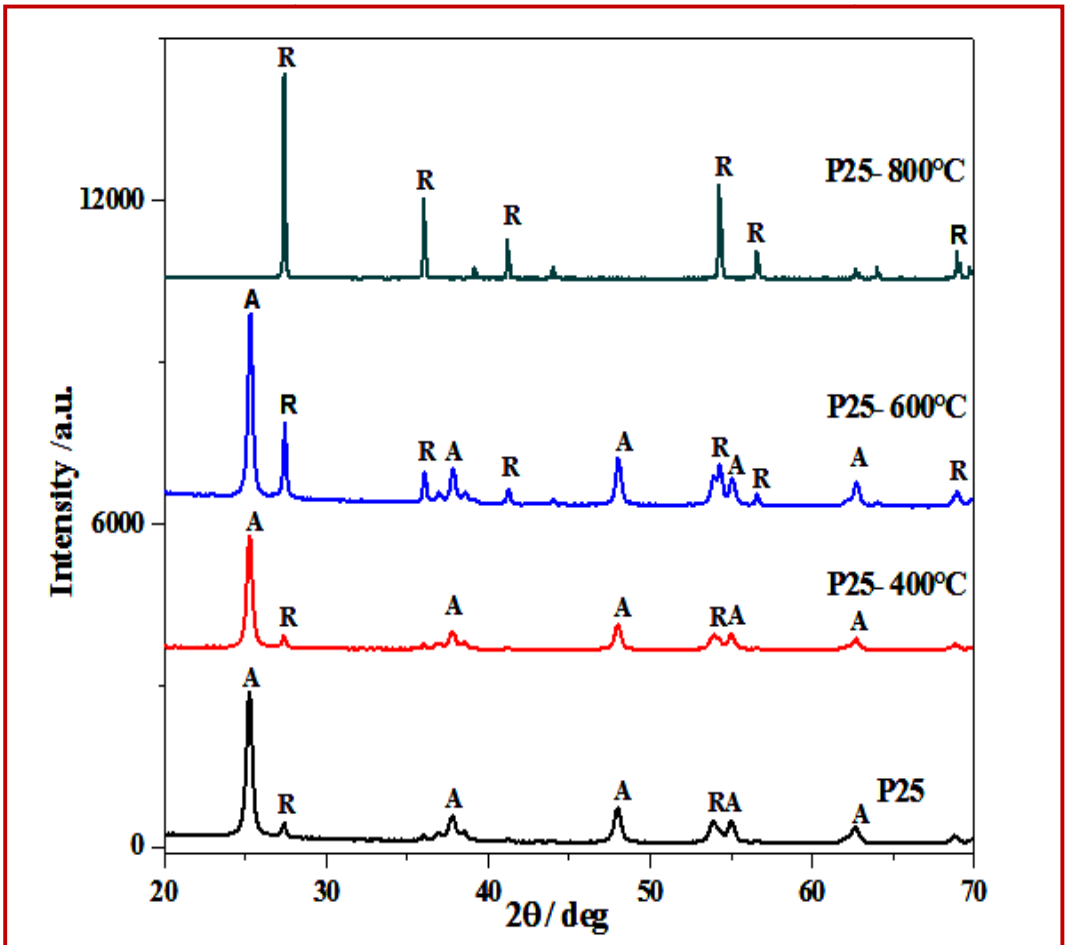

Fig. 1 XRD patterns of sintered P25-TiO_2 in air for 2 h at different temperature.

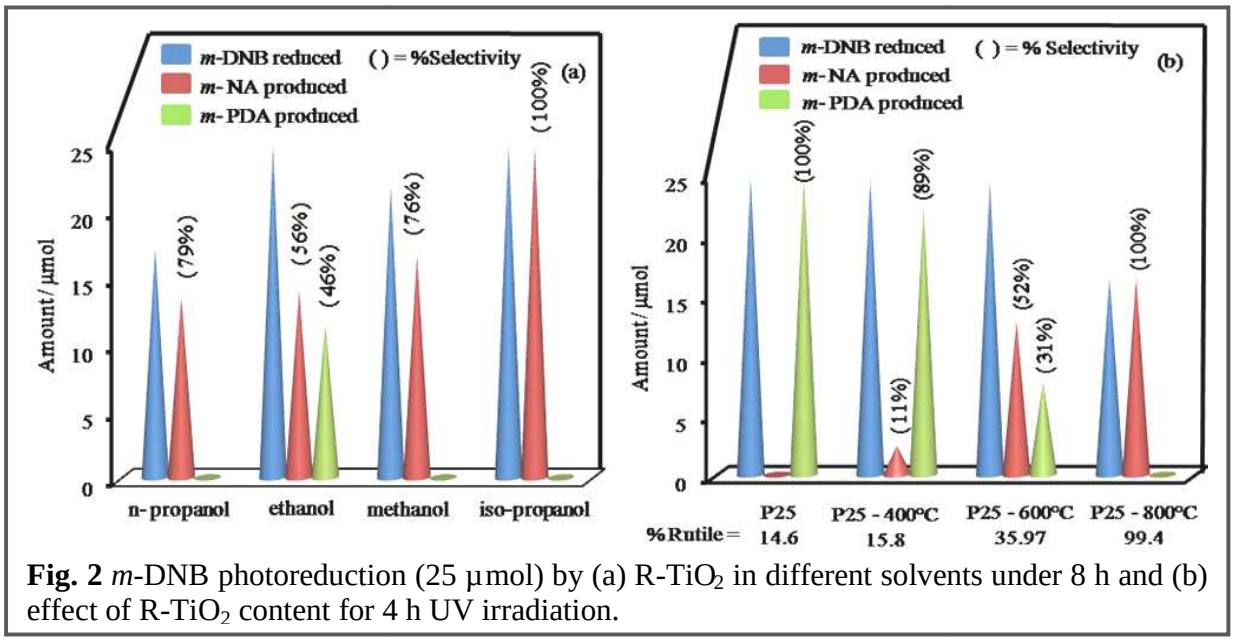

Fig. 2 *m*-DNB photoreduction (25 µmol) by (a) R-TiO_2 in different solvents under 8 h and (b) effect of R-TiO_2 content for 4 h UV irradiation.

electrons for reduction process and makes it a suitable solvent for the selective reduction of various nitroaromatics [8] as reported in literature. Fig. 2b showed that *m*-DNB (25 µmol) is selectively reduced to 100% *m*-PDA (25 µmol) by anatase-rutile mixed P25-TiO_2 catalyst and thereafter decreases with gradual increase in *m*-NA yield as a function of increased rutile content, and reached to 100% *m*-NA yield by pure (99%) R-TiO_2 after 4 h UV irradiation.

A comparative HPLC pattern (Fig. 3) shows a clear separation of *m*-PDA (t_R =2.9 min), *m*-NA (t_R =3.6 min) and *m*-DNB (t_R =4.6 min) peaks in a mixture (5 mM) of authentic samples (Fig. 3a), *m*-DNB reduction by R-TiO_2 for 8 h irradiation (Fig. 3b) displayed *m*-NA formation at t_R =3.6 min and *m*-DNB reduction by P25-TiO2 displayed *m*-PDA formation at t_R =2.9 min (Fig. 3c). The amount of *m*-DNB reduced is also subsequently decreased because of the low photoactivity

The amount of *m*-DNB reduced is

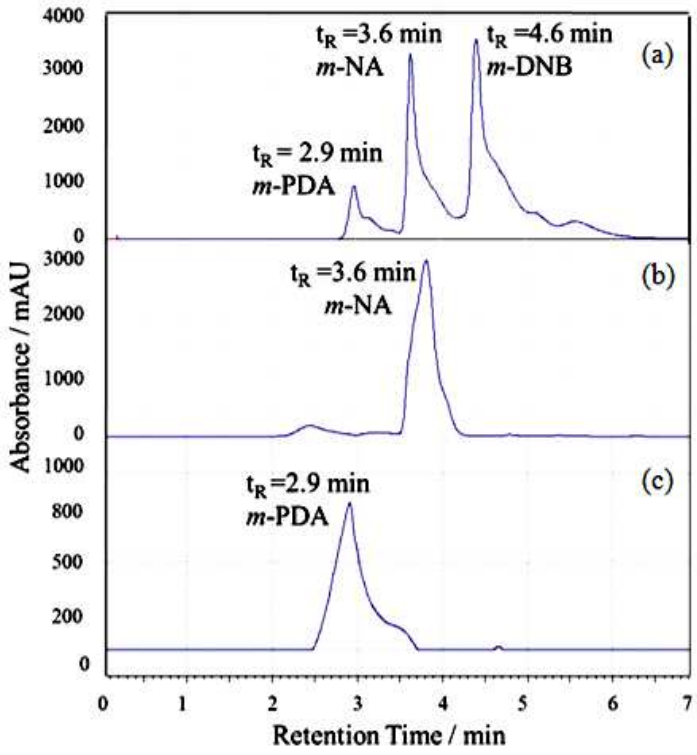

Fig. 3 HPLC pattern of (a) mixture of authentic *m*-DNB, *m*-NA, *m*-PDA (25 µmol each) and photoreduction of *m*-DNB (25 µmol) (b) with R-TiO_2 produces *m*-NA (25 µmol) during 8h (c) with P25-TiO_2 produces *m*-PDA (25 µmol) during 4 h UV irradiation.

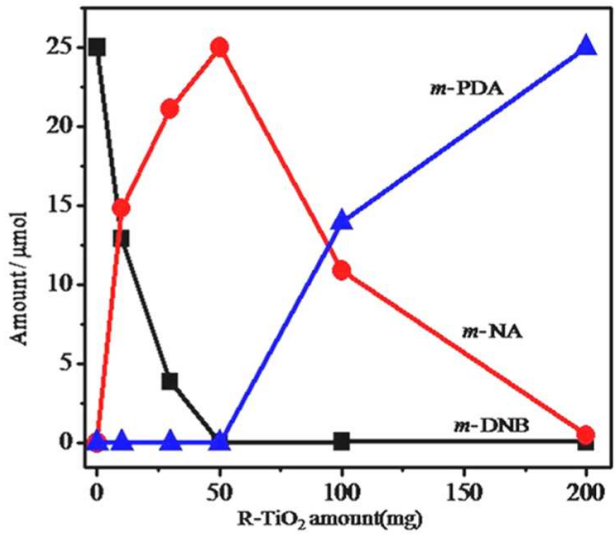

Fig. 4 *m*-DNB photoreduction (25 µmol) by R-TiO_2 (50-200 mg) in iso-propanol for 8 h irradiation.

also subsequently decreased because of the low photoactivity of R-TiO_2. Fig. 4 demonstrated that *m*-NA yield is highly improved with the increased amount of R-TiO_2, and exhibits maximum *m*-NA yield by 50 mg catalyst, and beyond this amount, the second –NO_2 group of *m*-NA starts reducing to give *m*-PDA as the final product. This can be well explained on the basis of availability of higher number of active sites of rutile TiO_2 for interaction with nitro group that resulted in rapid reduction of both –NO_2 groups. The amount of *m*-DNB is gradually reduced with increased amount (17.9 µmol) of *m*-NA along with little amount (3 µmol) of *m*-PDA produced by P25-TiO_2 during 2.5 h UV light irradiation and thereby, *m*-NA gets converted into 100% *m*-PDA (25 µmol) after 4 h light exposure (Fig. 5a) In contrary, complete reduction of *m*-

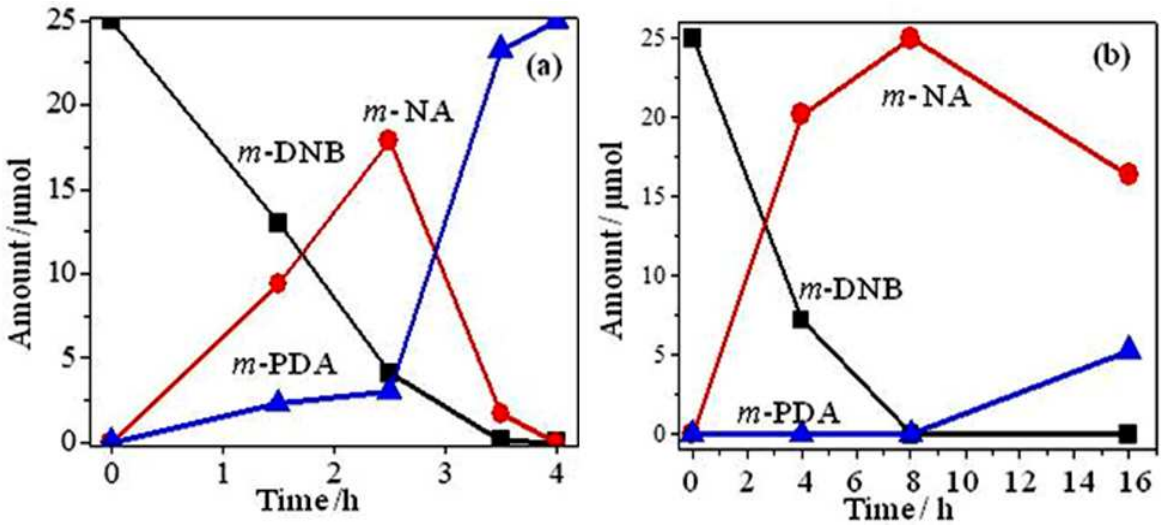

Fig. 5 Time course of *m*-DNB reduction by (a) P25-TiO_2 and (b) R-TiO_2 under UV irradiation

DNB to *m*-NA by R-TiO_2 is clearly observed after 8 h reduction and thereafter irradiation (> 8 h) led to less amount of *m*-PDA formation as shown in Fig. 5b. The efficiency of –NO_2 reduction to –NH_2 group is further verified by simultaneous analysis of acetone formed [11] during oxidation of iso-propanol under photoirradiation. It found that the amount of acetone formed is higher when both the –NO_2 groups are reduced to *m*-PDA than one –NO_2 reduction to *m*-NA formation as evident in the differences in peak area/height of acetone (t_R=1.2 min) in the GC chromatogram (Fig.6).

The GC-MS analysis revealed that a single sharp peak at t_R =5.5 min (Fig. 7a) for *m*-PDA and at t_R =8.1 min for *m*-NA (Fig. 7b) production by P25 and R-TiO_2 catalysts, respectively, evidencing cent percent yield and selectivity of the obtained products whose mass (Fig. 7c and 7d)

fragmentation is also matched with the respective authentic samples , confirmed the purity of *m*-NA and *m*-PDA. Thus it was found that *m*-DNB efficiently and selectively reduced by the increased percentage of rutile content and reached to the highest rate by pure R-TiO_2 as compared to no appreciable reduction of NB under low intensity of UV light. These findings are little different from the selective reduction [25] of $–NO_2$ to $–NH_2$ group by R-TiO_2 particles (obtained from P25-TiO_2 with HF dissolution) using high power Xe lamp (2 kW, 27.3 W/m^2) illumination. This fact suggests that the substituent and the position of $–NO_2$ group on the NB ring have an important role in the reduction process because the electron withdrawing groups that lower the electron density on a $–NO_2$ group present on *meta* position favour the rapid conversion of the $–NO_2$ into $–NH_2$ group and hence reduce the nucleophilicity of the resulting *m*-NA as observed in *m*-DNB reduction by P25-TiO_2. As the $–NO_2$ group in *para* position imparted less electronic induction than *meta* $–NO_2$ group, the selectivity of *p*-DNB (24 µmol) reduction to *p*-NA (17 µmol, 69%) is notably decreased without any production of *p*-PDA by R-TiO_2. This impact of $–NO_2$ substituent are further supported by the fact that almost no reduction (1-2 µmol) of NB to aniline (1 µmol) occurs by R-TiO_2 even after 8 h irradiation. However, P25-TiO_2 being its mixed anatase-rutile phase has higher catalytic activity, hence, 25 µmol *p*-DNB is reduced to 20 µmol *m*-PDA (82%)

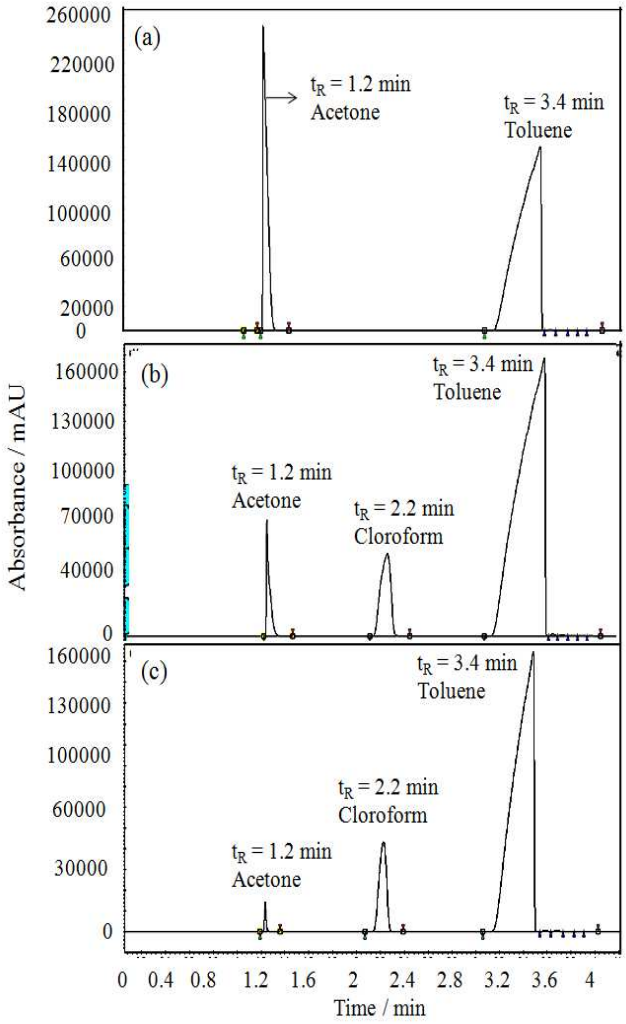

Fig. 6 GC pattern of (a) mixture of authentic acetone and toluene (1:1 v/v) and acetone produced during the photoreduction of *m*-DNB (25 µmol) into (b) *m*-PDA (25 µmol) with P25-TiO_2 during 4 h UV irradiation (c) *m*-NA (25 µmol) with R-TiO_2 during 8h UV irradiation.

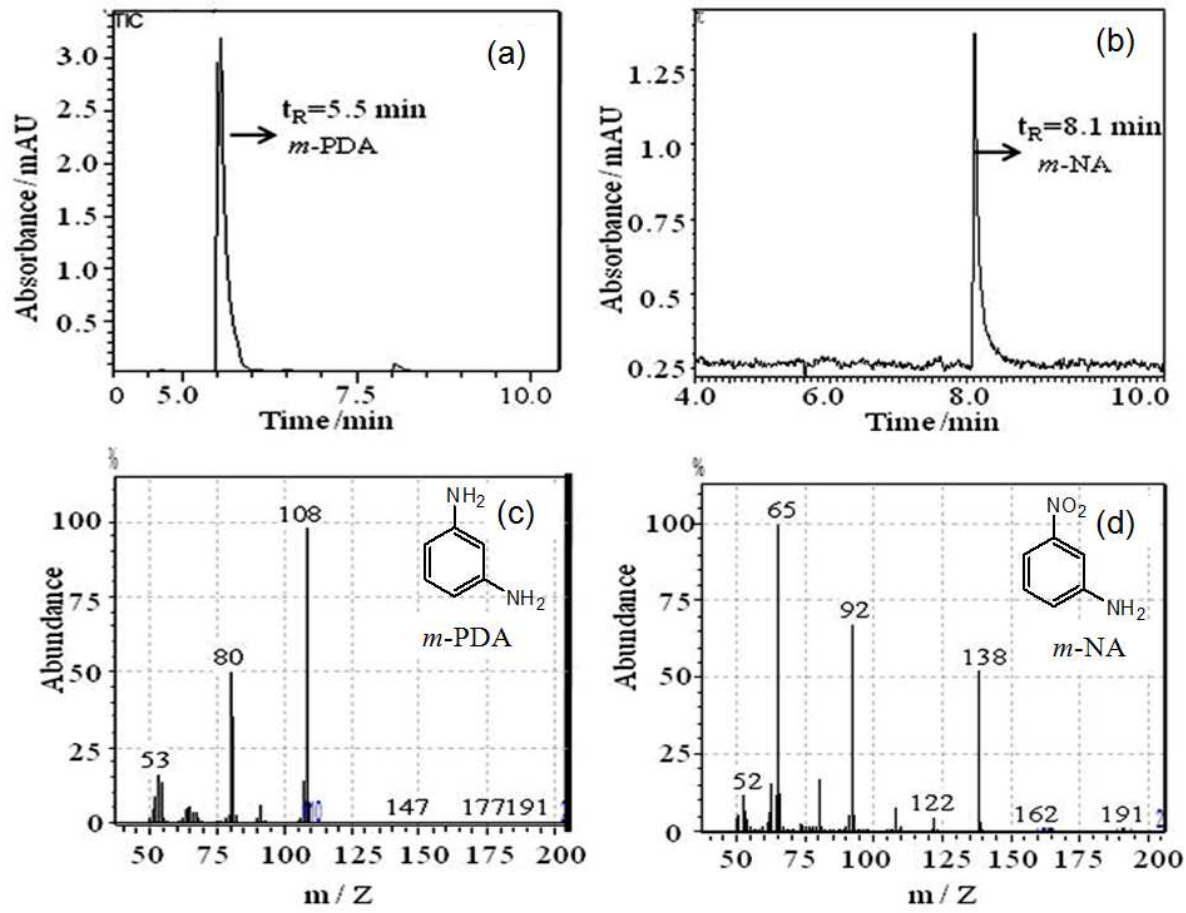

Fig. 7 GC chromatographs of photoreduction products of m-DNB (a) m-PDA with P25-TiO_2 after 4 h (b) *m*-NA with R-TiO_2 after 8 h, and (c, d) corresponding MS spectra with respective structural formulas *(inset).*

and 5 µmol *p*-NA (17%) relative to 14 µmol reduction of NB to 9 µmol aniline (66%) formation only after 4 h UV irradiation. Further, photoreduction of *m*-chloronitrobenzene by P25-TiO_2 gives *m*-chloroaniline (25 µmol) in 4 h, whereas R-TiO_2 gives less yield of *m*-chloroaniline (4 µmol) in 8 h as –Cl group is weakly electron withdrawing as compare to $–NO_2$ group which signifies that effect of different substituent present on *meta* position will also influence $–NO_2$ group reduction rate.

The measured surface area 56 m^2g^{-1} of P25 is notably reduced with increased rutile contents on increasing sintering temperature i.e., 38, 30 and 18 m^2g^{-1} at 400, 600 and 800 °C respectively. Therefore, although *m*-DNB reduction rate is decreased from 6.25 to 3.12 µmol/h, till the selectivity of *m*-NA yield is considerably improved because of the drastic changes in surface

electronic properties of R-TiO_2 with increased crystallinity [29] where fewer defect sites appeared to promote *m*-NA formation. The low photoreactivity of R-TiO_2 may probably due to less surface OH concentration leading to poorer O_2 adsorption essentially required for proficient capturing of photoexcited electron [30-32] and hence, exhibits fast recombination of e^-–h^+ pairs relative to P25-TiO_2 catalyst. Many studies [24-33] have revealed that strong oxidation of TiO_2 at elevated temperatures leads to the formation of a metal-deficient oxide and predominant defects in TiO_2 are oxygen vacancies that are important reactive agents for many surface reactions and thereby enhanced the photocatalytic activity due to mid gap induced states. The active sites for –NO_2 reduction on R-TiO_2 are the Ti^{3+} atoms [26,33] located at the oxygen vacancies on the R-TiO_2 surface behave as the adsorption site for DNB and the trapping site for conduction band electrons. Experimental results showed that rutile particles possess {011} and {110} faces, and the anatase particles exposed with {001} and {011} crystal faces, where the electronic energy levels of the {110} face are found to be lower than {011} face helping the quick separation of photoexcited electrons and holes for the rutile [34,35] than anatase particles. This variation in surface energy of the conduction and valence band of different crystal faces and their atomic arrangements thus affect the TiO_2 photoreactivity; hence facilitate the nitro-to-amine conversion by the surface-trapped electrons, enabling *m*-NA formation.

2.4 Conclusions

It is demonstrated that both the P25-TiO_2 and R-TiO_2 could be potentially utilized for the selective reduction of nitroaromatics possessing multifunctional reducible groups in *ortho, meta* and *para* position without any control of irradiation time. Thus proper selection of electron donating or withdrawing substituent's in the aromatic moiety would be highly beneficial and have a wide scope of several other desired products to obtain.

2.5 References

[1] P.F. Vogt, J.J. Gerulis, Ullmann's Encyclopedia of Industrial Chemistry. ''Aromatic Amines'', Wiley-VCH, Verlag GmbH & Co. KGaA, Weinheim, 2005, p. 2.

[2] L. Yingxin, C. Jixiang, Z. Jiyan, Chin. J. Chem. Eng. 15 (2007) 63.

[3] F.C. Lizana, S.G. Quero, N. Perret, M.A. Keane, Catal. Lett. 127 (2009) 25.

[4] Y. Chen, J. Qiu, X. Wang, J. Xiu, J. Catal. 242 (2006) 227.

[5] H. Rojas, G. Borda, P. Reyes, M. Brijaldo, J. Valencia, J. Chil. Chem. Soc. 56 (2011) 793.

[6] D.P. He, H. Shi, Y. Wu, B.Q. Xu, Green Chem. 9 (2007) 849.

[7] A. Corma, P. Serna, Science, 313 (2006) 332.

[8] H. Zhu, X. Ke, X. Yang, S. Sarina, H. Liu, Angew. Chem. 122 (2010) 9851.

[9] S. Kundu, S. Lau, H. Liang J. Phys. Chem. C 113 (2009) 5150.

[10] M.M. Telkar, J.M. Nadgeri, C.V. Rode, R.V. Chaudhari, Appl. Catal. A: Gen. 295 (2005) 23.

[11] Y.X. Liu, J.X. Chen, J.Y. Zhang, Chin. J. Chem. Eng. 15 (2007) 63.

[12] M.S. Wrighton, Chem. Eng. News 57 (1979) 29.

[13] M.A. Fox, Nouv. J. Chim. 11 (1987) 129.

[14] T. Kanno, T. Oguchi, H. Sakuragi, K. Tokumm, Tetrahedron Lett. 21 (1980) 467.

[15] J.A. Dean, In Handbook of Organic Chemistry, ed. McGraw Hill, New York, 1987, section 8.

[16] F. Mahdavi, T.C. Bruton, Y. Li, J. Org. Chem. 58 (1993) 744.

[17] A. Maldotti, L. Andreotti, A. Molinari, S. Tollari, A. Penoni, S. Cenini, J. Photochem. Photobiol. A: Chem. 133 (2000) 129.

[18] D.S. Bhatkhande, V.G. Pangarkar, A.A.C.M. Beenackers, Water Res. 37 (2003) 1223.

[19] R.J. Tayade, R.G. Kulkarni, R.V. Jasra, Ind. Eng. Chem. Res. 45 (2006) 922.

[20] H. Wang, J. Yan, W. Chang, Z. Zhang, Catal. Commun. 10 (2009) 989.

[21] R.J. Tayade, D.L. Key Mater. Sci. Forum 657 (2010) 62.

[22] Y. Li, L. Wang, In Nanocrystalline Semiconductor Materials, ed. P. Kamat, D. Meisel, Elsevier, New York, 1996.

[23] B. Pal, T. Torimoto, K. Okazak, B. Ohtani, Chem. Commun. 5 (2007) 483.

[24] C.J. Li, G.R. Xua, B. Zhang, J.R. Gonga, Appl. Catal. B: Environ. 115 (2012) 201.

[25] A. Hakki, R. Dillert, D.W. Bahnemann, Phys. Chem. Chem. Phys. 15 (2013) 2992.

[26] Y. Shiraishi, Y. Togawa, D. Tsukamoto, S. Tanaka, T. Hirai, ACS Catal. 2 (2012) 2475.

[27] S.C. Li, U. Diebold, J. Am. Chem. Soc. 132 (2010) 64.

[28] R.A. Spurr, H. Myers, Anal. Chem. 29 (1957) 760.

[29] S.Yurdakal, G. Palmisano, V. Loddo,O. Alagoz, V. Augugliaro, L. Palmisano, Green Chem. 11 (2009) 510.

[30] A. Kudo, Y. Miseki, Chem. Soc. Rev. 38 (2009) 253.

[31] K. Kobayatawa, Y. Nakazawa, M. Ikada, Y. Sato, A. Fujshima, Ber. Bunsen-Ges. Phys.Chem. 94 (1990) 1439.

[32] R. Campostrini, G. Carturan, L. Palmisano, M. Schiavello, A. Sclafani, Mater. Chem. Phys. 38 (1994) 277.

[33] S. Yin, H. Hasegawa, D. Maeda, M. Ishitsuka, T. Sato, J. Photochem. Photobio A: Chem. 163 (2004) 1.

[34] T. Ohno, K. Sarukawa, M. Matsumura, New J. Chem. 26 (2002) 1167.

[35] Y. Aoyama, Y. Oaki, R. Ise, H. Imai, Cryst. Eng. Comm. 14 (2012) 1405.

Chapter 3: Influence of coinage and platinum group metal co-catalysis for the photocatalytic reduction of *m*-dinitrobenzene by P25 and rutile TiO_2

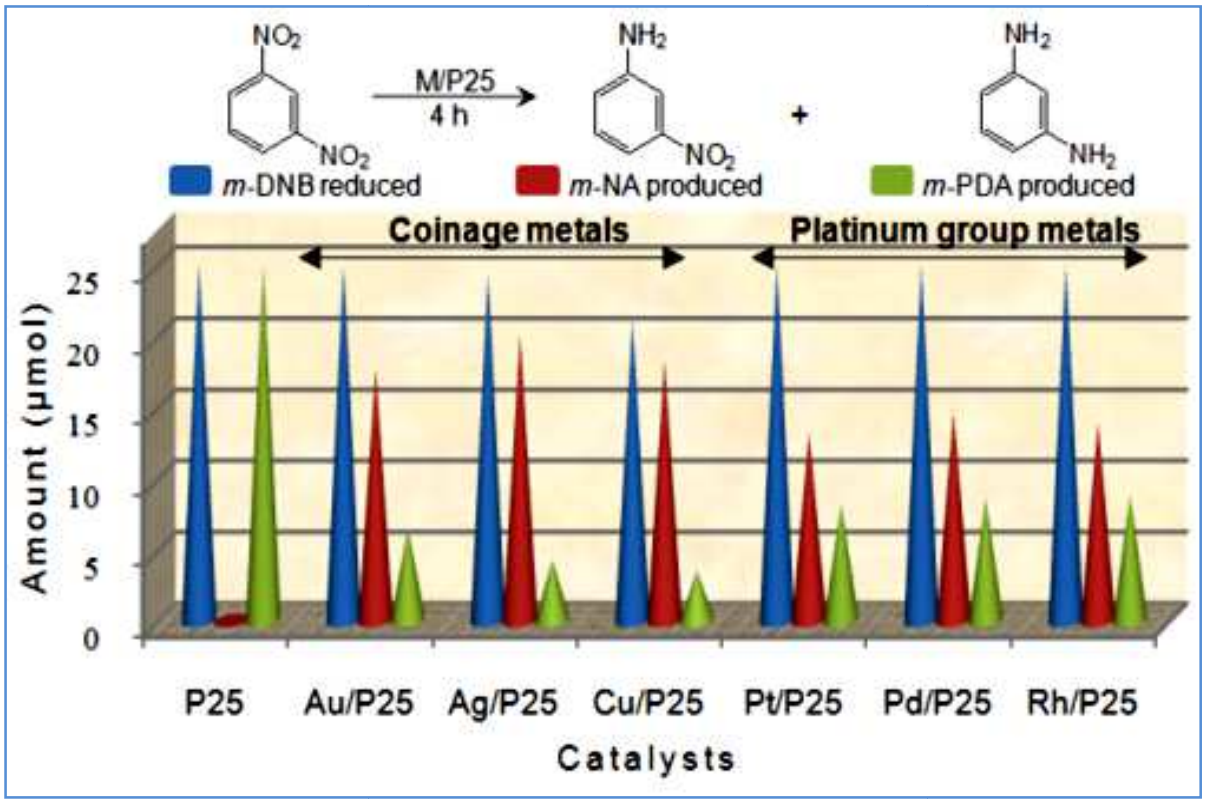

3.1 Introduction

Mixed phase P25-TiO_2 possessing a high surface adsorption affinity, more specific surface area, hydroxylated surface morphology, and better charge separation by rapid electron transfer from rutile (3.0 eV) to anatase (3.2 eV) crystal makes it superior photocatalyst [1−5] for many applications. Whereas, pure rutile TiO_2 (R-TiO_2) phase is generally regarded as less photoactive because of less surface OH concentration and poorer O_2 adsorption essentially required for rapid capturing of photoexcited electrons. Hence, exhibits fast recombination of e^-/h^+ pairs [6−11] that reduced the R-TiO_2 photocatalytic activity (PCA) relative to P25-TiO_2 catalyst. Recently, TiO_2 is utilized for selective reduction of nitroaromatics, benzonitrile to benzylamine, nitrobenzene to aniline and aryl azides to amines etc. and oxidation of alcohols to aldehydes, benzene to phenol [12−17] etc. under UV light irradiation. It revealed that though better PCA was achieved by either pure anatase or mixed P25-TiO_2 crystals generally give a mixture of product distribution, however, desired selectivity in organic conversion is not obtained in many instances. Hence, R-TiO_2 is recently employed [18−21] for the selective oxidation of benzyl alcohol to benzaldehyde, reduction of nitrobenzene to aniline, *m*-nitrotoluene to *m*-aminotoluene and nitroorganics reduction.

As R-TiO_2 is less active and more selective than anatase/P25, it takes longer duration of light irradiation for reduction of nitroaromatics, as also mentioned in our previous [22] report; R-TiO_2 gives 100% selectivity and yield of *m*-nitroaniline (*m*-NA) formation after 8 h irradiation as compared to 3−4 h irradiation in case of P25-TiO_2 which produces *m*-NA and *m*-phenylenediamine (*m*-PDA) during *m*-dinitrobenzene (*m*-DNB) reduction. The PCA for selective reduction can be further improved by Fe, Au, Ag, Cu, Pt, Pd, Ru and Rh etc. deposition onto TiO_2 as evident in photooxidation [23−26] reactions. Generally metal (M) deposition on TiO_2 surface forms a metal-semiconductor Schottky barrier that serves as a trap for photoexcited electrons [27−29], and thereby improved the charge separation efficiency for enhanced oxidation-reduction rate of the surface adsorbed organic substrates. This charge separation and Fermi level equilibration in M/TiO_2 composites are reported to be influenced by the nature, amount, size of distribution, reduction potential, Fermi energy/work function [30] and electronegativity of the deposited metal as depicted in ***Scheme 1***. Metals which have lower reduction potential than the conduction band/Fermi energy of TiO_2 are preferred, as more and more electrons get transfer to the metal and further to the reacting species and alter the reduction

efficiency. Although a few reports such as M-TiO_2/CdS composites (M = Pt, Pd, Rh and Fe) were studied for selective conversions [31] of lysine to pipecolinic acid formation, however, the effect of the different nature of metal loading on TiO_2 for selective reduction of nitroaromatics is not reported so far.

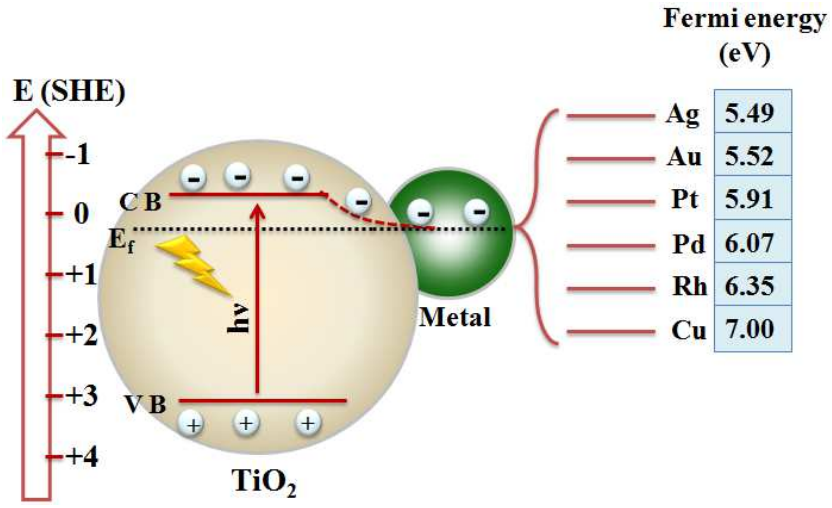

Scheme 1: Schematic illustration of Fermi level equilibration and charge transfer process occur at various metal-TiO_2 interfaces.

Hence, present research highlights the comparative effect of coinage (Au, Ag and Cu) and platinum group (Pt, Pd and Rh) metals co-catalysts deposition onto P25 and R-TiO_2 for improving the PCA for *m*-DNB reduction to optimize the product selectivity and yield upon shorter duration of light illumination.

3.2 Experimental section

3.2.1 Preparation of R-TiO_2 nanoparticles

R-TiO_2 nanoparticles were prepared by a standard method as reported elsewhere [22] and mentioned in *section-5.2.1* of chapter 1.

3.2.2 Metal (Au, Ag, Cu, Pt, Pd, Rh) photodeposition

Metal loading (0.2-1 wt%) onto prepared R-TiO_2 or P25-TiO_2 powder was done by using a photodeposition technique [32] as mentioned in *section- 5.2.2* of chapter 1.

3.2.3 Characterization techniques

As synthesized M/TiO_2 samples were characterized by DRS (*section-5.3.1*), XRD (*section-5.3.2)* BET (*section-5.3.3),* PL (*section-5.3.4)* and TEM (*section-5.3.5)* techniques discussed in detail in chapter 1.

3.2.4 Photocatalytic activity for m-DNB reduction: Photoreduction of *m*-DNB (25 µmol) was carried out with bare or M/TiO_2 powder as per procedure given in *section-5.4.1* (chapter 1). Reaction samples were analyzed by HPLC *(section-5.4.2)* and GC-MS *(section-5.4.3)* techniques as given in chapter 1.

3.3 Results and discussion

3.3.1 Optical, structural and morphological analysis of M/TiO_2 composites

Fig. 1a shows the absorption spectra of different metals (1 wt%) photodeposited P25-TiO_2 powder samples. The bare P25-TiO_2 sample exhibited a strong peak at 386 nm, which is attributed to the electronic transition from oxygen 2p orbital's in the valence band to the titanium 3d orbital's in the conduction band. In comparison to P25-TiO_2, the absorption onset in slightly red-shifted to 403 nm in Cu/TiO_2 and thereby varied to a little extent due to charge transfer transitions between the metal ion electrons and the TiO_2 conduction, depending upon the nature of M deposits over TiO_2 surface. However, Au and Ag loading displayed a characteristic surface plasmon resonance (SPR) band at 450 and 550 nm, respectively.

During UV light irradiation, the adsorbed metal ions on TiO_2 are reduced by the photoexcited electrons in conduction band as $M^{n+} + ne^- \rightarrow M^0$, and randomly deposited over the surface. It is well reported [33−35] that Au^{3+}, Ag^+, Cu^{2+}, Pt^{4+}, Pd^{2+} and Rh^{3+} ions are generally reduced to their metallic state because of their suitable reduction potential/work function that lies below the conduction band position of TiO_2. Hence, photoreduction of metal ions onto the respective

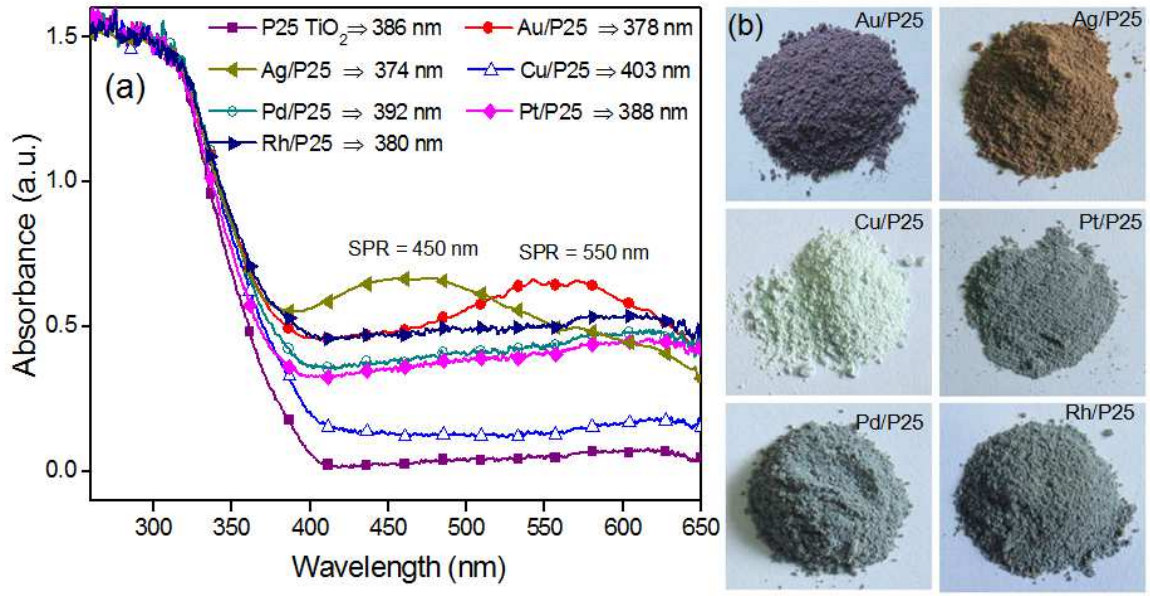

Fig. 1 Absorption spectra of different (a) metal (1 wt%) deposited P25-TiO_2 powders and (b) their colors.

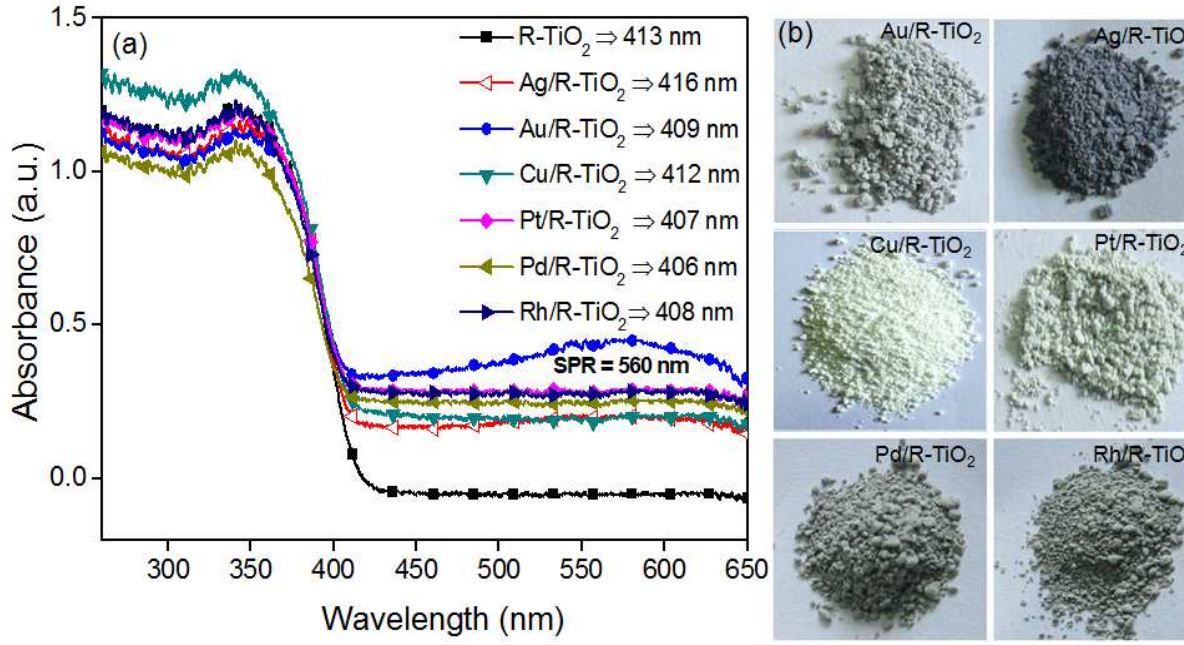

Fig. 2 Absorption spectra of (a) 1 wt% metal deposited rutile titania, and (b) their corresponding colors.

titania nanoparticles led to a significant change in their colors, as shown in Fig.1b.

As shown in Fig. 2a, the absorbance onset at 413 nm for bare R-TiO_2 does not induce any notable shift even after metal deposition, which is confirmed by the limit in color variation from light grey to dark grey (Fig. 2b). The decrease in intensity of absorption edge at 340 nm of R-TiO_2 relative to P25-TiO_2 is due to enhanced scattering of light by larger crystallites [36] formed by the calcination of P25-TiO_2, owing to the difference in surface morphologies, crystallite size, phase structure, and compositions.

The band gaps of bare and various metals deposited samples were calculated by using Tauc relation [37], which is given by $\alpha h\nu = A (h\nu - E_g)^n$, where α is the absorption coefficient, $h\nu$ is the photon energy, A is a constant and E_g is the band gap of the material, exponent n is the type of the transition (n = ½ for direct, 2 for indirect band gap). The exact value of the band gap is determined by extrapolating the straight-line portion of $\alpha h\nu$ versus E_g graph to the x-axis. It can be seen from the Fig. 3a that Au/P25 exhibits band gap energy 3.38 eV and Pt/P25 possess band gap of 3.24 eV relative to 3.2 eV for pure P25-TiO_2 sample. While metals loading did not modify the band energy relative to 3.0 eV of pure R-TiO_2, and comparative changes in band gap energy between different M/P25 and M/R-TiO_2 did not demonstrate any significant difference except Ag, Au and Cu loading which increased the band gap energy in a small extent relative to

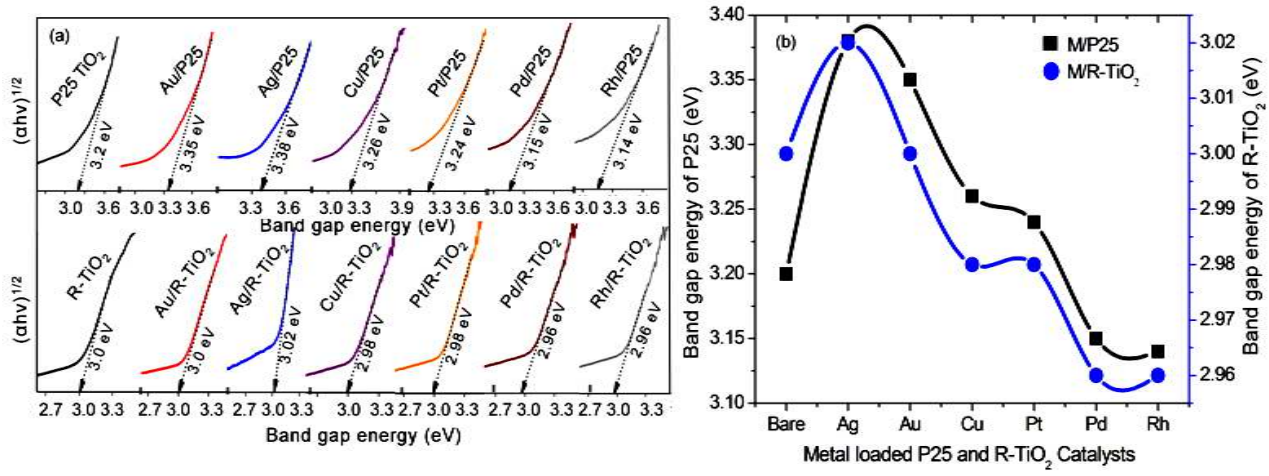

Fig. 3 (a) The plot of $(\alpha h\nu)^{1/2}$ function versus the band gap energy of various pure and deposited samples. (b) Variation in the band gap energy of pure and metal deposited samples.

bare TiO_2 as observed in Fig. 3b. Ag, Au and Cu loading which increased the band gap energy in a small extent relative to bare TiO_2 as observed in Fig. 3b.

The photoluminescence (PL) spectra in Fig. 4a showed that P25-TiO_2 exhibited a set of the emission bands in the range of 400-550 nm indicated that commercial available P25 material is not much crystalline due to the presence of many surface defect sites. The band at 404 nm is attributed to band edge emission; originate from the recombination of photoexcited electron-hole pair's and the emission bands at 423 nm, 446 nm, 460 nm is assigned to shallow-trap state near absorption band edge emission, correspond to the presence of oxygen vacancies, [38] whereas,

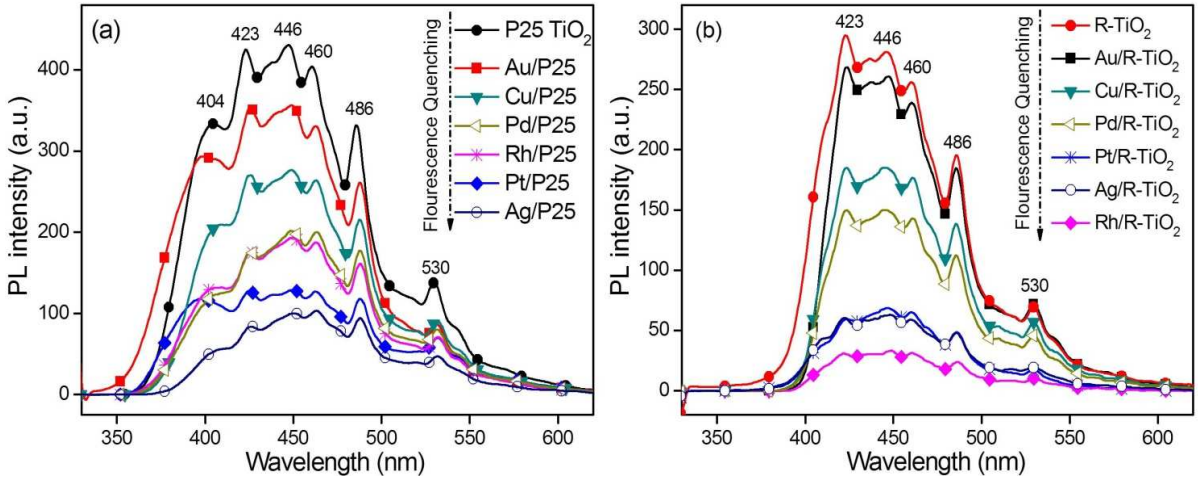

Fig. 4 Change in photoluminescence spectra of (a) P25 and (b) rutile after 1 wt% loading of different metals.

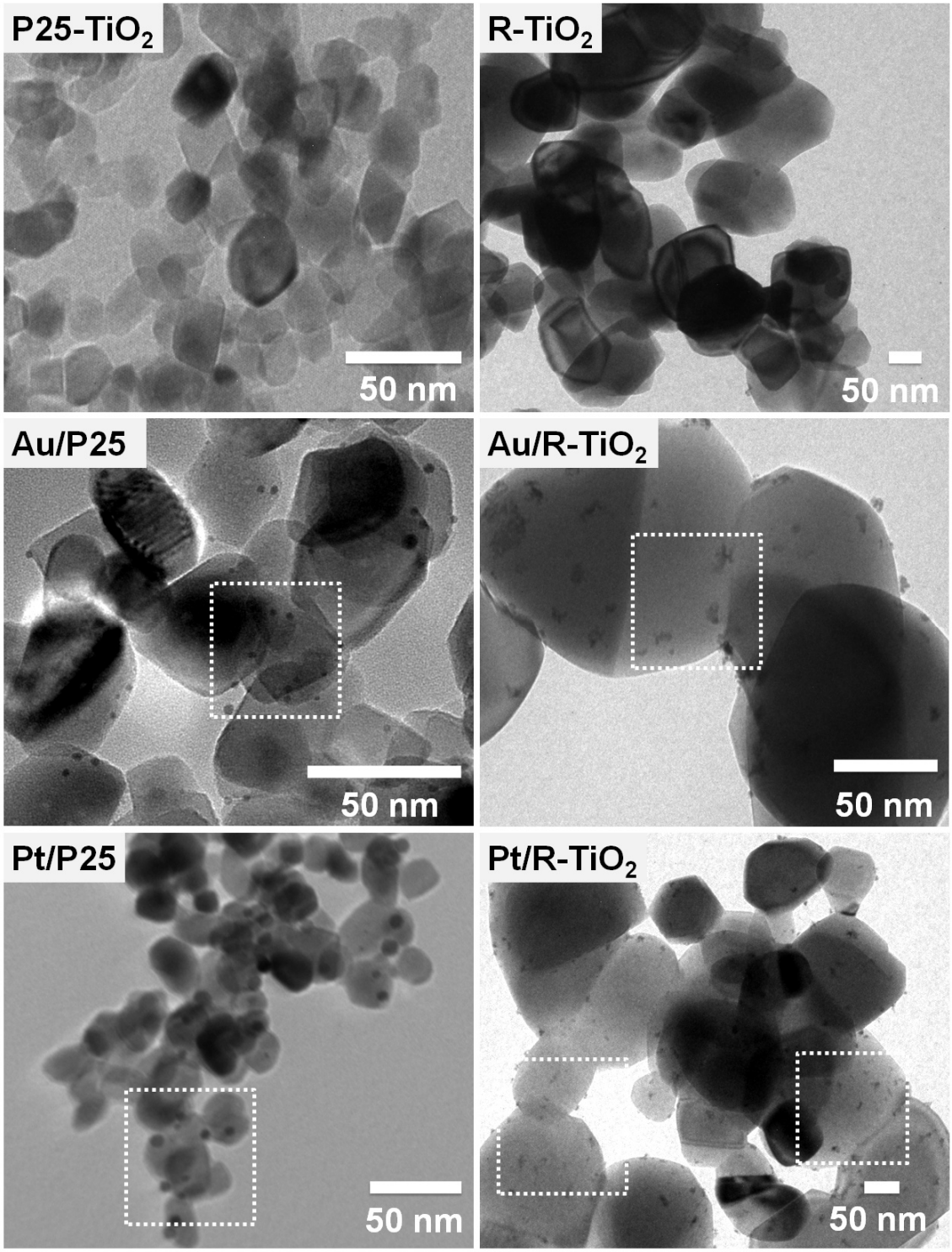

Fig. 5 TEM images of (a) P25-TiO_2 (b) Rutile TiO_2 (c) 1 wt% Au/TiO_2 (d) 1wt% Au/R-TiO_2 (e) 1 wt% Pt/TiO_2 and (f) 1wt% Pt/R-TiO_2 composites.

bands at 486 nm and 530 nm corresponds to the deep-trap states far below the band edge emissions and collectively called surface state emissions. These charge carriers are generally trapped by oxygen vacancies and surface hydroxyl groups, which contribute in their visible luminescence [39]. After deposition of 1 wt% M onto the TiO_2 surface always quench the PL intensity depending on the kind of M deposits, where Ag and Pt loading led to a maximum reduction in PL intensity as compared to Au deposition and bare P25 catalysts. While Rh, Pt and Ag deposition displayed higher PL quenching relative to bare and Au loaded R-TiO_2. This could be attributed to effective shuttling of photogenerated photo generated charge carriers from TiO_2 surface to deposited M islands that prevent the recombination and hence quench the PL emission. Similar defects have been observed in case of R-TiO_2 except the band at 404 nm as shown in Fig. 4b and the intensity of emission peak at 423 nm is higher than that of 400 nm indicates that the M/TiO_2 nanoparticles having more surface states dominate the excitonic emission.

TEM photographs in Fig. 5 revealed that pure P25 and R-TiO_2 having size around 25 nm and 122 nm. This large difference in the size distribution of P25 and R-TiO_2 was probably due to the induced growth of crystallite size after high temperature calcination at 800

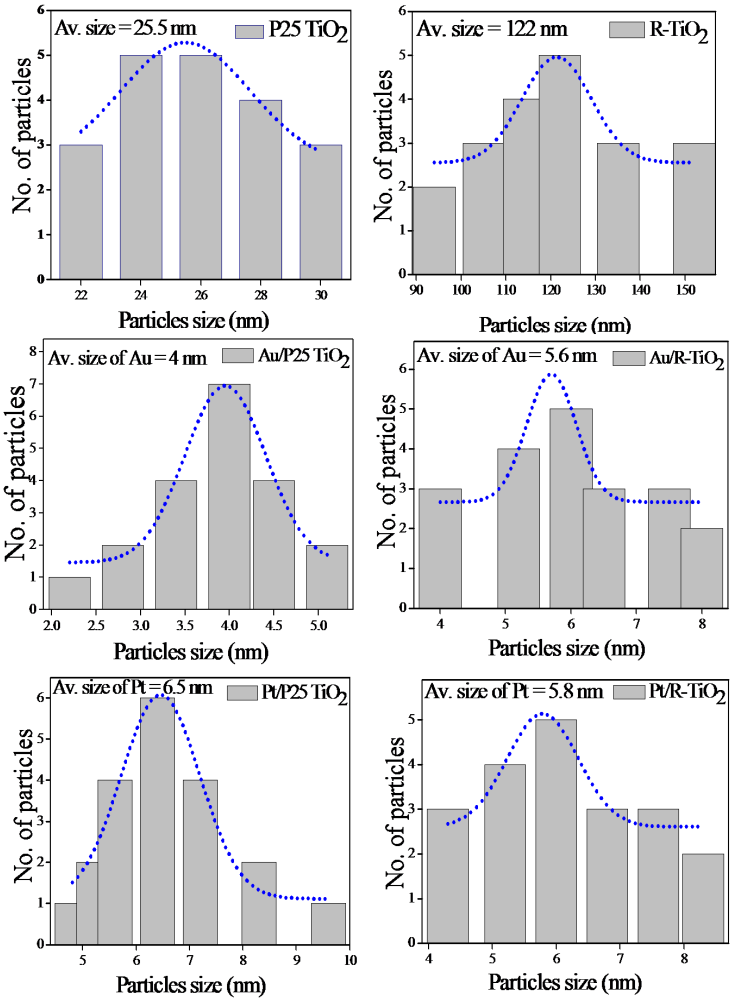

Fig. 6 Size distribution P25, rutile and 1 wt% Au & Pt loaded TiO_2 nanocomposites.

°C. Many smaller Au nanoparticles of average size ~4 nm and ~5 nm were found to be uniformly deposited over P25-TiO_2 and R-TiO_2 surface, respectively, while Pt nanoparticles of size ~6 nm were found to be homogeneously distributed on both the TiO_2 (evaluated by considering 20 particles) follows Gaussian curve fitting (Fig. 6). It can be seen from the XRD pattern (Fig. 7) that the characteristic mixed anatase-rutile P25-TiO_2 and rutile TiO_2 phase has been observed with a good degree of crystallinity. Notably, 1 wt% M loading did not show any characteristic diffraction peak because of their low concentration in the sample.

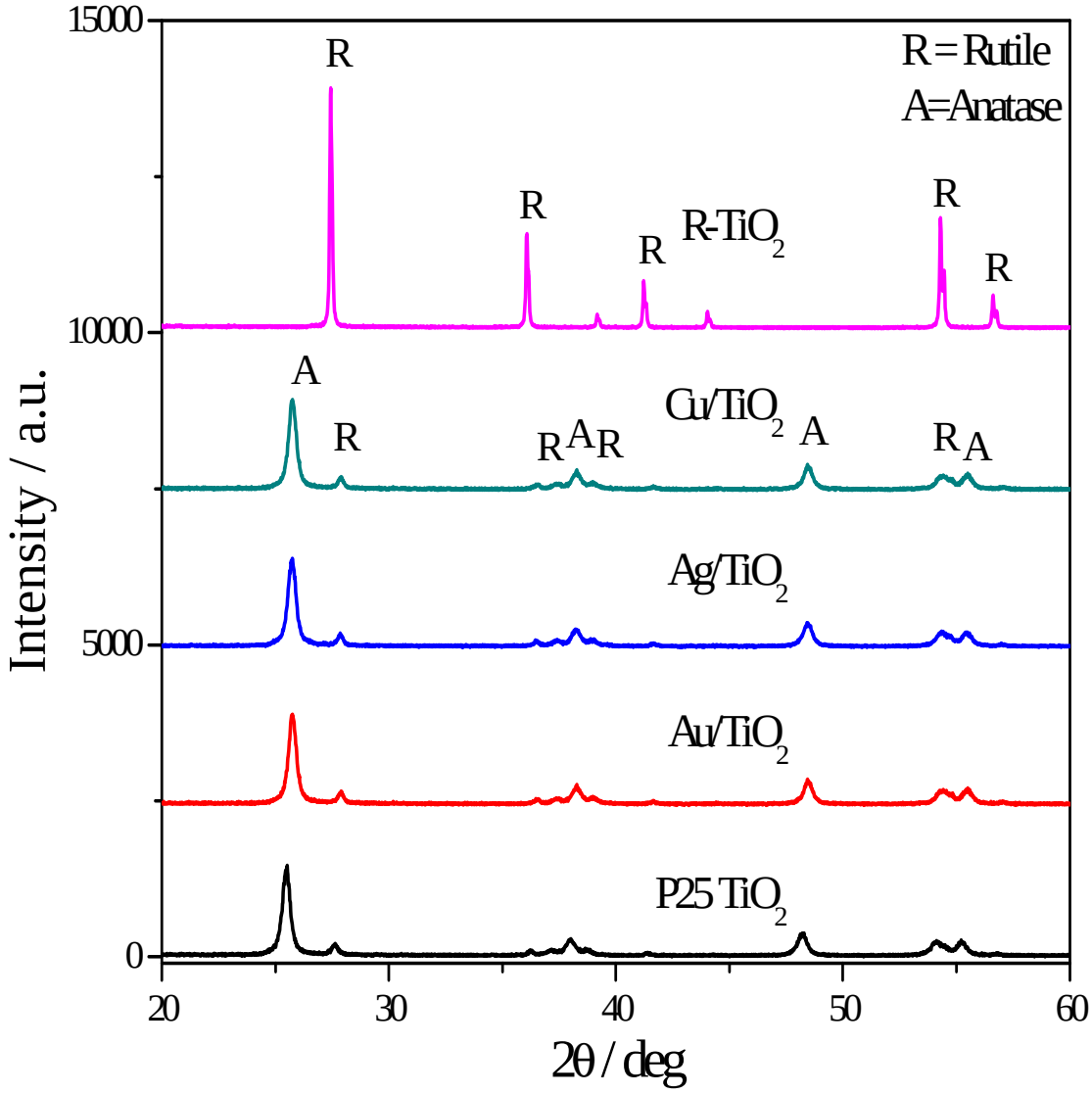

Fig. 7 X-ray diffraction pattern of pure and 1 wt% metal (M = Au, Ag and Cu) deposited TiO_2 nanocomposites.

3.3.2 Photocatalytic study

Fig. 8 shows the reduction of *m*-DNB to *m*-PDA and *m*-NA formation after 4 h UV irradiation and their distribution with 0.2−1 wt% metals (Au, Ag, Pt and Pd) loaded P25-TiO_2 catalysts. It

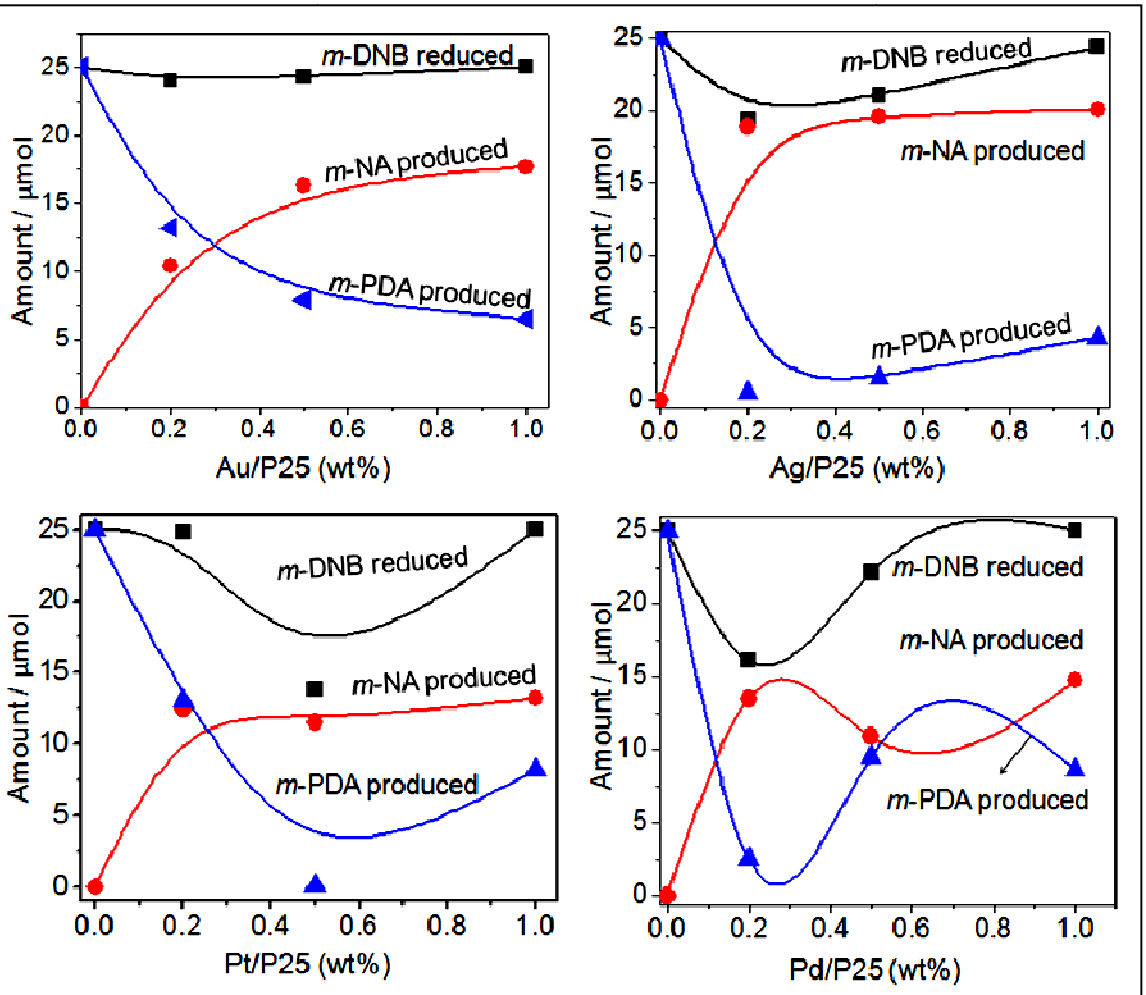

Fig. 8 *m*-DNB photoreduction products with different amount of Au, Ag, Pt and Pd deposited P25-TiO_2 catalysts.

found that always *m*-DNB (25 µmol) is selectively reduced to 100% *m*-PDA by bare P25-TiO_2 and thereby *m*-NA formation started increased upto 80% (20 µmol) with decreasing *m*-PDA yield (5 µmol) with increased amount (0.2-1 wt%) of Au and Ag loading as in Fig. 8. Notably, the same trend is also observed in case of Pt and Pd loaded P25-TiO_2 with relatively low yield (<12 µmol) of *m*-PDA and (59%) *m*-NA (~14.7 µmol) during *m*-DNB photoreduction, evidencing higher co-catalytic activity of Au and Ag than Pt and Pd metal imparted to TiO_2 photocatalysts. The GC-MS patterns are as shown in Fig. 9.

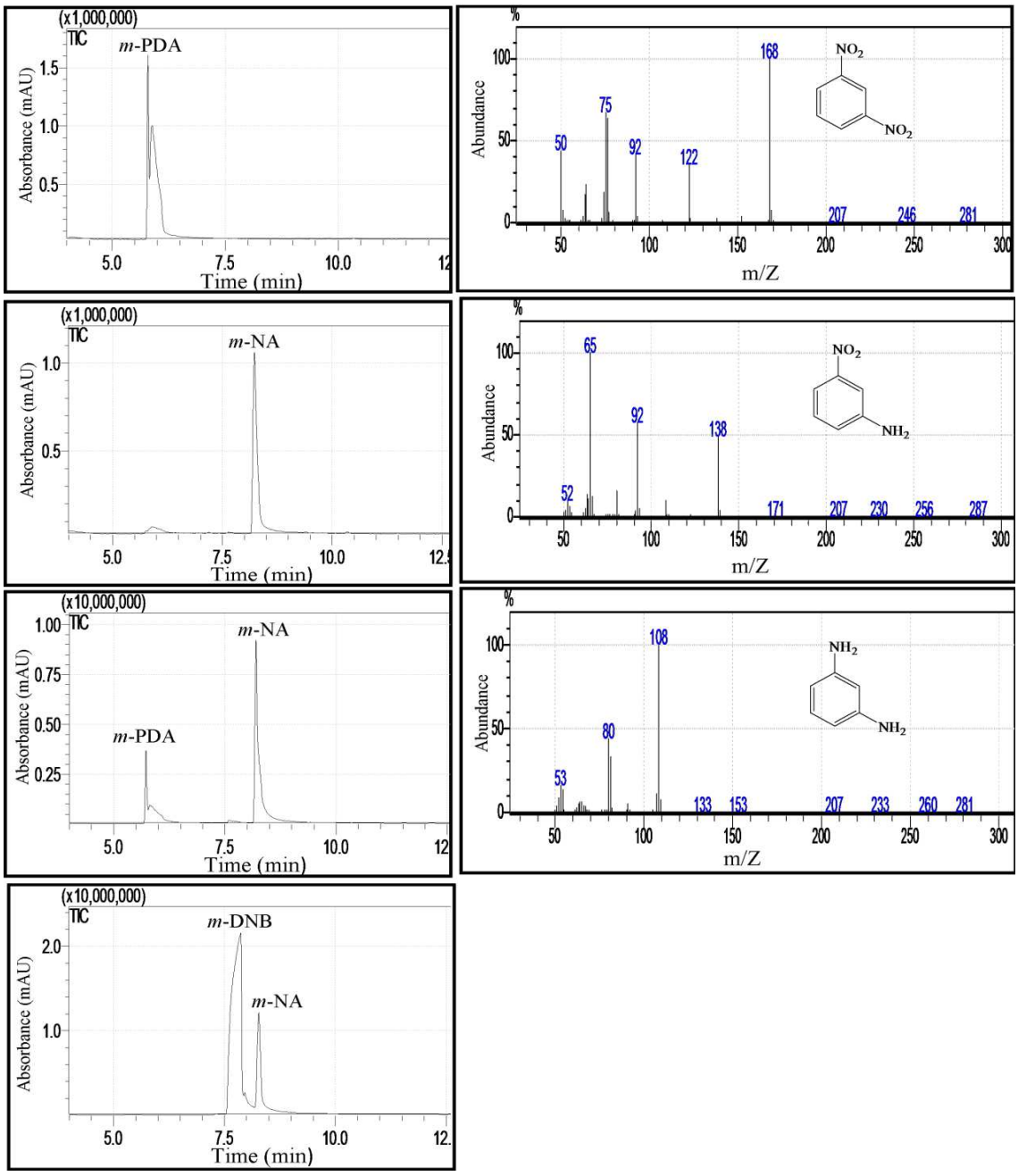

Fig. 9 GC –MS analysis of *m*-DNB photoreduction samples. GC pattern of (a) *m*-PDA produced by P25 in 4 h (b) *m*-NA produced by R-TiO_2 in 8 h (c) Products of 1 wt% Ag/TiO_2 in 4 h (d) *m*-NA produced by 1 wt% Pt/R-TiO_2 in 8 h. MS pattern of (e) *m*-DNB (f) *m*-NA (g) *m*-PDA

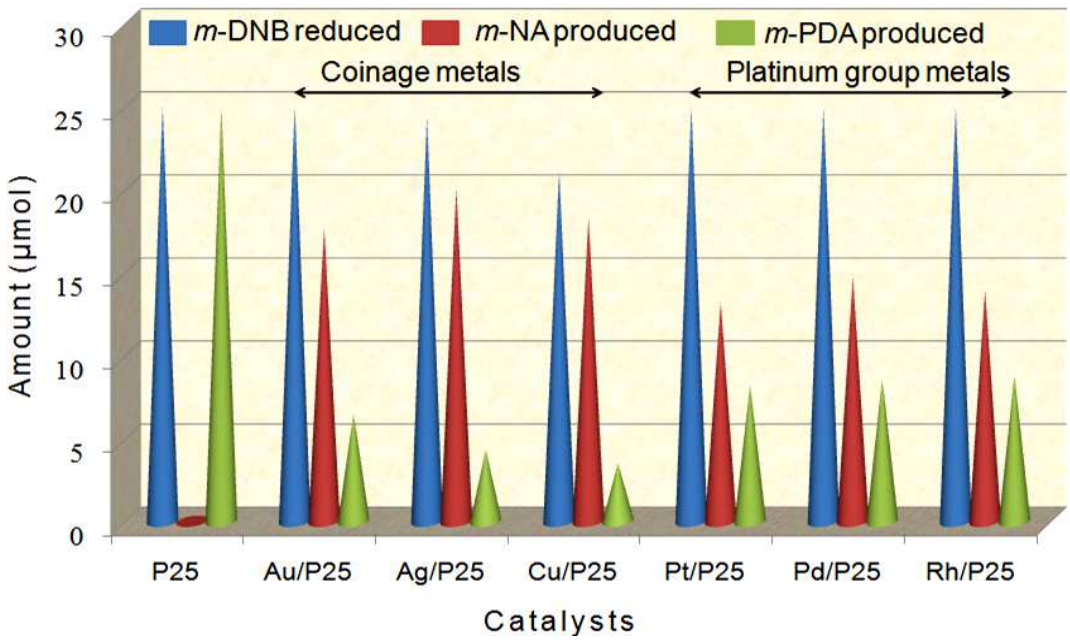

Fig. 10 *m*-DNB reduction by 1 wt% coinage metal and platinum group metals loaded P25-TiO_2 under 4 h UV light irradiation.

Fig. 10 showed comparative products distribution, where *m*-NA selectivity and yield is significantly enhanced by coinage metal loading relative to 100% *m*-PDA yield by bare P25-TiO_2 during 4 h irradiation. Whereas, bare R-TiO_2 always exhibited the highest photoactivity for 100% selective reduction of *m*-DNB to *m*-NA formation, and 1 wt% metals loading significantly reduced the photoreactivity even after 8 h light irradiation as shown in Fig. 11.

The selectivity of the photocatalytic reduction is ascribed [40−42] to the presence of face specific reactive sites on rutile crystals which is predominantly terminated by {110}, {100} and {011} faces, whereas the anatase particles exposed with {001} and {011} faces. It is reported [43, 44] that reduction plane associated with anatase {011} face contains a rich array of defects compared to reduction plane of R-TiO_2 {110}. These defect sites are identified as Ti^{3+} which behave as an active site [20] on the TiO_2 surface and are necessary for adsorption and the conversion of nitro group to amine. Further, the improved crystallinity [45] of R-TiO_2 may also contribute to the product selectivity obtained during the photo reduction photoreduction. It found that surface area (Table 1) 56 m^2g^{-1} of P25 is reduced to 18 m^2g^{-1} for R-TiO_2 due to increased particle size after high temperature treatment and 1 wt% M deposition always decreased the surface area of P25 and R-TiO_2 to 45-35 m^2g^{-1} and 4-8 m^2g^{-1} , respectively, does not seem to have any beneficial

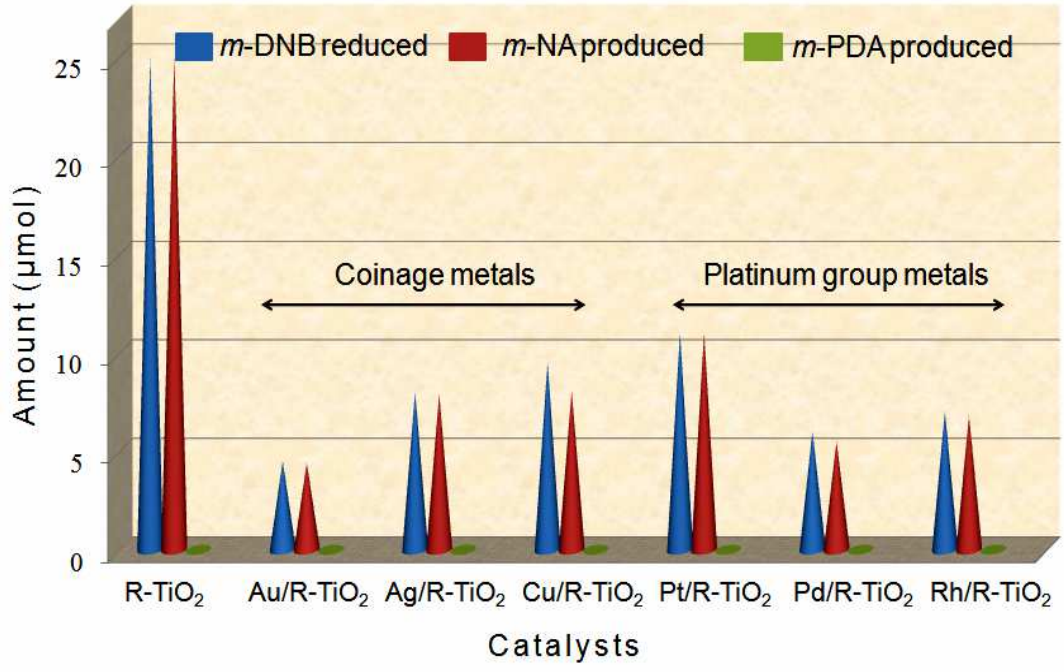

Fig. 11 *m*-DNB reduction by 1 wt% coinage and platinum group loaded R-TiO_2 under R-TiO_2 under 8 h UV light irradiation.

effects to PCA. This decreased surface area of TiO_2 by M loading probably because of the surface coverage [23] of smaller metal nanoparticles on the porous surface of TiO_2.

The fluctuation in the co-catalytic activity of coinage and platinum group metals could be attributed [46, 47] to the differences in the Fermi energy, work function, electron affinity and redox potential etc. which usually facilitate electron accumulation in the metal nanodeposits depending upon the extent of Fermi level equilibration between conduction band electrons of TiO_2 and loaded metals (Scheme 1). It is evident that owing to lower work function 4.2 eV of Pt than 5.5 eV of Au, the conduction band electrons of TiO_2 may be easily transferred to Pt deposits. It is also reported [48] that metals like Pt quickly discharge electrons to the substrate, unlike Au and Ag, which store a fraction of electrons captured from conduction band of TiO_2 and thus exhibiting higher co-

Table 1. Specific surface area of 1 wt% M/TiO_2 nanocomposites.

Sample	Surface area (m^2g^{-1})
P25-TiO_2	56.00
Au/P25	42.00
Ag/P25	35.00
Cu/P25	38.00
Pt/P25	41.00
Pd/P25	45.00
Rh/P25	38.87
R-TiO_2	18.00
Au/R-TiO_2	3.87
Ag/R-TiO_2	5.40
Cu/R-TiO_2	6.70
Pt/R-TiO_2	7.80
Pd/R-TiO_2	4.50
Rh/R-TiO_2	5.50

catalytic activity of 1 wt% Pt/TiO_2 that simultaneously reduced two NO_2 groups of *m*-DNB to selective formation of *m*-PDA relative to one -NO_2 group reduction to *m*-NA formation by 1 wt% Au/TiO_2 after 4 h UV irradiation. Moreover, plasmonic interaction of platinum group metals having characteristics absorption bands in the UV-region could impart crucial effects on the charge transfer kinetics and energetic for superior co-catalytic activity of M-TiO_2 photocatalysis under UV light irradiations.

3.4 Conclusion

In summary, 1 wt% metal loading on P25 and R-TiO_2 does not seem to improve the PCA except the improved selectivity by M/P25 which is opposite to high PCA for oxidation reactions by M/TiO_2 catalysts generally observed. Coinage metals e.g., Ag/P25 exhibit higher selectivity (80%) and yield for *m*-NA formation. Irrespective of the nature of metal loading, the *m*-DNB photoreduction is always notably reduced as compared to the highest photoreactivity of bare R-TiO_2 that produces 100% *m*-NA. This decrease in PCA for the nitro group reduction by all M/TiO_2 could thus be attributed to the decrease in active Ti^{3+} sites available on the surface after metal nanodeposits loading that might also act as a recombination centre for photoexcited charge species.

3.5 References

[1] H. Yuzawa, T. Mori, H. Itoh, H. Yoshida, J. Phys. Chem. C 116 (2012) 4126.

[2] D. Friedmann, C. Mendive, D. Bahnemann, Appl. Catal. B: Environ. 99 (2010) 398.

[3] C.N.R. Rao, A. Govindaraj, Adv. Mater. 21 (2009) 4208.

[4] S. Sarina, H.Y. Zhu, Z.F. Zheng, S.E. Bottle, J. Chang , Chem. Sci. 3 (2012) 2138.

[5] K. Fuku, T. Kamegawa, K. Mori, H. Yamashita, Chem. Asian J. 7 (2012) 1366.

[6] Y. Yang, H. Zhong, C. Tian, Res. Chem. Intermed. 37 (2011) 91.

[7] H. Kawaguchi, T. Wejima, Kagaku Kogaku Ronbun 9 (1983) 107.

[8] H. Kawaguchi, Environ. Technol. Lett. 5 (1984) 471.

[9] V. Augugliaro, L. Palmisano, A. Sclafani, C. Minero, E. Pelizzetti, Toxicol. Environ. Chem. 16 (1988) 89.

[10] M. Addamo, V. Augugliaro, A. Di Paola, E. Garcıa Lopez, V. Loddo, G. Marci, R. Molinari, L. Palmisano, M. Schiavello, J. Phys. Chem. B 108 (2004) 3303.

[11] S. Bakardjieva, J. Šubrt, V. Štengl, M.J. Dianez, M.J. Sayagues, Appl. Catal. B: Environ. 58 (2005) 193.

[12] A. Maldotti, L. Andreotti, A. Molinari, S. Tollari, A. Penoni, S. Cenini, J. Photochem. Photobiol. A: Chem. 133 (2000) 129.

[13] T. Zhang, L. You, Y. Zhang, Dyes Pigm. 68 (2006) 95.

[14] K. Imamura, T. Yoshikawa, K. Nakanishi, K. Hashimoto, H. Kominami, Chem. Comm. 49 (2013) 10911.

[15] H. Huanga, J. Zhoua, H. Liu, Y. Zhou, Y. Fenga, J. Hazard. Mater. 178 (2010) 994.

[16] V. Augugliaro, H. Kisch, V. Loddo, M.J. López-Muñoz, C. Márquez-Alvárez, G. Palmisano, L. Palmisano, F. Parrino, S. Yurdakal, Appl. Catal. A: Gen 349 (2008) 189.

[17] Y. Shiraishi, N. Saito, T. Hirai, J. Am. Chem. Soc. 127 (2005) 12820.

[18] C.J. Li, G.R. Xua, B. Zhang, J.R. Gonga, Appl. Catal. B: Environ. 115 **(**2012) 201.

[19] A. Hakki, R. Dillert, D.W. Bahnemann, Phys. Chem. Chem. Phys. 15 (2013) 2992.

[20] Y. Shiraishi, Y. Togawa, D. Tsukamoto, S. Tanaka, T. Hirai, ACS Catal. 2 (2012) 2475.

[21] S.C. Li, U. Diebold**,** J. Am. Chem. Soc. 132 (2010) 64.

[22] J. Kaur, B. Pal, Cat. Comm. 53 (2014) 25–28.

[23] C.G. Silva, R. Juarez, T. Marino, R. Molinari, H. Garicia, J. Am.Chem. Soc. 133 (2011) 595.

[24] S. Sakthivel, M.V. Shankar, M. Palanichamy, B. Arabindoo, D.W. Bahnemann, V. Murugesan, Water Res. 38 (2004) 3001.

[25] N. Zhang, S. Liu, X. Fu, Y.J. Xu, J. Phys. Chem. C 115 (2011) 9136.

[26] A. Kumar, A.K. Jain, J. Photochem. Photobiol. A: Chem. 1564 (2003) 207.

[27] K. Li, B. Chai, T. Peng, J. Mao, L. Zan, ACS Catal. 3 (2013) 170.

[28] Y. Ma, Q. Xu, X. Zong, D. Wang, G. Wu, X. Wang, C. Li, Energy Environ. Sci. 5 (2012) 6345.

[29] A. Tanaka, S. Sakaguchi, K. Hashimoto, H. Kominami, ACS Catal. 3 (2013) 79.

[30] V. Subramannian, E.E. Wolf, P.V. Kamat, J. Am. Chem. Soc. 126 (2004) 4943.

[31] B. Ohtani, B. Pal, S. Ikeda, Catal. Surv. Asia 7 (2003) 165.

[32] U. Diebold, Surf. Sci. Rep. 48 (2003) 53.

[33] M.I. Litter, Appl. Catal. B: Environ. 23 (1999) 89.

[34] H. Reiche, W.W. Dunn, A.J. Bard, J. Phys. Chem. 83 (1979) 2248.

[35] M.D. Ward, A.J. Bard, J. Phys. Chem. 86 (1982) 3599.

[36] J.G. Yu, H.G Yu, B. Cheng, X.J. Zhao, J.C. Yu, W.K. Ho, J. Phys. Chem. B 107 (2003) 13871.

[37] R. Singh, B. Pal, Mater. Res. Bull. 48 (2013) 1403.

[38] N.D. Abazovic, L. Mirenghi, I.A. Jankovic, N. Bibic, D.V. Sojic, B.F. Abramovic, M.I. Comor, Nanoscale Res. Lett 4 (2009) 518.

[39] S. Mathew, A.K. Prasad, T. Benoy, P.P. Rakesh, M. Hari, T.M. Libish, P. Radhakrishnan, V.P.N. Nampoori, C.P.G. Vallabhan, J. Fluoresc. 22 (2012) 1563.

[40] M.A. Behnajady, N. Modirsha, H.M. Shokri, B. Rad, Global NEST J. 10 (2008) 1.

[41] S. Wendt, R. Schaub, J. Matthiesen, E.K. Vestergaard, E. Wahlstrom, M.D. Rasmussen, P. Thostrup, L.M. Molina, E. Lagsgaard, I. Stensgaard, B. Hammer, F. Besenbacher, Surf. Sci. 598 (2005) 226.

[42] O. Bikondoa, C.L. Pang, R. Ithnin, C.A. Muryn, H. Onishi, G. Thornton, Nat. Mater. 5 (2006) 189.

[43] S. Wendt, J. Matthiesen, R. Schaub, E.K. Vestergaard, E. Lagsgaard, F. Besenbacher, B. Hammer, Phys. Rev. Lett. 96 (2006) 066107.

[44] Z. Zhang, O. Bondarchuk, J.M. White, B.D. Kay, Z. Dohnalek, J. Am. Chem. Soc. 128 (2006) 4198.

[45] S. Yurdakal, G. Palmisano, V. Loddo, V. Augugliaro, L. Palmisano, J. Am. Chem. Soc. 130 (2008) 1568.

[46] P.V. Kamat, Pure Appl. Chem. 74 (2002) 1693.

[47] K.T. Ranjit, T.K. Varadarajan, B. Viswanathan 96 (1996) 181.

[48] H. Choi, W.T. Chen, P.V. Kamat, ACS Nano 6 (2012) 4418.

Chapter 4: Selective formation of benzo[c]cinnoline by photocatalytic reduction of 2,2′-dinitrobiphenyl using TiO_2 and under UV light irradiation

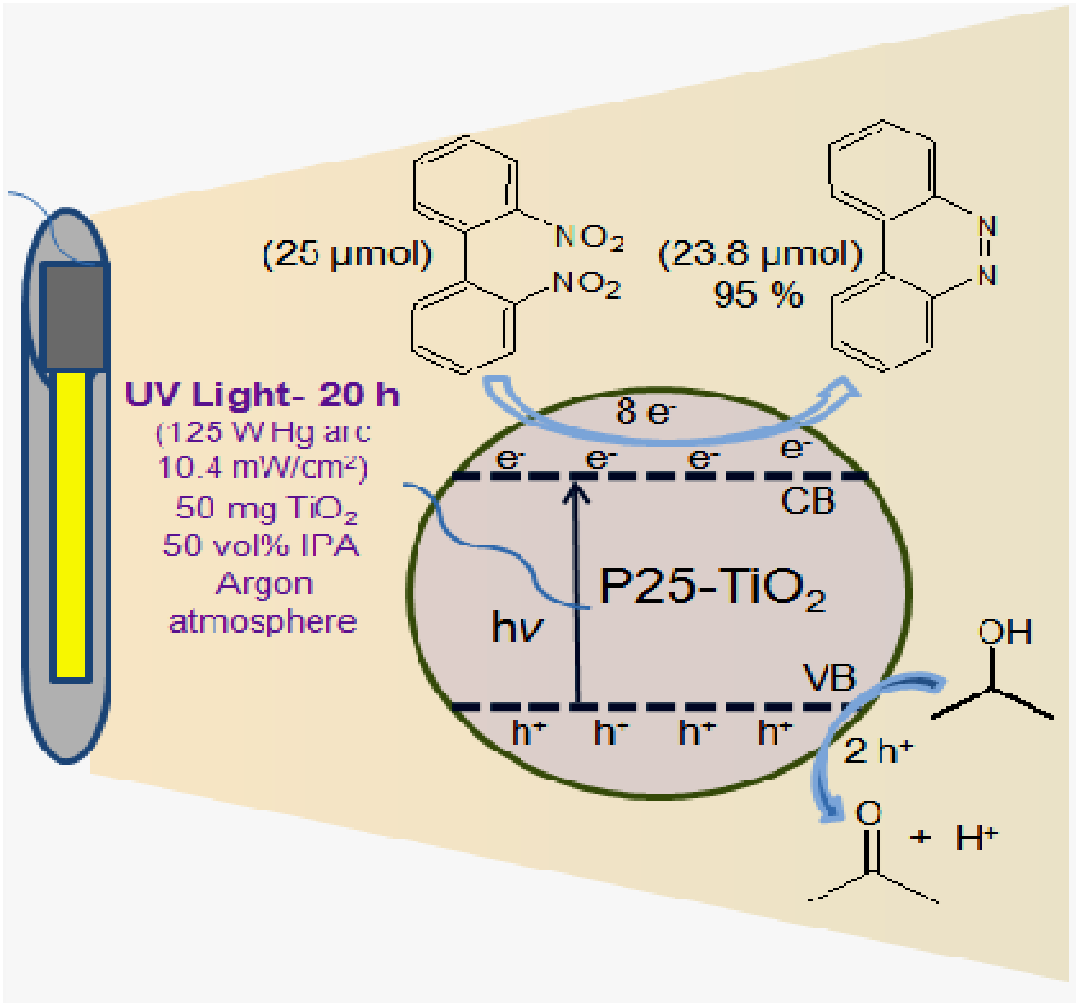

4.1 Introduction

Benzo[c]cinnoline (BC) is a very important organic compound used in manufacturing of dyes, electrochromic polymers, coloured polyamide fibres and it has microbial and herbicidal activities [1-3]. It is typically synthesized by reduction of 2,2′-dinitrobiphenyl (DNBP) [4,5] with Raney Ni [6] and Pd-C [7,8], Zn [9], Fe^{+2} oxalate [10], Fe [11], $LiAlH_4$ [12,13], triethyl phosphate [14], Fe-carbonyl [15], and by electrochemical methods [16]. These conventional methods require harsh conditions such as strong reducing agents, high pressure and temperature, expensive solvents, and leave toxic by-products. Hence, a greener, environmentally benign and mild photocatalytic reaction process by nontoxic TiO_2 catalyst under light irradiation could have beneficial advantages for the highly selective production of BC from DNBP reduction under ambient conditions.

Nitroaromatics reduction by TiO_2 under UV irradiation has been recently reported [17,18] to be feasible due to its higher conduction band energy (− 0.85 V) than the reduction potential −0.5 V *vs*. SCE of $–NO_2$ group [19,20]. Nitrobenzene reduction to aniline and azoxybenzene by photoirradiated CdS, WO_3, ZnO, TiO_2, and SiO_2@Rh–CdS composites [21-25], formation of 4-ethoxy-1,2,3,4-tetrahydroquinoline [26] and cyclic imino acids [27], synthesis of 2-methylpiperazine by (TiO_2 or CdS)–zeolites [28], *etc*. are demonstrated. Photocatalytic reduction of *m*-dinitrobenzene for selective formation of *m*-phenylenediamine (100%) by P25-TiO_2 and *m*-nitroaniline (100%) by rutile TiO_2, and *p*-dinitrobenzene to a mixture of products is reported [29] to be due to the electron withdrawing effect and the position of the $–NO_2$ group in the benzene moiety. However, little information has been known to date about the reduction behaviour of $–NO_2$ groups present in two separate benzene rings of biphenyl compounds.

In this context, this research demonstrated for the first time that photocatalytic reduction of DNBP led to highly selective yield of BC (Scheme 1) along with small amount of other amino derivatives by P25-TiO_2 (Degussa, a mixture of 70% anatase and 30% rutile) under controlled UV light irradiation.

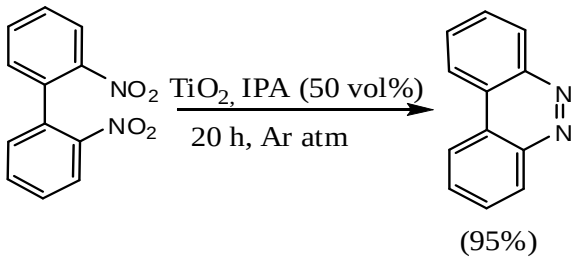

(95%)

Scheme 1. Photocatalytic reduction of DNBP to BC by TiO_2 under UV irradiation.

4.2 Experimental section

4.2.1 Photoreduction reaction

The reduction was carried out in a rubber capped-sealed test tube containing 5 mL aqueous iso-propanol (IPA, 50 vol%), 50 mg P25-TiO_2 (TiO_2) and 25 µmol DNBP suspension under an argon atmosphere with constant magnetic stirring and UV light (125 W Hg arc, 10.4 $mWcm^{-2}$) irradiation for different time periods. The reaction products are quantitatively analysed by HPLC (*section -5.4.2*), GC-MS (*section-5.4.5*) and NMR (*section-5.4.4*) techniques as discussed in chapter 1.

4.3 Results and discussion

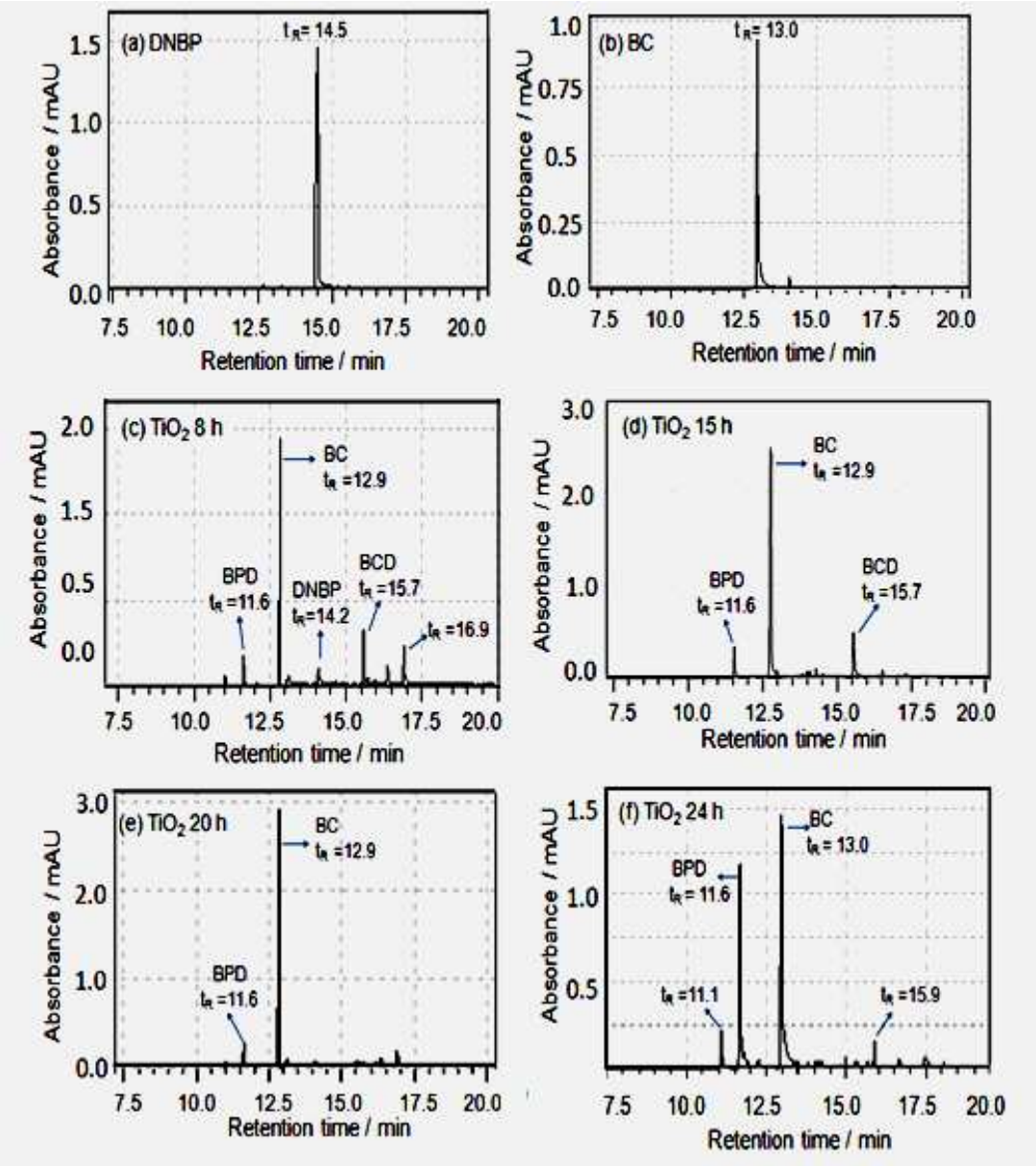

Fig. 1 GC pattern of authentic (a) DNBP (25 µmol) (b) BC (7.5 µmol) and photoreduction products of DNBP (25 µmol) by TiO_2 after (c) 8 h (d) 15 h (e) 20 h (f) 24 h UV irradiation.

Fig. 1a and b showed the GC chromatographs of the authentic sample showing a single peak of DNBP (25 µmol) at t_R = 14.5 min and BC (7.5 µmol) at t_R = 13 min. Fig. 1c reveals that after DNBP reduction by TiO_2 during 8 h irradiation, a number of GC peaks at t_R = 11.6, 12.9, 15.7 and 16.9 min including few smaller peaks evolved due to the formation of various reduction products. The peak height at t_R = 14.2 min for DNBP is decreased due to its complete reduction, and with the passage of 15-24 h irradiation (Fig. 1d-f), the intensity of all the peaks is reduced except a smaller peak at t_R = 11.6 min, and a major peak at t_R = 12.9-13.0 min is found to be significantly enhanced (Fig. 1e) after DNBP reduction for 20 h irradiation. The peak at t_R = 15.7 min is not observed after 15 h, whereas the peak intensity at t_R = 11.6 min is seen to be almost same upto 20 h and beyond that it is notably increased with simultaneous decrease in the peak

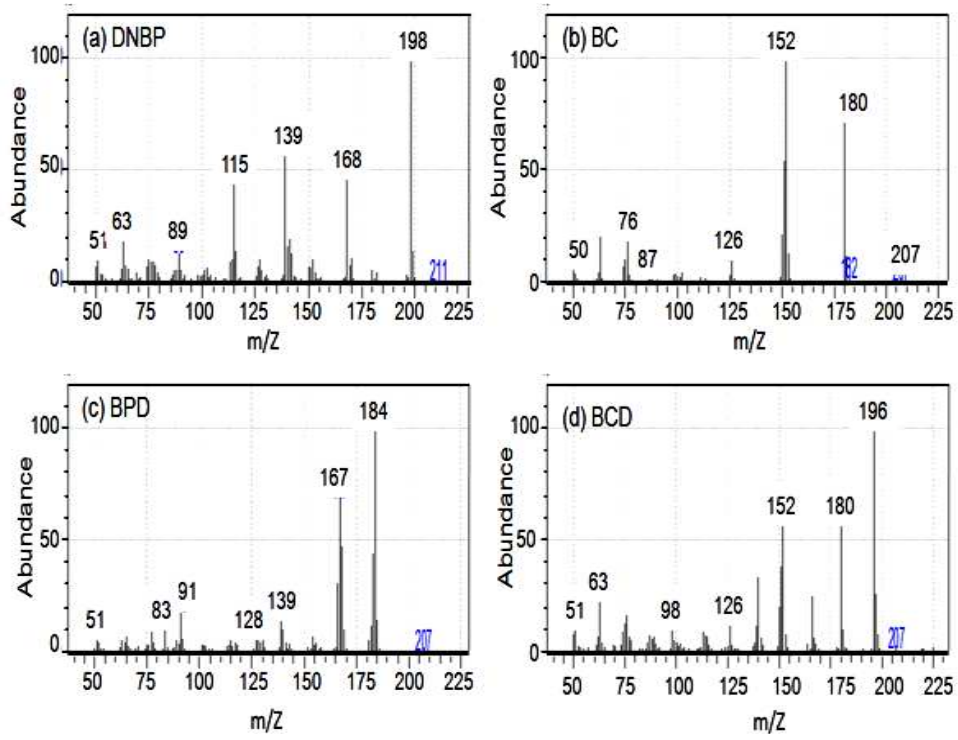

Fig. 2 Mass spectral analysis of DNBP and its reduction products.

height at t_R = 12.9 min after 20-24 h UV light irradiation.

The mass spectrum analysis of authentic DNBP (Fig. 2a) and its reduction products, confirmed the formation of BC (Fig. 2b) at t_R = 12.9 min, biphenyldiamine(BPD, Fig. 2c) at t_R = 11.6 min, and benzo[c]cinnoline dioxide (BCD, Fig. 2d) at t_R = 15.7 min, during DNBP reduction by TiO_2

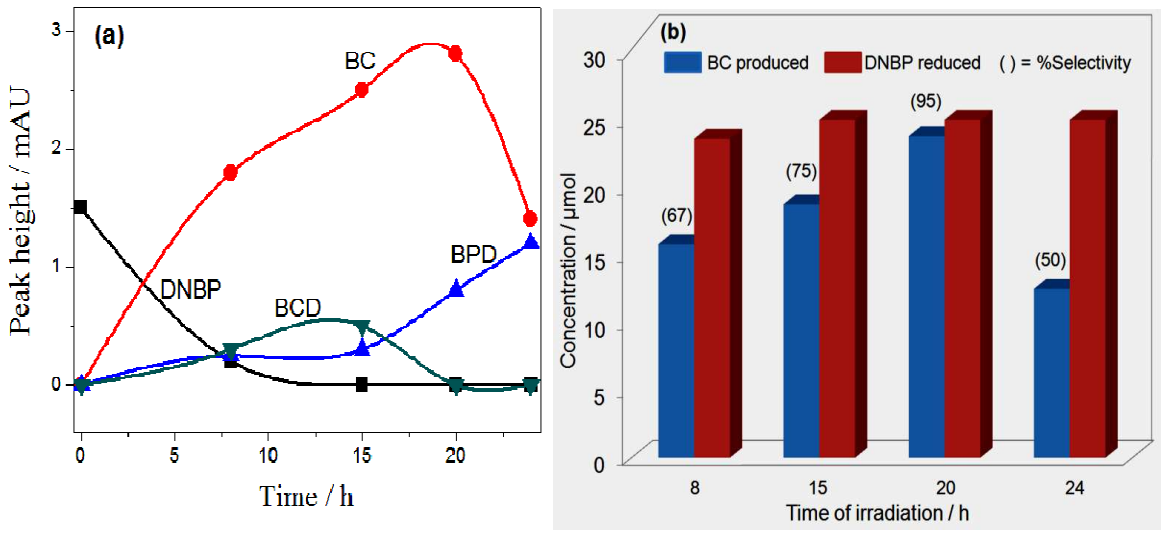

Fig. 3 (a) Time course graph (peak height variation) of different products of DNBP reduction and (b) BC yield and selectivity as a function of UV irradiation time.

for different time periods. Fig. 3a shows the variation in the peak heights of three major reduction products BCD, BC and BPD with decreased DNBP concentration and increased UV irradiation time.

It is found that DNBP almost selectively reduced to BC along with the formation of a BPD after 20 h. It further revealed that BCD is formed upto 15 h irradiation, whereas BPD is increased with a decrease in the amount of BC formed beyond 20-24 h reduction. By comparing 7.5 µmol commercial authentic BC samples, the yield and selectivity of BC obtained by DNBP (25 µmol) reduction using TiO_2 under UV irradiation for 8-24 h gradually increased from 67% to a maximum of 23.8 µmol (95%) of BC during 20 h and thereby, remarkably decreased beyond 20-24 h irradiation due to its self-reduction to BPD. HPLC

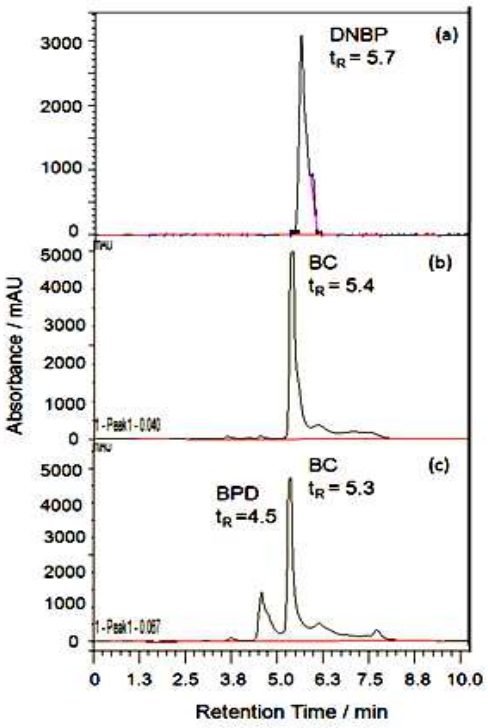

Fig. 4 HPLC Chromatograms of (a) DNBP authentic (25 µmol) (b) BC authentic (25 µmol) (c) reduction products of DNBP (25 µmol) with TiO_2 by 20 h light irradiation produced 23.7 µmol BC.

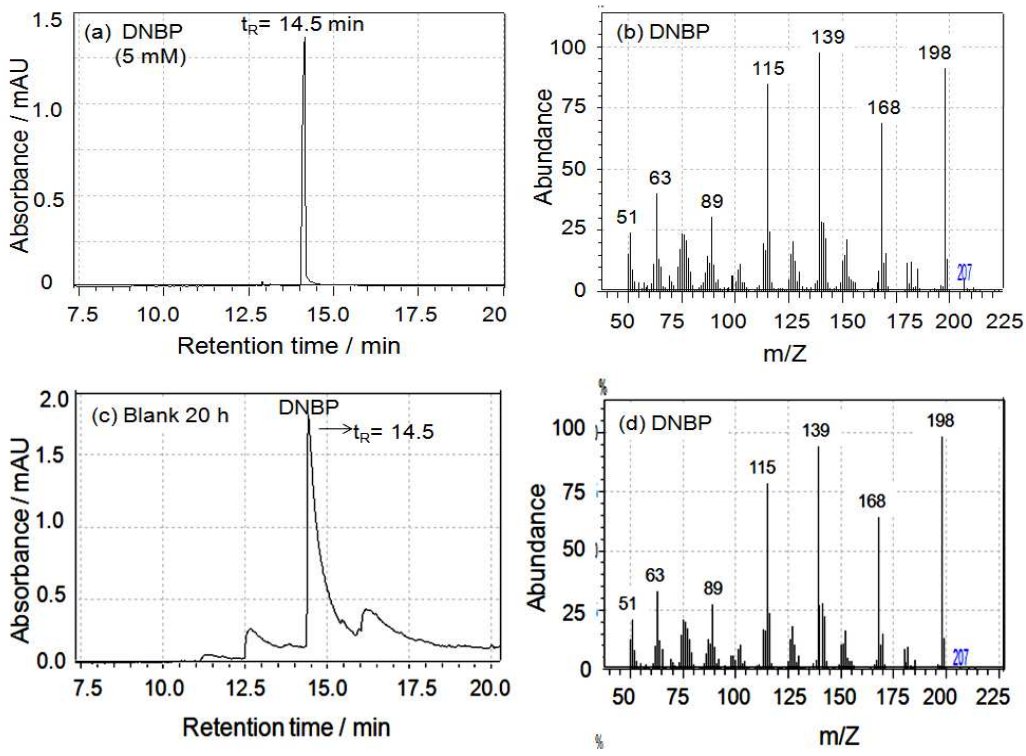

Fig. 5 GC pattern of authentic DNBP (5 mM = 25 µmol) (b) its mass spectra (c) blank reaction after 20 h of UV irradiation and (d) its mass spectra showing mass of DNBP corresponding to peak at t_R = 14.5 min .

analysis (Fig. 4) also revealed the formation of ~23.7 µmol of BC. In a blank test, no such reduction of DNBP occurred without the TiO_2 catalyst after 20 h of UV light irradiation (Fig. 5), thus confirming the photocatalytic nature of DNBP reduction reaction. The reproducibility was further judged by another set of experiments carried out under similar conditions, which produced ~23.2 µmol of BC relative to 23.8 µmol in the first run.

The ^{1}H-NMR (400 MHz, $CDCl_3$) spectral analysis (Fig. 6) shows the peaks observed for: DNBP authentic at d 8.20 (d, 2H, *J* = 8.24 Hz, ArH), 7.70 (t, 2H, *J* = 7.32 Hz, ArH), 7.60 (t, 2H, *J* = 8.24 Hz, ArH), 7.30 (dd, 2H, *J* = 7.76 Hz, ArH); BC authentic (Fig. 6b) at d 8.76–8.74 (m, 2H, ArH), 8.59–8.57 (m, 2H, ArH), 7.94–7.89 (m, 4H, ArH). BC formed by DNBP photoreduction shows NMR (Fig. 6c) peaks at d 8.77–8.74 (m, 2H, ArH), 8.61–8.59 (m, 2H, ArH), and 7.94–7.91 (m, 4H, ArH) that almost closely match (except for some small peaks of other unidentified products) with the characteristic NMR spectra of the authentic BC sample. BPD produced after 24 h irradiation showed peaks at δ 7.54-7.50 (m, 4H, ArH), 7.30 (t, 2H, J =

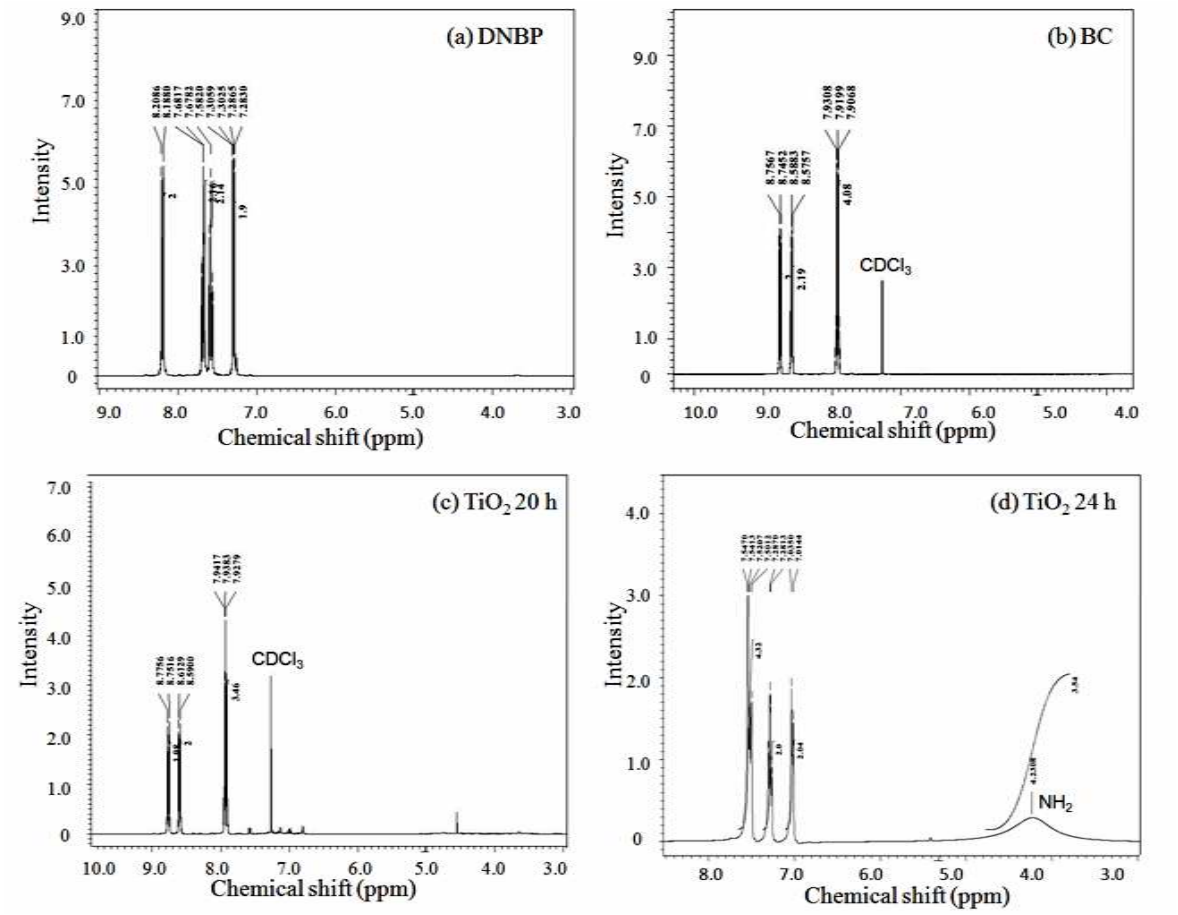

Fig. 6. NMR spectra of authentic (a) DNBP (b) BC and DNBP reduction product by TiO_2 after (c) 20 h and (d) 24 h UV irradiation.

7.8 Hz, ArH) and 7.23 (d, 2H, J = 8.24 Hz, ArH) and a typical broad peak for NH_2 protons at 4.23 (bs, 4H, NH_2) is also seen in Fig. 6d which are quite different from the NMR spectra of DNBP and BC. On the basis of obtained detected reduction products, it is revealed that the rate determining step for DNBP photocatalytic reduction using TiO_2 is the selective formation of BC *via* some transient intermediates; nitroso and hydroxylamine derivatives BCD, azoxy compounds and few unidentified products by following reaction pathways in **scheme 2**. It is reported [30,25] that this intermediate sequence RNO_2-RNO-RNHOH-RNH_2 is generally formed during many nitroaromatics photoreduction. GC chromatographs (Fig. 1) also further support that these short lived products (e.g., BCD) disappeared with increasing irradiation time. BPD production took place to a lesser extent *via* direct reduction of the hydroxylamine derivative (path-I) during initial hours (8-20 h), and beyond that more amount of BPD (path-II) is formed probably due to

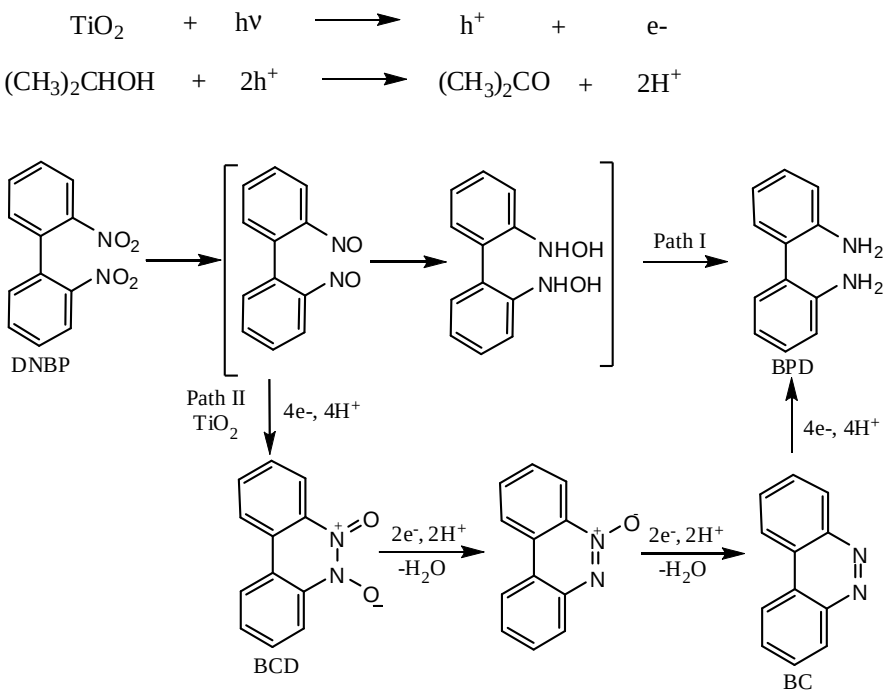

Scheme 2. Possible reaction pathways of DNBP reduction by TiO_2 and UV light irradiation.

self-reduction of as-produced BC during 8-20 h irradiation. The photoexposure of TiO_2 (band gap energy = 380-390 nm) with UV light generates electrons in the conduction band and holes in the valence band, where two NO_2 groups of DNBP are sequentially reduced to NH_2 groups in BPD by $12e^-$, and complete reduction of DNBP by irradiated TiO_2 required $8e^-$ for the BC

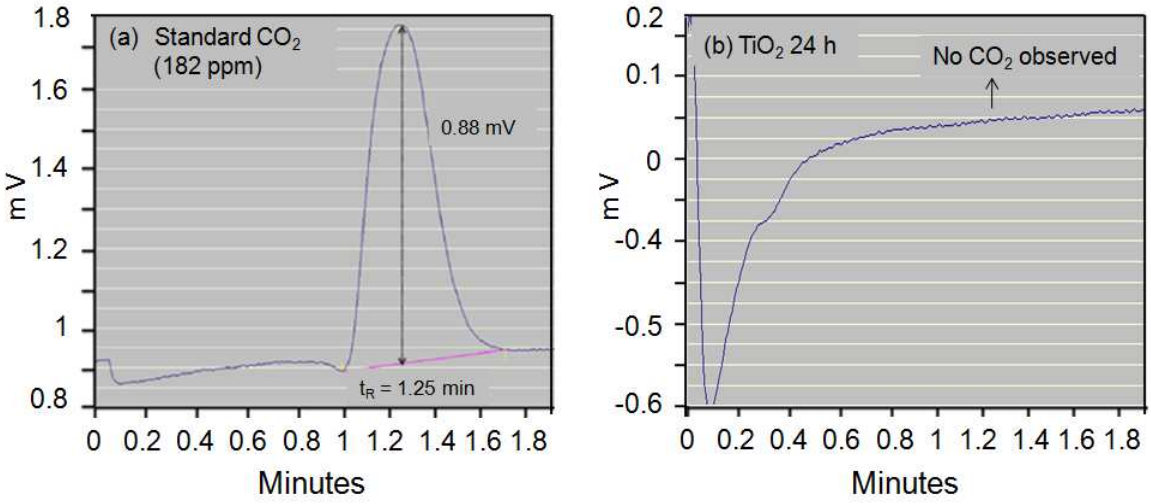

Fig. 7 GC chromatographs of (a) Standard CO_2 of 180 ppm (b) DNBP reaction with TiO_2 after 24 h of UV light irradiation (no peak for CO_2 at 1.25 min).

formation through various intermediate reduction steps. Furthermore, over oxidation of acetone into CO_2 was not observed as confirmed by GC analysis (Fig. 7). It is also observed that the reduction process is accompanied by the simultaneous oxidation of iso-propanol (hole scavenger) to acetone (t_R = 1.2 min) whose amount (Fig. 8) increased with (20 to 24 h) irradiation time, and no H_2 production is detected by photoexcited holes (h^+) in the valence band under UV irradiation.

The phoreduction reaction of DNBP with pure rutile TiO_2 nanoparticles was also performed under UV light irradiation upto 24 h, under similar experimental conditions. The HPLC and GC data showed no change in the DNBP peak height and not formation of any other product. Hence, DNBP was not reduced with pure rutile TiO_2 nanoparticles.This could be attributed due to slow photoactivity of rutile TiO_2 nanoparticles under UV light irradiation. Also, it is reported in literature that higher surface area may also play a major role in adsorption of reactants resulting in higher photocatalytic activity.

The rutile samples in the present study, exhibit lower surface area of 18 m^2g^{-1} as compare to P25-TiO_2 nanoparticles which posses a higher surface area of 56 m^2g^{-1} and the reactions were performed under UV light irradiation.

Thus, it is evident that DNBP undergoes intramolecular reductive cyclization reactions by TiO_2 because of the close spatial proximity [5] of the interacting NO_2 groups that lie in two different benzene rings separately relative to their location in the same benzene moiety in various dintirobenzenes. Such redox combined photocatalytic reactions like selective photoreduction of o-dinitrobenzene to

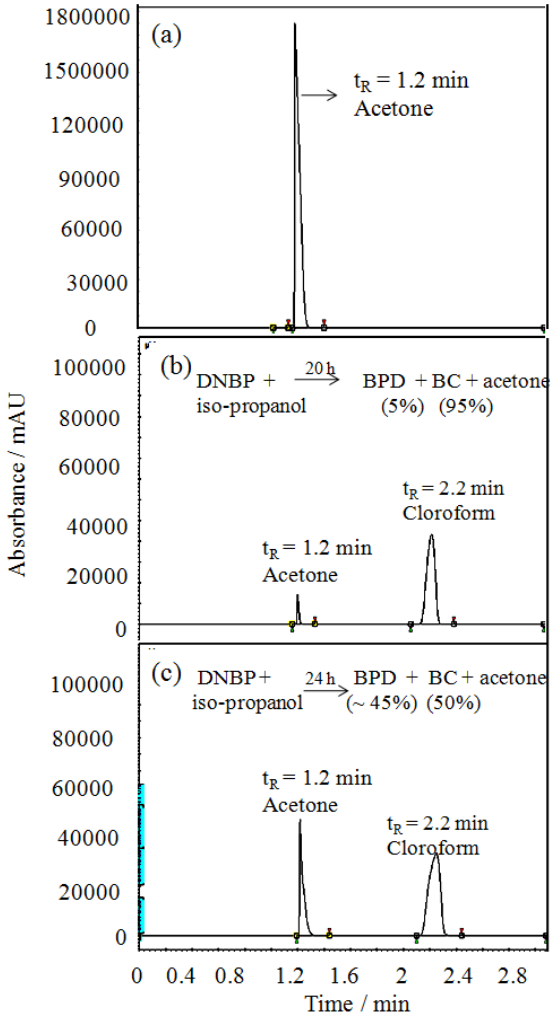

Fig. 8 GC pattern of (a) authentic acetone sample (b) acetone produced by the photoreduction of DNBP (25 µmol) by TiO_2 during 20 h and (c) 24 h UV irradiation.

benzimidazole (96%) by TiO_2 [31], and formation of pipecolinic acid [32] from L-lysine irradiation are reported to be highly efficient for practical applications. Depending on the position (1:2, 1:3 and 1:4) of -NO_2 functionality [29,31] and the extent of the electron withdrawing effect of -NO_2 groups imparted to benzene ring, dinitrobenzene is reduced to a variety of reduction products by both P25-TiO_2 and rutile TiO_2 under controlled UV irradiation. However, the pure rutile TiO_2 nanoparticles of size nm does not have any photoreactivity for DNBP reduction upto 24 h under experimental conditions.

4.4 Conclusion

The non-conventional production of BC from DNBP reduction by TiO_2 and UV light where the yield and selectivity could be simply tuned by light irradiation under ambient conditions without using any costly toxic solvent and reducing agents is experimented for the first time using inexpensive and non-toxic titania catalyst. This photoreduction process could be extended to synthesis of other N-heterocyclic compounds, which requires harsh experimental conditions in conventional techniques.

We are grateful to Prof. Ashok Kumar Malik, Punjabi University, Patiala, India for GC-MS analysis.

4.5 References

[1] E. Killic, S. Aktan, Commun. Fac. Sci. Uni. Ank. Series B 47 (2001) 37.

[2] N. Minagawa, K. Kaneko, S. Sajo, A. Yoshimoto, Biosci. Biotechnol. Biochem**.** 5**7** (1993) 1577.

[3] T. Eicher, S. Hauptmann, The Chemistry of Heterocycles, Wiley-VCH, Weinheim, 2003.

[4] J.W. Barton, J.W. Barton, in Advances in Heterocyclic Chemistry, ed. A.R. Katritzky and A.J. Boulton, Academic Press,NewYork, 1979, vol. 24, pp. 151–185.

[5] R.E. Buntrock, E.C. Taylor, Chem. Rev. 68 (1968) 209.

[6] J.L. Everett, W.C.J. Ross, J. Chem. Soc**.** (1949) 1972.

[7] A. Etienne, G. Izoret, Bull. Socc. **C**him. Fr. (1964) 2897.

[8] H. Stetter, A.I. Schwarz, Chem. Ber. 90 (1957) 1349.

[9] J. Radell, L. Spialter, J. Hollander, J. Org. Chem. 21 (1956) 1051.

[10] D.V. Banthorpe, E.D. Hughes, C. Ingold, J. Chem Soc. 2 (1962) 386.
[11] P.Z. Slack, R. Slack, Nature 160 (1947) 437.
[12] J.F. Corbett, P.F. Holt, J. Chem. Soc**.** 3 (1960) 646.
[13] A. Etienne, R. Piat, Bull. Socc**. C**him. Fr. (1962) 292.
[14] J.I.G. Cadogan, M. Cameron-Wood, R.K. Mackie, R.J.G. Searle, J. Chem. Soc. 4 (1965) 831.
[15] J.E. Kmiecik, J. Org. Chem. 30 (1965) 2014.
[16] T. Wohlfahrt, J. Prakt. Chem. 65 (1902) 295.
[17] Y. Shiraishi, Y. Togawa, D. Tsukamoto, S. Tanaka, T. Hirai, ACS Catal. 2 (2012) 2475.
[18] Y. Shiraishi, H. Hirakawa, Y. Togawa, Y. Sugano, S. Ichikawa, T. Hirai, ACS Catal. 3 (2013) 2318.
[19] M.A. Fox, Nouv. J. Chim. 11 (1987) 129.
[20] J.A. Dean, Handbook of Organic Chemistry, New York, 1987.
[21] R.J. Tayade, R.G. Kulkarni, R.V. Jasra, Ind. Eng. Chem. Res. 45 (2006) 922.
[22] H. Wang, J. Yan, W. Chang, Z. Zhang, Catal. Comm. 10 (2009) 989.
[23] R.J. Tayade, D.L. Key, Mater. Sci. Forum, 657 (2010) 62.
[24] Y. Li, L. Wang, Nanocrystalline Semiconductor Materials, Elsevier, New York, 1996.
[25] B. Pal, T. Torimoto, K. Okazak, B. Ohtani, Chem. Comm. 5 (2007) 483.
[26] K.H. Park, H.S. Joo, K.I. Ahn, K. Jun, Tetrahedron Lett. 36 (1995) 5943.
[27] B. Ohtani, S. Tsuru, S. Nishimoto, T. Kagiya, K. Izawa, J. Org. Chem. 55 (1990) 5551.
[28] V. Kambala, S. Rao, M. Subrahmanyam, Photochem. Photobiol. Sci. 1 (2002) 597.
[29] J. Kaur, B. Pal, Cat. Com., 53 (2014) 25.
[30] R.E. Moore, A. Furst, J. Org. Chem. 23 (1958) 1504.
[31] H. Wang, R.E. Partch, Y. Li, J. Org. Chem. 62 (1997) 5222.
[32] B. Pal, S. Ikeda, H. Kominami, Y. Kera, B. Ohtani, J. Catal. 217 (2003) 152.

Chapter 5: Crystal phase and shape dependent photoactivity of titania for nitroaromatics reduction under UV light irradiation

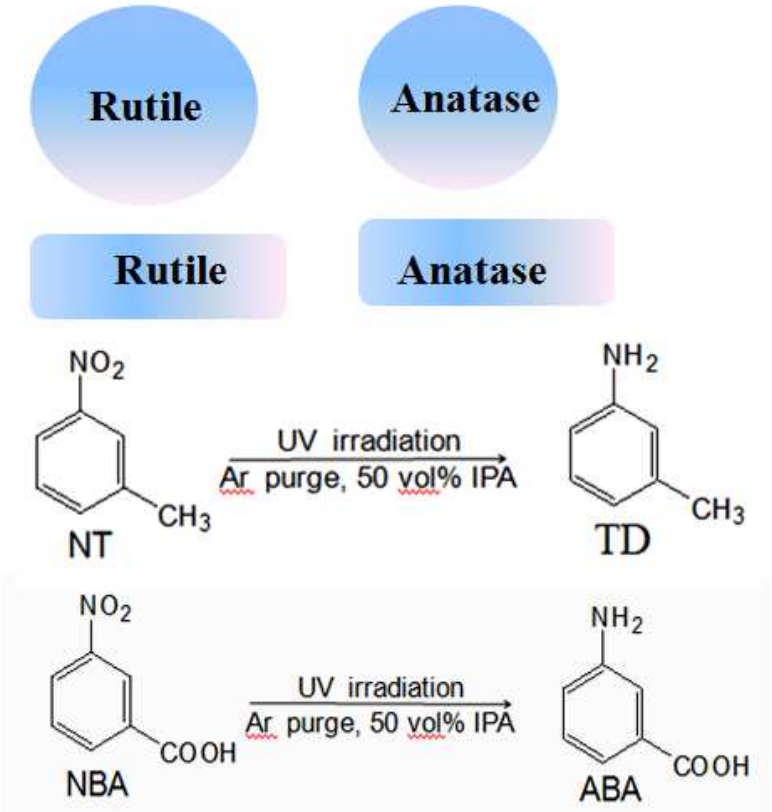

5.1 Introduction

Titanium dioxide (TiO_2) semiconductor, nowadays is used for greener synthesis of aminoaromatics by one step reduction [1-4] of nitroaromatics. The production of aminoaromatics from nitroaromatics is of great interest because aminoaromatics are important intermediates for the synthesis [5-8] of dyes, antioxidants, herbicides, polymers, pharmaceuticals and other fine chemicals. These can be prepared easily by the reduction of nitroaromatics using catalytic hydrogenation, zinc, tin, iron, Au/SiO_2, Au/Al_2O_3, Pd/TiO_2, Pt-Ne bimetallic nanoparticles [9-16] and $Pt\text{-}TiO_2$ a variety of other reduction conditions. The draw backs of all these methods include the requirement of toxic solvents, strong reducing agents like $NaBH_4$, expensive metals like Au/Pt, reactions at high pressure and temperature and generation of toxic byproducts. Whereas the use of titania for the photoreduction of nitroaromatics is highly advantageous over all these methods because it is a cheap, non-toxic, generates no harmful byproduct and require room temperature and pressure conditions. Also, conduction band energy of TiO_2 is −0.85 V in comparison to −0.5 V vs SCE of the $–NO_2$ group, so NO_2 is preferably reduced [17-21] over aceto, cyano, and aldehyde functionality present in the same compound.

It is reported that anatase TiO_2 usually shows much higher photocatalytic activity than rutile TiO_2. However, some recent reports show the improved selectivity of rutile TiO_2 nanoparticles [22-25] for selective oxidation of aromatic alcohols to aldehydes, photoreduction of nitroaromatics to aminoaromatics such as *m*-nitrotoluene photoreduction to *m*-aminotoluene. Further, it is reported [26] that rutile nanoparticles show 100% yield and selectivity of *m*-dinitrobenzene photoreduction to *m*- nitroaniline. Also, metal (coinage and platinum group) loading also improves the selectivity of $P25\text{-}TiO_2$ for the photoreduction of *m*-dinitrobenzene [27] while metal loading does not shows significant improvement in rutile TiO_2 nanoparticles photoactivity.

Further, the photocatalytic activity of anatase and rutile nanoparticles can also be improved by changing their morphology [28-31] from spherical to rod. The advantages of one-dimensional nanorods over nanospheres as photocatalyst are that the one-dimensional geometry facilitates fast and long distance electron transport, exhibit higher specific surface area, light absorption increases because of the larger length-to-diameter ratio. The improved photoactivity of rutile nanorods [32] has been observed for Rhodamine B degradation (low temp) and gas-phase decomposition of acetaldehyde. Herein, we investigated the potential application of anatase and

rutile titania nanorods and nanospheres for the improved photoreduction of nitroaromatics such as *m*-nitrobenzoic acid (*m*-NBA) and *m*- nitrotoluene (*m*-NT).

5.2 Experimental section

5.2.1 Synthesis of titania nanostructures of different crystal phase, size and shape

ANR were synthesized by a hydrothermal method as reported elsewhere [33] and briefly described in *section 5.2.4* of chapter 1. ANP were synthesized by sol-gel [34] method as mentioned in *section 5.2.5* of chapter 1. RNP were synthesized by the calcination of commercially available Degussa P25 TiO_2 powder at 800 ˚C in a muffle furnace for 2 h. RNR were synthesized through a seed-mediated growth process [35] as discussed in *section 5.2.3* of chapter 1.

5.2.2 Characterization techniques

As synthesized TiO_2 samples were characterized by DRS *(section-5.3.1),* XRD *(section-5.3.2)* BET *(section-5.3.3),* PL *(section-5.3.4),* TEM *(section-5.3.5),* TCSPC *(section-5.3.6)* as discussed in chapter 1.

5.2.3 Photocatalytic activity for nitroaromatics reduction

Photoreduction of *m*-NBA (25 µmol) and *m*-NT was carried out with as prepared TiO_2 samples as per procedure given in *section-5.4.1* (chapter 1). Reaction samples were analyzed by HPLC *(section-5.4.2)* techniques as given in chapter 1.

5.3 Results and discussion

5.3.1 Structural analysis

Crystalline phase of P25 TiO_2 and as prepared samples was analyzed by using XRD and are shown in Fig. 1. XRD profile of RNP shows highly intense peaks of rutile titania whereas RNR exhibited comparatively less intense peaks of rutile phase at 2θ = 27.5°, 36.5°, 41°, 54.1° and 56.5° and are assigned to the (110), (101), (200), (111), (210), (211) and (220) planes (JCPDS no. # 21-1276). However, ANP and ANR exhibited diffraction peaks at 2θ = 25.4°, 37.9°, 47.9°, 53.9° and 54.9° are assigned to (101), (004), (200), (105) and (211) planes (JCPDS no. # 21-1272) of anatase phase. BET surface area analysis exposed that surface of P25 is 45 m^2g^{-1} while that of ANP and ANR exihibited increased surface area of 89 m^2g^{-1} and 71 m^2g^{-1}, respectively. The surface area of RNP is 18 m^2g^{-1} while it increases to 69 m^2g^{-1} for RNR.

5.3.2. Morphological analysis

Morphology of the prepared samples was investigated through TEM analysis. TEM image of P25-TiO_2 exhibited spherical nanoparticles of average size 25-30 nm, RNP also exhibited spherical particles with the size of 120-130 nm while RNR exhibited rod like morphology with the size range (L×W = 28-30 nm × 3.5-3.8 nm) as shown in Fig. 2. TEM micrographs of ANP shows spherical nanoparticles of average size 8-10 nm and ANR shows the formation of rice like nanorods with size (L×W = 80-132 nm × 8-13 nm).

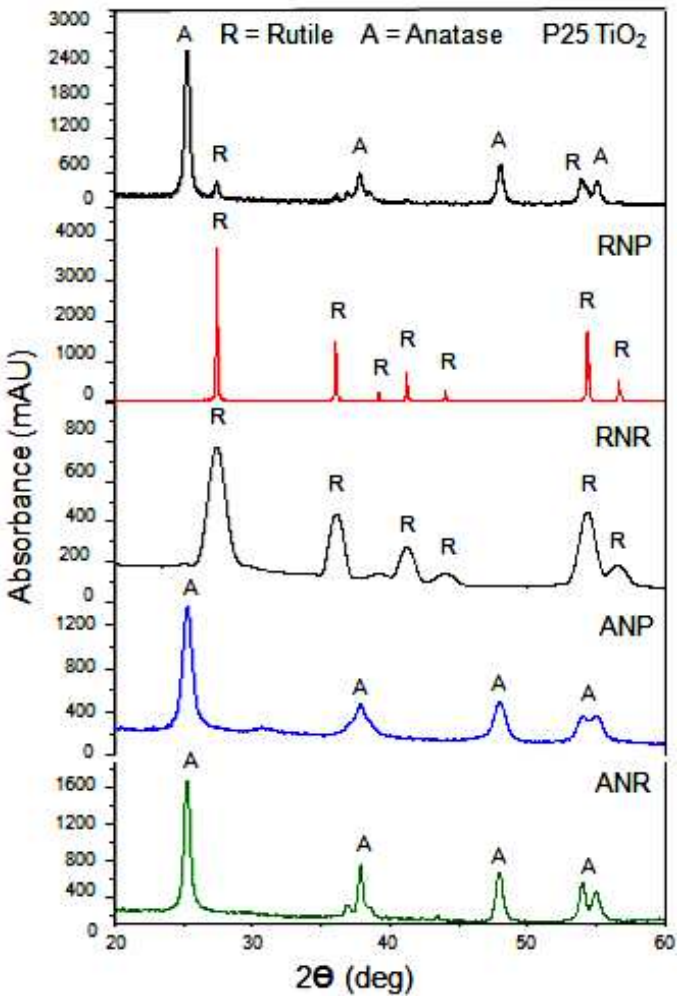

Fig. 1 XRD patterns of as prepared titania nanoparticles of different morphology.

5.3.3 Optical properties

Optical properties of as prepared TiO_2 samples were studied by recording UV-vis absorption spectra and emission spectra. In Fig. 3 absorption onset of P25-TiO_2 appears at 386 nm, whereas the absorption onset for ANP and ANR is blue shifted to 380 and 384 nm respectively. However, the absorption onset of RNP occurs at 413 nm which is further red shifted to 418 nm in RNR. Further, the band gap values of all these samples were calculated from Tauc plot using the equation

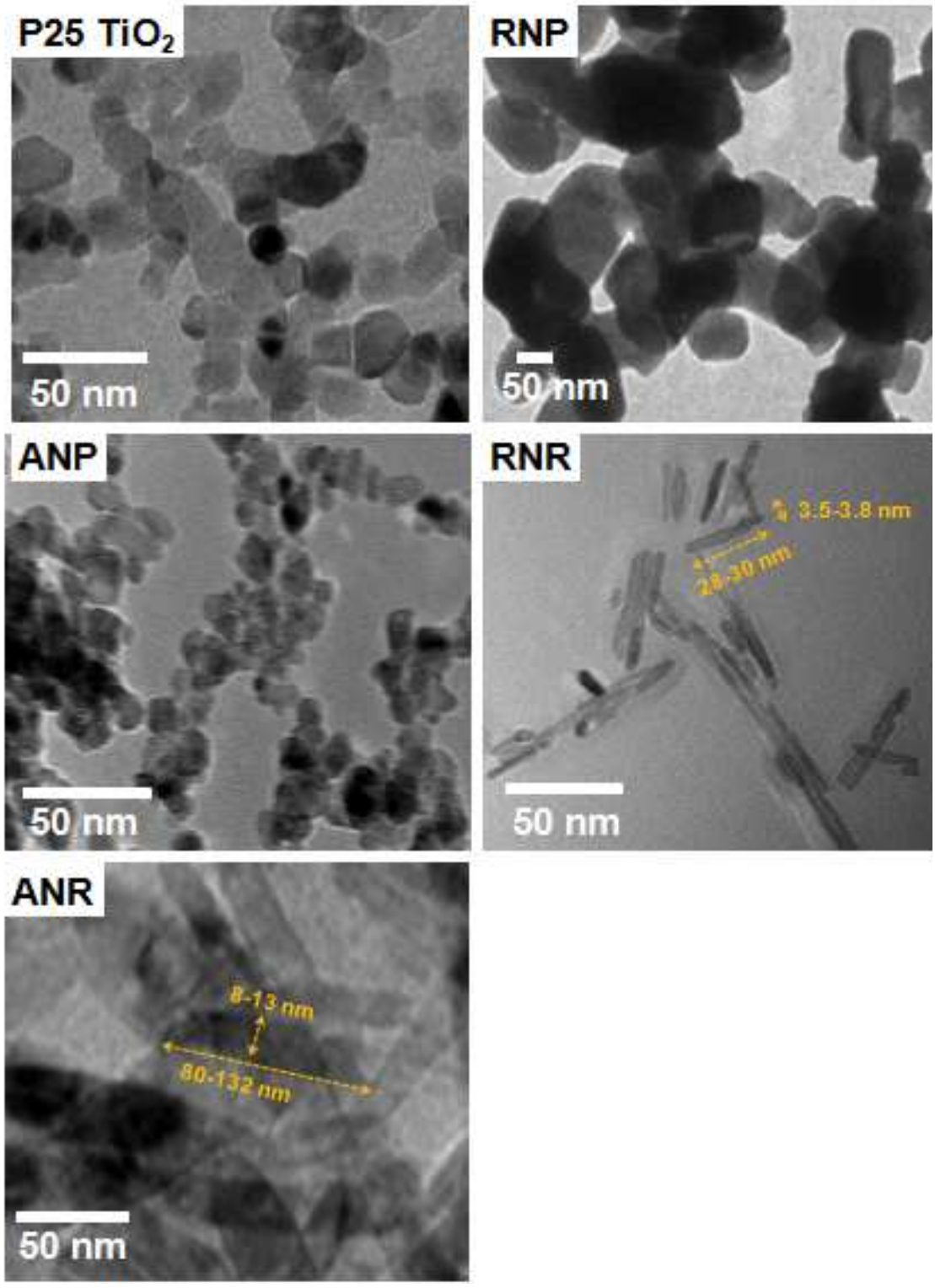

Fig. 2 TEM images of as prepared titania nanostructures

$$\alpha h\nu = A(h\nu - E_g)^n$$

where α = absorption coefficient,

hν = energy of photon,

A = constant,

Eg = band gap of the material

and n = index and its value depends upon on the nature of the electronic transition responsible for the absorption (n = 2 for indirect, 1/2 for direct band gap).

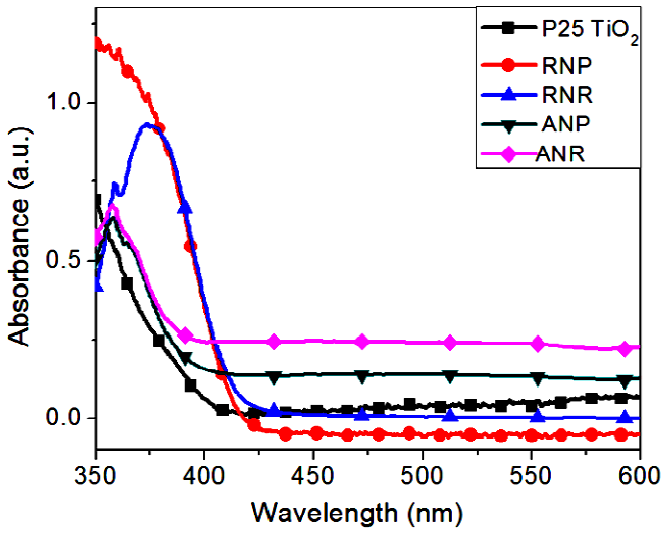

Fig. 3 Absorption spectra of different titania nanostructures

The band gap of the samples were calculated by extrapolating the straight-line portion of αhν versus Eg graph to the x-axis as shown in Fig. 4a. The band gap values varies from 3.0 eV for RNP to 3.21 eV for ANR (Fig. 4b) depending upon the phase and morphology. The low band gap exhibited by RNP and RNR expected to facilitate the efficient electron transfer and may serve as an efficient photocatalyst.

The emission in nanocrystalline TiO_2 is due to the defects resulting from under coordinated Ti^{4+} ions, oxygen vacancies, chemisorbed surface species, which result in the localized intra-band gap states that serve as electron traps. The photoluminescence (PL) spectra in Fig. 5a showed that TiO_2 nanostructures exhibit the emission bands from 400 to 550 nm range which indicates the occurrence of various surface defect sites. The emission peak, 403 nm, corresponds to a direct

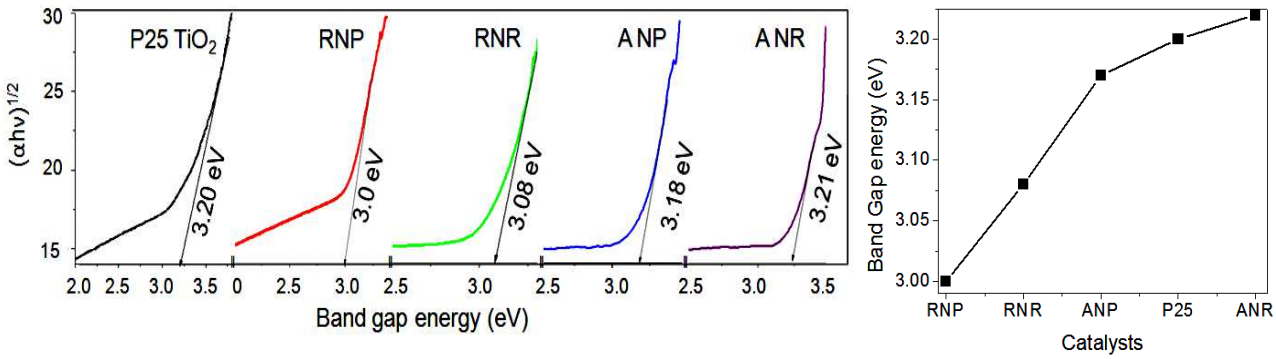

Fig. 4 (a) The plot of $(\alpha h\nu)^{1/2}$ function versus the band gap energy of various titania samples (b) Variation in the band gap energy of titania samples.

band emission of the fundamental band gap (3.2 eV) of anatase TiO_2, whereas the emission peak, 423 nm, is attributed to the self trapped excitons. The peak, 446 nm, relates to the emission process of oxygen vacancy defects in TiO_2 and the emission signal, 485 nm corresponds to the charge-transfer from Ti^{3+} to oxygen anion in a TiO_6^{8-} complex, related with oxygen vacancies at the TiO_2 surface [36-39]. The emission, 529 nm, can be related with anion vacancies on the surface of TiO_2 nanoparticles. The strong quenching in PL emission, in the case of RNR nanoparticles, has been attributed to the decrease in recombination rate of photo-generated electron–hole pairs.

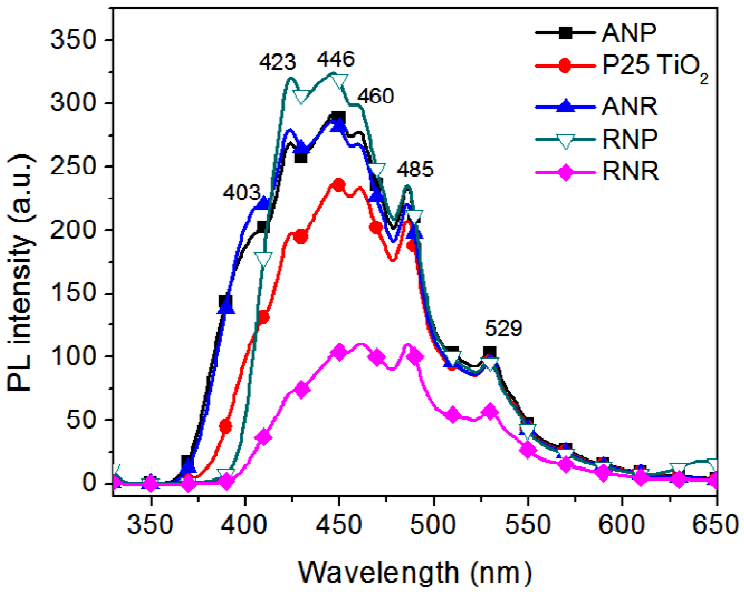

Fig. 5 Photoluminescence spectra of various titania nanostructures.

The average lifetime [40] of photoexcited e^-/h^+ pairs is calculated by time resolved fluorescence decays (Fig. 5) has been found to be gradually increased as 1.2, 1.5 and 2.1 ns for P25 TiO_2 ANP, ANR and respectively, confirming better delocalization of e^-–h^+ pairs in the lengthy

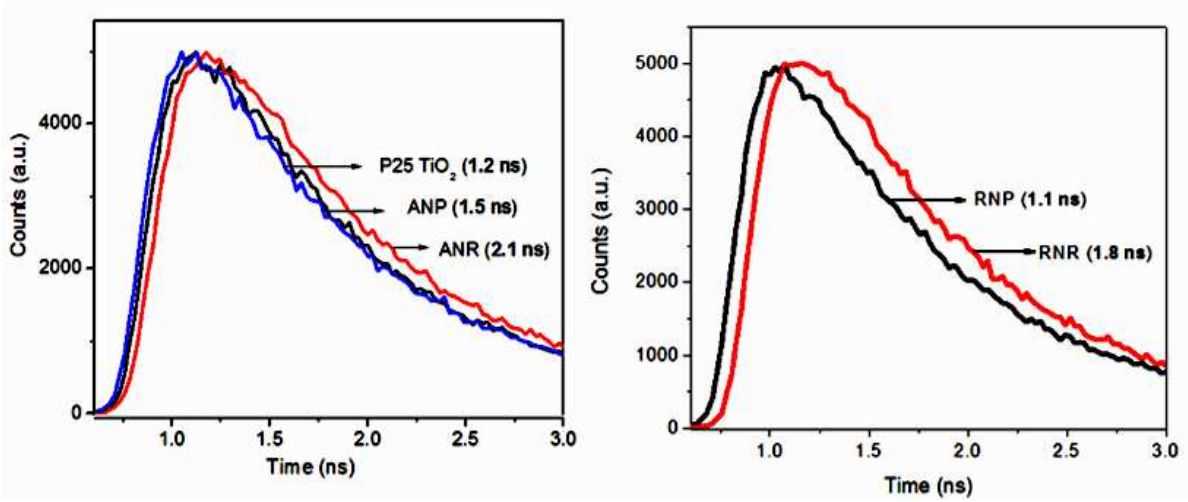

Fig. 6 Time resolved decay curves of titania nanostructures

crystalline NR. Also, average lifetime of RNP and RNR found to be 1.1 and 1.8 ns respectively.

5.3.4 Photocatalytic study

The photocatalytic activity of as prepared titania catalysts were evaluated by monitoring the photoreduction of *m*-NBA and *m*-NT. Fig.6a showed the selective reduction of *m*-NBA to *m*-ABA after 6 h UV irradiation with P25-TiO_2, ANP and ANR catalysts. It found that smaller ANP (8 nm) catalysts exhibits highest photoactivity for *m*-NBA reduction and produces *m*-ABA with 42 % yield as compared to 40 % and 30 % yield of P25 TiO_2 and ANR respectively. It could be probably due to increased surface area of ANP (89 m^2g^{-1}) owing to its smaller size as compare to 45 m^2g^{-1} and 71 m^2g^{-1} of P25 TiO_2 and ANR respectively. Fig. 6b showed the significant higher photoactivity for RNR (~ 3 times) as compared to RNP for *m*-NBA reduction into ABA under 8 h UV irradiation. The yield of *m*-ABA significantly increases upto 48% with RNR as compare to 18% with RNP catalysts. It could be attributed due to long distance electron transport along longitudinal length, higher surface area (69 m^2g^{-1}) of RNR available for

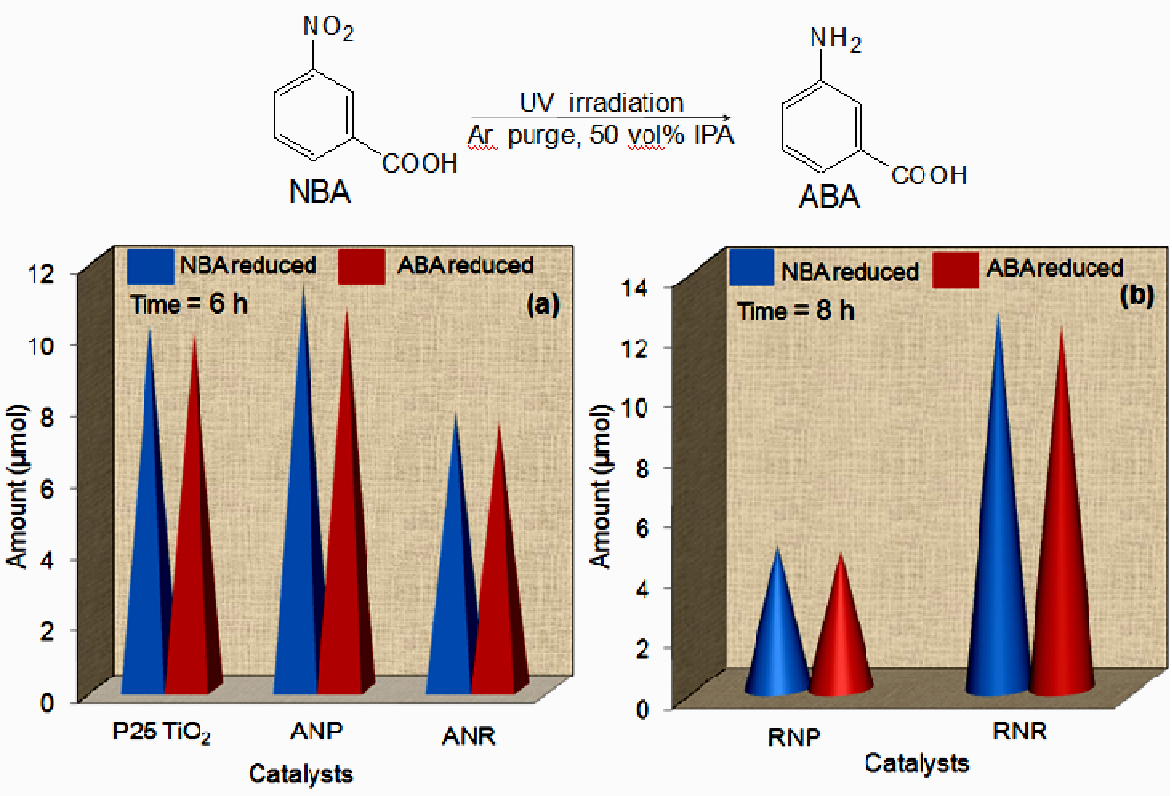

Fig. 6 *m*-NBA reduction under UV light irradiation by (a) P25-TiO_2, ANP and ANR for 6 h (b) RNP and RNR for 8 h

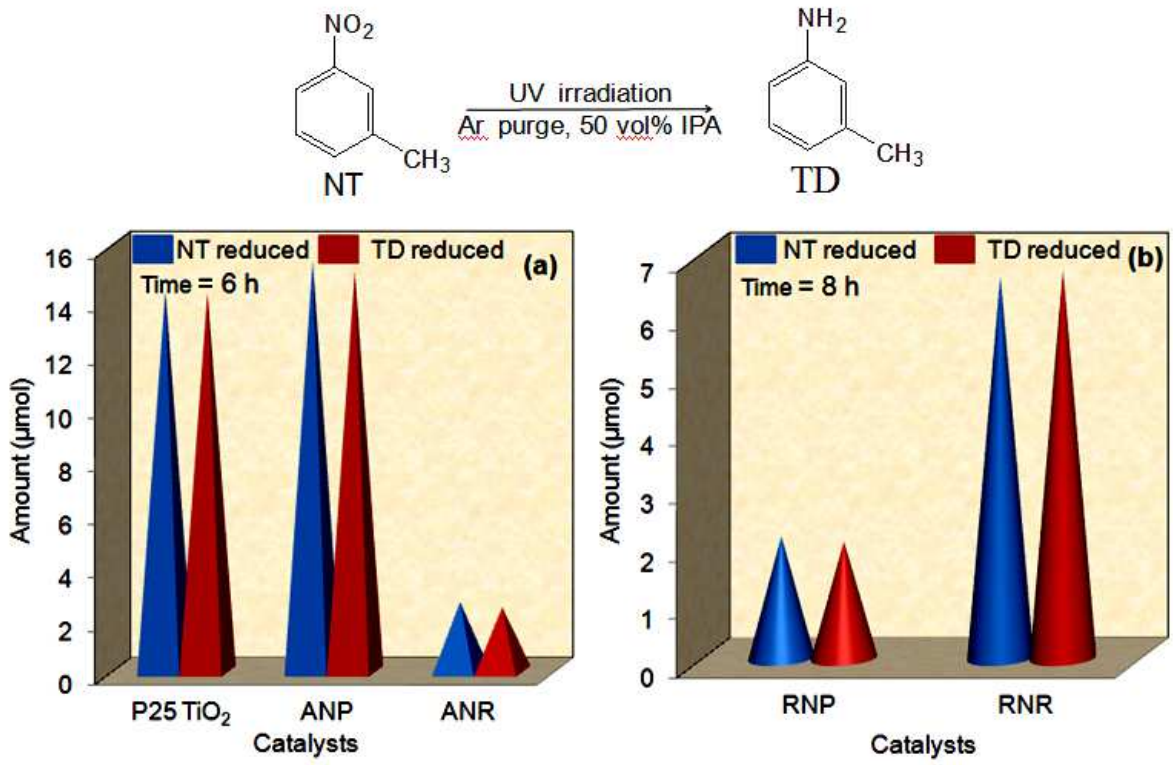

Fig. 7 *m*-NT reduction under UV light irradiation by (a) P25-TiO_2, ANP and ANR for 6 h (b) RNP and RNR for 8 h

adsorbtion and reduction of *m*-NBA as compare to lesser (18 m^2g^{-1}) surface area of RNP. Also, by changing the morphology from RNP to RNR the charge carrier time also enhances from 1.1 to 1.8 ns which also contributes to its enhanced photoactivity. Also, the obtained results shows that anatase titania nanostructures shows higher photoactivity in lesser irradiation time as compare to rutile nanostructures.

Further Fig. 7a also shows the same trend for *m*-NT reduction into *m*-toluidene (*m*-TD). It shows that ANP showed highest photoactivity for the reduction of *m*-NT and produces *m*-TD with yield 60 % under 6 h of UV irradiation. Also, RNR gives yield 26 % (~ 3 times) as compare to 8 % yield with RNP catalysts during 8 h UV irradiation. Fig. 8 shows that rate of reduction/hour for *m*-NBA and *m*-NT reduction with various catalysts follows the trend ANP> P25 TiO_2> RNR> ANR> RNP. This can be attributed to the fact [41, 42, 43] that reduction plane {011} related with anatase nanostructures contains a rich array of defects in comparison with reduction plane {110} of R-TiO_2. The defect sites are identified as Ti^{3+} which behave as an active site on the TiO_2 surface and are necessary for adsorption and the conversion of nitro group to amine.

The present results are also in agreement with literature that morphology, the exposed crystal faces, and their relative specific surface area seem to play the major roles in the their phocatalytic performance. Literature also reveals the superior photocatalytic activity of [44] the lengthy nanocrystals as compare spherical nanoparticles because of superior delocalization and reduced recombination rate of photoexcited e^-/h^+ pairs. Also, some reports [45] shows that other parameters such as band gap energy, surface defects, crystallinity and some electro-kinetic parameters etc might be also, responsible for better photoactivity of titania nanoparticles.

5.4 Conclusion

It is demonstrated that as prepared RNP, RNR, ANP, ANR could be potentially utilized for nitroaromatics photoreduction. RNR showed superior photoactivity (~ 3 times) as compared to RNP for the photoreduction of *m*-NT into *m*-toluidene (*m*-TD) and *m*-NBA into *m*-aminobenzoic acid (*m*-ABA) under 8 h UV irradiation. The obtained results show that the long distance electron transport along longitudinal length, larger surface area, quenched PL emission, increased lifetime of charge carriers of RNR as compare to RNP having lower surface area and charge carrier lifetime collectively contribute to its enhanced photocatalytic activity. Futhermore, ANP also shows higher photocatalytic activity than ANR owing to their smaller size and larger surface area as compare to ANR and P25-TiO_2 for *m*-NBA and *m*-NT photoreduction under 6 h UV light irradiation.

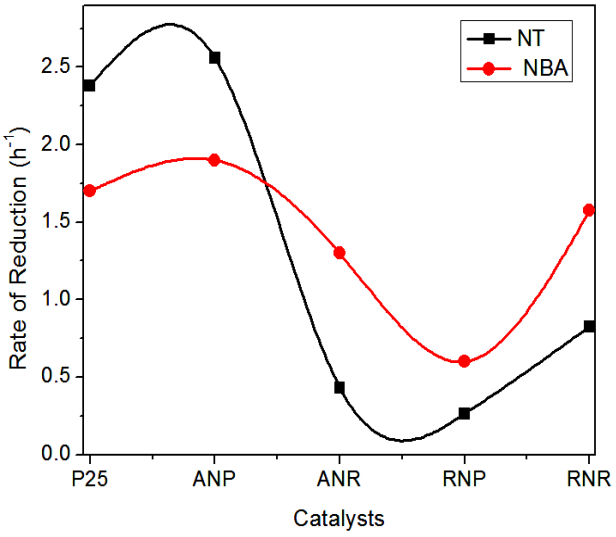

Fig. 8 Rate of reduction per hour of NT and NBA with various titania nanostructures

5.5 References

[1] H. Hirakawa, M. Katayama, Y. Shiraishi, H. Sakamoto, K. Wang, B. Ohtani, S. Ichikawa, S. Tanaka, T. Hirai, ACS Appl. Mater. Interfaces 7 (2015) 3797.

[2] M. Boronat, P. Concepcion, A. Corma, S. Gonzalez, F. Illas, P. Serna, J. Am. Chem. Soc. 129 (2007) 16230.

[3] O.V. Makarova, T. Rajh, M.C. Thurnauer, A. Martin, P.A. Kemme, D. Cropek, Environ. Sci. Technol. 34 (2000) 4797.

[4] X. Pan, Y. J. Xu, ACS Appl. Mater. Interfaces 6 (2014) 1879.

[5] P.F. Vogt, J.J. Gerulis, Ullmann's Encyclopedia of Industrial Chemistry. ''Aromatic Amines'', Wiley-VCH, Verlag GmbH & Co. KGaA, Weinheim, 2005, p. 2.

[6] L. Ying, C. Jixiang, Z. Jiyan, Chin. J. Chem. Eng. 15 (2007) 63.

[7] D. He, X. D. Jiao, P. Jiang, J. Wang, B. Q. Xu, Green Chem. 14 (2012) 111.

[8] Y. Zheng, K. Ma, H. Wang, X. Sun, J. Jiang, C. Wang, R. Li, J. Ma, Catal. Lett. 124 (2008) 268.

[9] F.C. Lizana, S.G. Quero, N. Perret, M.A. Keane, Catal. Lett. 127 (2009) 25.

[10] Y. Chen, J. Qiu, X. Wang, J. Xiu, J. Catal. 242 (2006) 227.

[11] H. Rojas, G. Borda, P. Reyes, M. Brijaldo, J. Valencia, J. Chil. Chem. Soc. 56 (2011) 793.

[12] D.P. He, H. Shi, Y. Wu, B. Q. Xu, Green Chem. 9 (2007) 849.

[13] X. Pan, Y. J. Xu, ACS Appl. Mater. Interfaces 6 (2014) 1879.

[14] J.J. Chen, W.K. Wang, W.W. Li, D.N. Pei, H.Q. Yu, ACS Appl. Mater. Interfaces 7 (2015) 12671.

[15] A. Corma, P. Serna, Science 313 (2006) 332.

[16] H. Zhu, X. Ke, X. Yang, S. Sarina, H. Liu, Angew. Chem. 122 (2010) 9851.

[17] M.S. Wrighton, Chem. Eng. News 57 (1979) 29.

[18] M.A. Fox, Nouv. J. Chim. 11 (1987) 129.

[19] T. Kanno, T. Oguchi, H. Sakuragi, K. Tokumm, Tetrahedron Lett. 21 (1980) 467.

[20] J.A. Dean, In Handbook of Organic Chemistry, ed. McGraw Hill, New York, 1987, section 8.

[21] F. Mahdavi, T.C. Bruton, Y. Li, J. Org. Chem. 58 (1993) 744.

[22] C.J. Li, G.R. Xu, B. Zhang, J.R. Gong, Appl. Catal. B: Environ. 115 (2012) 201.

[23] A. Hakki, R. Dillert, D.W. Bahnemann, Phys. Chem. Chem. Phys. 15 (2013) 2992.

[24] Y. Shiraishi, Y. Togawa, D. Tsukamoto, S. Tanaka, T. Hirai, ACS Catal. 2 (2012) 2475.

[25] S.C. Li, U. Diebold, J. Am. Chem. Soc. 132 (2010) 64.

[26] J. Kaur, B. Pal, Catal. Comm. 53 (2014) 25.

[27] J. Kaur, R. Singh, B. Pal, J. Mol. Catal. A: Chemical 397 (2015) 99.

[28] Q. Zhao, M. Li, J. Chu, T. Jiang, H. Yin, Appl. Surf. Sci. 255 (2009) 3773.

[29] J.C. Xu, M. Lu, X.Y. Guo, H.L. Lia, J. Mol. Catal. A: Chem. 226 (2005) 123.

[30] J. Yu, H. Yu, B. Cheng, C. Trapails, J. Mol. Catal. A: Chem. 249 (2006) 135.

[31] H. J. Yun, H. Lee, N. D. Kim, J. Yi, Electrochem. Comm. 11 (2009) 363.

[32] Z. Liu, X. Zhang, S. Nishimoto, M. Jin, D.A. Tryk, T. Murakami, A. Fujishima, Langmuir 23 (2007) 10916.

[33] J.N. Nian, H. Teng, J. Phys. Chem. B 110 (2006) 4193.

[34] K.V. Baiju, S. Shukla, K.S. Sandhya, J. James, K.G.K. Warrier J. Phys. Chem. C 111 (2007) 7612.

[35] A. Dessombz, D. Chiche, P. Davidson, P. Panine, C. Chaneac, J.P. Jolivet, J. Am. Chem. Soc. 129 (2007) 5904.

[36] N.D. Abazovic, L. Mirenghi, I.A. Jankovic, N. Bibic, D.V. Sojic, B.F. Abramovic, M.I. Comor, Nanoscale Res. Lett . 4 (2009) 518.

[37] S. Chaveanghong, S.M. Smith, J. Sudchanham, T. Amornsakchai, J. Microsc. Soc. Thail. 4 (2011) 36.

[38] X. Song, L. Gao, Langmuir 23 (2007) 11850.

[39] J. Liu, J. Li, A. Sedhain, J. Lin, H. Jiang, J. Phys. Chem. C 112 (2008) 17127.

[40] S. Khanchandani, S. Kundu, A. Patra, A.K. Ganguli, J. Phys. Chem. C 116 (2012) 23653.

[41] U. Aschauer, A. Selloni, Phys.Chem.Chem.Phys. 14 (2012) 16595.

[42] X. Peng, A. Chen, Appl. Phys. A 80 (2005) 473.

[43] B.S. Shirke , P.V. Korake, P.P. Hankare, S.R. Bamane, K.M. Garadkar, J Mater Sci: Mater Electron 22 (2011) 821.

[44] J. Yang, J.H. Zeng, S.H. Yu, L. Yang, G.E. Zhou, Y.T. Qian, Chem. Mater. 12 (2000) 3259-3263.

[45] I.S. Grover, V. Mutreja, S. Singh, B. Pal, Sci. & Soc. 9(2011) 169-174.

Conclusions

Summary of the work

Chapter 1: covers the brief introduction to the mechanism of TiO_2 photocatalysis, effect of shape, size, crystal phase and metal loading onto TiO_2, functional group transformations using TiO_2, related reports in the literature and the scope for selective photoreduction photo reduction of nitroaromatics by TiO_2 nanostructures.

Further, the detailed experimental methods and characterisation techniques used in the present study are also explained. This includes, synthesis of bare (nanospheres and nanorods), different crystal phase (anatase and rutile) and metal (Au, Ag, Cu, Pt, Pd, Rh) loaded titania nanostructures, the procedure for photoreduction of various nitroaromatics with as prepared catalysts, characterisation and product analysis techniques: Diffused reflectance spectroscopy (DRS), photoluminescence (PL), time resolved spectroscopy (TCSPC), X-ray diffraction (XRD), Transmission electron microscope (TEM), BET surface analyzer, High Performance Liquid Chromatography (HPLC), Gas chromatography-mass spectroscope (GC-MS), Gas chromatography (GC), Nuclear magnetic resonance spectroscope (NMR).

Chapter 2: Describes the effect of rutile TiO_2 content, solvent, catalyst amount, irradiation time, crystallinity, surface area and electron withdrawing groups for selective photoreduction of *m*-dinitrobenzene by P25-TiO_2 and R-TiO_2. Also, the photoreduction studies were carried out for nitrobenzene, *p*-dinitrobenzene and *m*-chloronitrobenzene for comparison. It is concluded from the work that both the P25-TiO_2 and R-TiO_2 could be potentially utilized for the selective reduction of nitroaromatics possessing multifunctional reducible groups in *ortho*, *meta* and *para* position. Further, the insertion of a second $–NO_2$ group in nitrobenzene ring has an important role in expediting $–NO_2$ reduction to $–NH_2$ as compared to a negligible reduction of nitrobenzene under similar conditions, indicating that electron withdrawing groups lower the electron density on $–NO_2$ present on meta position and favor quick reduction of the $–NO_2$ group. Thus proper selection of electron donating or withdrawing substituent's in the aromatic moiety would be highly beneficial and have a wide scope of several other desired products to obtain.

Chapter 3: Demonstrates the influence of coinage (Au, Ag and Cu) and platinum group metal (Pt, Pd, Rh) co-catalysis for the photocatalytic reduction of *m*-dinitrobenzene by P25 and R-

TiO_2. It has been concluded from the work that 1 wt% metal loading on P25 and R-TiO_2 does not seem to improve the PCA except the improved selectivity by M/P25 which is opposite to high PCA for oxidation reactions by M/TiO_2 catalysts generally observed. Further, coinage metals e.g., Ag/P25 exhibit higher selectivity and yield for *m*-NA formation. Irrespective of the nature of metal loading, the *m*-DNB photoreduction is always notably reduced as compared to the highest photoreactivity of bare R-TiO_2 that produces 100% *m*-NA. This decrease in PCA for the nitro group reduction by all M/TiO_2 could thus be attributed to the decrease in active Ti^{3+} sites available on the surface after metal nanodeposits loading that might also act as a recombination centre for photoexcited charge species.

Chapter 4: Describes the selective formation of benzo[c]cinnoline by photocatalytic reduction of 2,2′-dinitrobiphenyl using P25-TiO_2 under UV light irradiation. It is observed from the study that the non-conventional production of benzo[c]cinnoline from 2,2′-dinitrobiphenyl photoreduction by P25-TiO_2 and UV light, where the yield and selectivity could be simply tuned by light irradiation under ambient conditions without using any costly toxic solvent and reducing agents are experimented for the first time using inexpensive and non-toxic titania catalyst. This photoreduction process could be extended to other N-heterocyclic compounds synthesis that requires harsh experimental conditions in conventional techniques.

Chapter 5: Presented a fine insight for the crystal phase and shape dependent photoactivity of titania for nitroaromatics reduction under UV light irradiation. This chapter describes importance of different shapes and crystal phases of TiO_2 nanostructures such as RNP, RNR, ANP, ANR and P25-TiO_2 (70:30 anatase and rutile) for the PCA for *m*-nitrotoluene (*m*-NT) and *m*-nitrobenzoic (*m*-NBA) photoreduction under UV light irradiation. RNR showed superior photoactivity (~3 times) as compared to RNP for the selective photoreduction of *m*-NT into *m*-toluidine (*m*-TD) and *m*-NBA into *m*-aminobenzoic acid (*m*-ABA) under 8 h UV irradiation. The obtained results show that the long distance electron transport along longitudinal length, larger surface area, quenched PL emission, increased lifetime of charge carriers of RNR as compare to RNP having lower surface area and charge carrier lifetime collectively contribute to its enhanced PCA. Futhermore, ANP of size 8-10 nm having surface area 89 m^2g^{-1} also shows higher PCA than anatase nanorods of size (L×W = 80-132 nm × 8-13 nm and surface area = 71

m^2g^{-1}) and P25-TiO_2 (25-30 nm) for *m*-NBA and *m*-NT photoreduction under 6 h UV light irradiation. The overall rate of reduction/hour for *m*-NBA and *m*-NT photoreduction with all of these catalysts has been found to vary in the following order ANP> P25-TiO_2> RNR> ANR> RNP. Thus, the photoactivity of rutile TiO_2 for the selective photoreduction of nitroaromatics can be enhanced by tuning the morphology from spheres to rods. Also, the effect of available surface area for reduction, crystal phase also plays an important role in the reduction of nitroaromatics.

Future Scope

After concluding the present work, it can be suggested that efforts are required for the selective reduction of nitroaromatics which possess multifunctional reducible groups in *ortho, meta* and *para* position with rutile nanoparticles, nanorods and P25 titania nanostructures. Synthesis of N-heterocyclic compounds that requires harsh experimental conditions in conventional techniques can also be investigated with P25-TiO_2.

List of Publications

Papers in SCI/refereed journals

1. **Jaspreet Kaur** and Bonamali Pal, "Selective formation of benzo[c]cinnoline by photocatalytic reduction of 2,2'-dinitrobiphenyl using TiO_2 and under UV light irradiation" ***Chemical Communications*** 51 (2015) 8500-8503. **(IF = 6.834)**
2. **Jaspreet Kaur** and Bonamali Pal, "100% selective yield of *m*-nitroaniline by rutile TiO_2 and *m*-phenylenediamine by P25-TiO_2 during *m*-dinitrobenzene photoreduction" ***Catalysis Communications*** 53 (2014) 25–28. **(IF = 3.699)**
3. **Jaspreet Kaur**, Rohit Singh and Bonamali Pal, "Influence of coinage and platinum group metal co-catalysis for the photocatalytic reduction of *m*-dinitrobenzene by P25 and rutile TiO_2" ***Journal of Molecular Catalysis A: Chemical*** 397 (2015) 99–105. **(IF = 3.679)**
4. **Jaspreet Kaur** and Bonamali Pal, "Crystal phase and shape dependent photoactivity of titania for nitroaromatics reduction under UV light irradiation" under preparation.

List of papers/poster presented in conferences

1. **Jaspreet Kaur** and Bonamali Pal**, "**Metal (Au, Ag, Pt) -TiO_2 Nanocomposites for the Selective Photoreduction of *m*-Dinitrobenzene" International Conference on Emerging Technologies- Micro to Nano **(ETMN-2013)** held at BITS Pilani, KK Birla Goa Campus, Goa, India in February 23rd-24th , 2013.
2. **Jaspreet Kaur** and Bonamali Pal, "Selective photoreduction of nitroaromatics by metal loaded TiO_2 nanocomposites" National Conference on Innovative Molecules for Sustainable Future **(NCIMS-2013)** held at Thapar University, Patiala, India in October 24 th -26 th , 2013.
3. **Jaspreet Kaur** and Bonamali Pal, "Photoreduction of 3-substituted nitrobenzenes by P25 and silver loaded titania nanoparticles" International Conference on Nanoscience and Technology **(Nanoscitech -2014)** held at Panjab University, Chandigarh, India in February 13th-15th, 2014.
4. **Jaspreet Kaur** and Bonamali Pal, "Reduction of nitroaromatics by rutile nanoparticles under ultraviolet light" National Conference on New Frontiers in Chemical Sciences **(NFCS-2014)** held at Khalsa College, Patiala, India in November 15th, 2014.
5. **Jaspreet Kaur** and Bonamali Pal, "Selective photoreduction of nitroaromatics by bare and metal (Au, Ag, Cu) loaded rutile nanoparticles" International Conference on Recent Advances in

Nanoscience and Nanotechnology **(ICRAN-2014)** held at Jawahar Lal Nehru University, New Delhi, India in December 15-16th, 2014.

6. **Jaspreet Kaur** and Bonamali Pal, "Enhanced photoreduction of nitroaromatics by pure rutile nanorods" National Conference on **(SACOS 2015)** held at Punjabi University, Patiala, India ***(Awarded 2nd Prize)*** in February 15-16th, 2015.

ChemComm

COMMUNICATION

View Article Online
View Journal

Cite this: DOI: 10.1039/c5cc02713f

Received 1st April 2015,
Accepted 10th April 2015

DOI: 10.1039/c5cc02713f

www.rsc.org/chemcomm

Selective formation of benzo[c]cinnoline by photocatalytic reduction of 2,2′-dinitrobiphenyl using TiO_2 and under UV light irradiation†

Jaspreet Kaur and Bonamali Pal*

Photocatalytic reduction of 25 μmol 2,2′-dinitrobiphenyl in 50% aqueous iso-propanol and 50 mg P25-TiO_2 under an argon atmosphere and 20 h UV light irradiation selectively produced 23.8 μmol of benzo[c]cinnoline (95%), and 2,2′-biphenyldiamine (5%) whose amount gradually increased with the irradiation time beyond 20–24 h due to further reduction of benzo[c]cinnoline.

Benzo[*c*]cinnoline (BC) is a very important organic compound used in manufacturing of dyes, electrochromic polymers, coloured polyamide fibers and has microbial and herbicidal activities.[1–3] It is typically synthesized by reduction of 2,2′-dinitrobiphenyl (DNBP)[4,5] with RANEY® Ni[6] and Pd-C,[7,8] Zn,[9] Fe^{+2} oxalate,[10] Fe,[11] $LiAlH_4$,[12,13] triethyl phosphite,[14] Fe-carbonyl,[15] and by electrochemical[16] methods. These conventional methods require harsh conditions such as strong reducing agents, high pressure and temperature, expensive solvents, and leave toxic byproducts. Hence, a greener, environmentally benign and mild photocatalytic reaction process using a nontoxic TiO_2 catalyst under light irradiation could have beneficial advantages for the highly selective production of BC from DNBP reduction under ambient conditions.

Nitroaromatics reduction by TiO_2 under UV irradiation has been recently reported[17,18] to be feasible due to its higher conduction band energy (−0.85 V) than the reduction potential −0.5 V *vs.* SCE of the $-NO_2$ group.[19,20] Nitrobenzene reduction to aniline and azoxybenzene by photoirradiated CdS, WO_3, ZnO, TiO_2, and SiO_2@Rh–CdS composites,[21–25] formation of 4-ethoxy-1,2,3,4-tetrahydroquinoline[26] and cyclic imino acids,[27] synthesis of 2-methylpiperazine by (TiO_2 or CdS)–zeolites,[28] *etc.* are demonstrated. Photocatalytic reduction of *m*-dinitrobenzene for selective formation of *m*-phenylenediamine (100%) by P25-TiO_2 and *m*-nitroaniline (100%) by rutile TiO_2, and *p*-dinitrobenzene to a mixture of products is reported[29] to be due to the electron withdrawing effect and the position of the $-NO_2$ group in the benzene moiety. However, little information has been known to date about the reduction behaviour of $-NO_2$ groups present in two separate benzene rings of biphenyl compounds.

In this context, this research demonstrated for the first time that photocatalytic reduction of DNBP led to highly selective yield of BC (Scheme 1) along with a small amount of other amino derivatives by P25-TiO_2 (Degussa, a mixture of 70% anatase and 30% rutile) under controlled UV light irradiation. The reduction was carried out in a rubber capped-sealed test tube containing 5 mL aqueous iso-propanol (IPA, 50 vol%), 50 mg P25-TiO_2 (TiO_2) and 25 μmol DNBP suspension under an argon atmosphere with constant magnetic stirring and UV light (125 W Hg arc, 10.4 mW cm^{-2}) irradiation for different time periods. The reaction products are quantitatively analysed by HPLC, GC-MS and NMR techniques (ESI†).

Fig. 1a and b show the GC chromatographs of the authentic sample showing a single peak of DNBP (25 μmol) at t_R = 14.5 min and BC (7.5 μmol) at t_R = 13 min. Fig. 1c reveals that after DNBP reduction by TiO_2 during 8 h irradiation, a number of GC peaks at t_R = 11.6, 12.9, 15.7 and 16.9 min including few smaller peaks evolved due to the formation of various reduction products. The peak height at t_R = 14.2 min for DNBP is decreased due to its complete reduction, and with the passage of 15–24 h irradiation (Fig. 1d–f), the intensity of all the peaks is reduced except for a smaller peak at t_R = 11.6 min, and a major peak at t_R = 12.9–13.0 min is found to be significantly enhanced (Fig. 1e) after DNBP reduction for 20 h irradiation. The peak at t_R = 15.7 min is not observed after 15 h, whereas the peak intensity at t_R = 11.6 min is

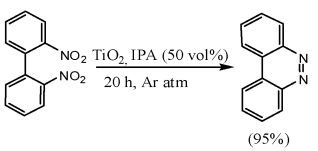

Scheme 1 Photocatalytic reduction of DNBP to BC by TiO_2 under UV irradiation.

School of Chemistry and Biochemistry, Thapar University, Patiala, Punjab, India. E-mail: bpal@thapar.edu; Fax: +91 175 2364498; Tel: +91 175 2393491

† Electronic supplementary information (ESI) available: HPLC, GC, GC-MS and NMR analysis techniques. See DOI: 10.1039/c5cc02713f

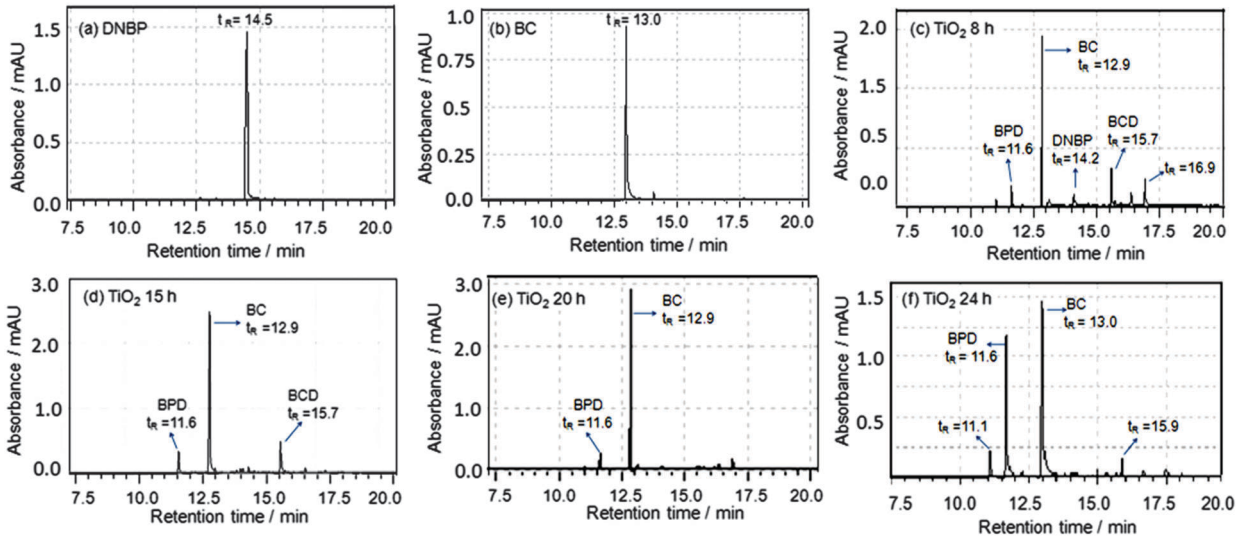

Fig. 1 GC pattern of authentic (a) DNBP (25 μmol), (b) BC (7.5 μmol) and photoreduction products of DNBP (25 μmol) by TiO_2 after (c) 8 h, (d) 15 h, (e) 20 h, (f) 24 h UV irradiation.

seen to be almost the same up to 20 h and beyond that it is notably increased with a simultaneous decrease in the peak height at t_R = 12.9 min after 20–24 h UV light irradiation.

The mass spectrum analysis of authentic DNBP (Fig. 2a) and its reduction products confirmed the formation of BC (Fig. 2b) at t_R = 12.9 min, biphenyldiamine (BPD, Fig. 2c) at t_R = 11.6 min, and benzo[*c*]cinnoline dioxide (BCD, Fig. 2d) at t_R = 15.7 min during DNBP reduction by TiO_2 for different time periods. Fig. 3a shows the variation in the peak heights of three major reduction products BCD, BC and BPD with decreased DNBP concentration and increased UV irradiation time. It is found that DNBP almost selectively reduced to BC along with the formation of a small amount of BPD after 20 h. It further revealed that BCD is formed up to 15 h irradiation, whereas BPD is increased with a decrease in the amount of BC formed beyond 20–24 h reduction. By comparing 7.5 μmol commercial authentic BC samples, the yield and selectivity of BC obtained by DNBP (25 μmol) reduction using

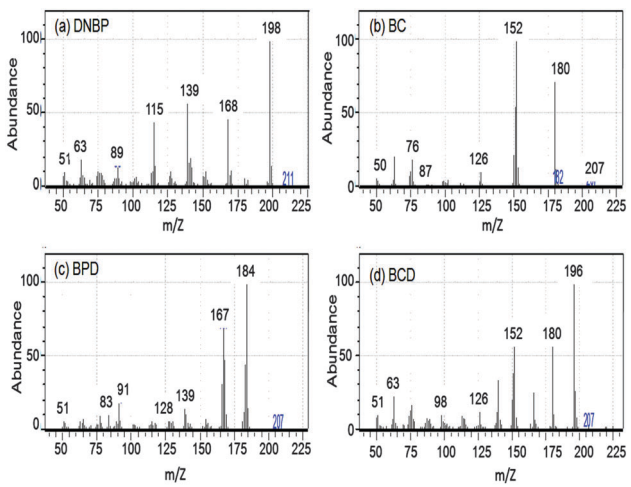

Fig. 2 Mass spectral analysis of DNBP and its reduction products.

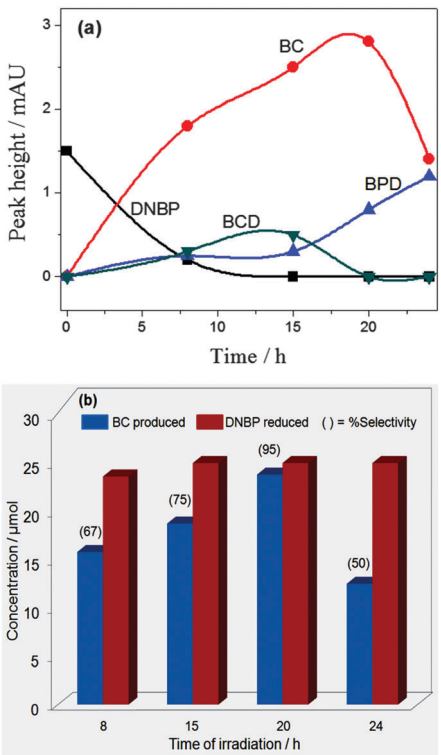

Fig. 3 (a) Time course graph (peak height variation) of different products of DNBP reduction and (b) BC yield and selectivity as a function of UV irradiation time.

TiO_2 under UV irradiation for 8–24 h gradually increased from 67% to a maximum of 23.8 μmol (95%) of BC during 20 h and thereby, remarkably decreased beyond 20–24 h irradiation due to its self-reduction to BPD. HPLC analysis (Fig. S1, ESI†) also revealed the formation of ~23.7 μmol of BC. In a blank test, no such reduction of DNBP occurred without the TiO_2 catalyst after 20 h of UV light irradiation (Fig. S2, ESI†), thus confirming

the photocatalytic nature of DNBP reduction reaction. The reproducibility was further judged by another set of experiments carried out under similar conditions, which produced ~23.2 μmol of BC (Fig. S3c, ESI†) relative to 23.8 μmol in the first run.

The ^{1}H-NMR (400 MHz, $CDCl_3$) spectral analysis (Fig. S4, ESI†) shows the peaks observed for: DNBP authentic at δ 8.20 (d, 2H, J = 8.24 Hz, ArH), 7.70 (t, 2H, J = 7.32 Hz, ArH), 7.60 (t, 2H, J = 8.24 Hz, ArH), 7.30 (dd, 2H, J = 7.76 Hz, ArH); BC authentic (Fig. S4b, ESI†) at δ 8.76–8.74 (m, 2H, ArH), 8.59–8.57 (m, 2H, ArH), 7.94–7.89 (m, 4H, ArH). BC formed by DNBP photoreduction shows NMR (Fig. S4c, ESI†) peaks at δ 8.77–8.74 (m, 2H, ArH), 8.61–8.59 (m, 2H, ArH), and 7.94–7.91 (m, 4H, ArH) that almost closely match (except for some small peaks of other unidentified products) with the characteristic NMR spectra of the authentic BC sample. BPD produced after 24 h irradiation showed peaks at δ 7.54–7.50 (m, 4H, ArH), 7.30 (t, 2H, J = 7.8 Hz, ArH) and 7.23 (d, 2H, J = 8.24 Hz, ArH), and a typical broad peak for NH_2 protons at 4.23 (bs, 4H, NH_2) is also seen in Fig. S4d (ESI†) which are quite different from the NMR spectra of DNBP and BC.

On the basis of the obtained detected reduction products, it is revealed that the rate determining step for DNBP photocatalytic reduction using TiO_2 is the selective formation of BC *via* some transient intermediates; nitroso and hydroxylamine derivatives BCD, azoxy compounds and few unidentified products by following reaction pathways in Scheme 2. It is reported[25,30] that this intermediate sequence RNO_2–RNO–RNHOH–RNH_2 is generally formed during many nitroaromatics photoreduction. GC chromatographs (Fig. 1) also further support that these short lived products (*e.g.*, BCD) disappeared with increasing irradiation time. BPD production took place to a lesser extent *via* direct reduction of the hydroxylamine derivative (path-I) during initial hours (8–20 h), and beyond that more amount of BPD (path-II) is formed probably due to self-reduction of as-produced BC during 8–20 h irradiation. The photoexposure of TiO_2 (band gap energy = 380–390 nm) with UV light generates electrons in the conduction band and holes in the valence band, where two NO_2 groups of DNBP are sequentially reduced to NH_2 groups in BPD by 12e$^-$, and complete reduction of DNBP by irradiated TiO_2 required 8e$^-$ for the BC formation through various intermediate reduction steps. It is also observed that the reduction process is accompanied by the simultaneous oxidation of iso-propanol (hole scavenger) to acetone (t_R = 1.2 min) whose amount (Fig. S5, ESI†) increased with (20 to 24 h) irradiation time, and no H_2 production is detected by photoexcited holes (h^+) in the valence band under UV irradiation. Furthermore, over oxidation of acetone to CO_2 was not observed as confirmed by GC analysis (Fig. S6, ESI†).

Thus, it is evident that DNBP undergoes intramolecular reductive cyclization reactions by TiO_2 because of the close spatial proximity[5] of the interacting NO_2 groups that lie in two different benzene rings separately relative to their location in the same benzene moiety in various dinitrobenzenes. Such redox combined photocatalytic reactions like selective photoreduction of *o*-dinitrobenzene to benzimidazole (96%) by TiO_2,[31] and formation of pipecolinic acid[32] from L-lysine irradiation are reported to be highly efficient for practical applications. Depending on the position (1 : 2, 1 : 3 and 1 : 4) of –NO_2 functionality[29,31] and the extent of the electron withdrawing effect of –NO_2 groups imparted to the benzene ring, dinitrobenzene is reduced to a variety of reduction products by both P25-TiO_2 and rutile TiO_2 under controlled UV irradiation. However, the pure rutile TiO_2 phase does not have any photoreactivity for DNBP reduction under the same experimental conditions.

The non-conventional production of BC from DNBP reduction by TiO_2 and UV light where the yield and selectivity could be simply tuned by light irradiation under ambient conditions without using any costly toxic solvent and reducing agents is experimented for the first time using an inexpensive and non-toxic titania catalyst. This photoreduction process could be extended to synthesis of other N-heterocyclic compounds, which requires harsh experimental conditions in conventional techniques.

We are grateful to Prof. Ashok Kumar Malik, Punjabi University, Patiala, India, for GC-MS analysis.

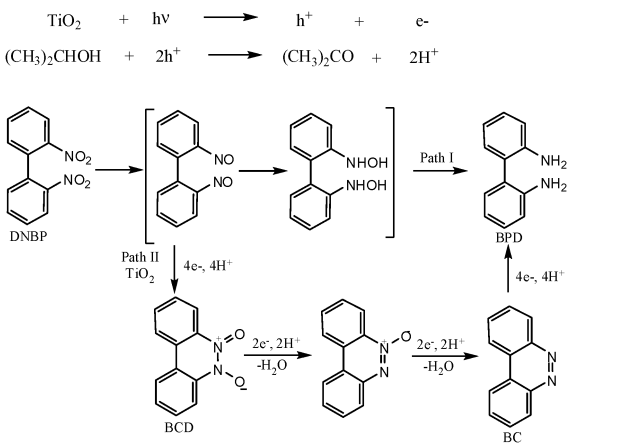

Scheme 2 Possible reaction pathways of DNBP reduction by TiO_2 and UV light irradiation.

Notes and references

1 E. Killic and S. Aktan, *Commun. Fac. Sci. Univ. Ankara, Ser. B: Chem. Chem. Eng.*, 2001, **47**, 37.
2 N. Minagawa, K. Kaneko, S. Sajo and A. Yoshimoto, *Biosci., Biotechnol., Biochem.*, 1993, **57**, 1577.
3 T. Eicher and S. Hauptmann, *The Chemistry of Heterocycles*, Wiley-VCH, Weinheim, 2003.
4 J. W. Barton, in *Advances in Heterocyclic Chemistry*, ed. A. R. Katritzky and A. J. Boulton, Academic Press, New York, 1979, vol. 24, pp. 151–185.
5 R. E. Buntrock and E. C. Taylor, *Chem. Rev.*, 1968, **68**, 209.
6 J. L. Everett and W. C. J. Ross, *J. Chem. Soc.*, 1949, 1972.
7 A. Etienne and G. Izoret, *Bull. Soc. Chim. Fr.*, 1964, 2897.
8 H. Stetter and A. I. Schwarz, *Chem. Ber.*, 1957, **90**, 1349.
9 J. Radell, L. Spialter and J. Hollander, *J. Org. Chem.*, 1956, **21**, 1051.
10 D. V. Banthorpe, E. D. Hughes and C. Ingold, *J. Chem. Soc.*, 1962, **2**, 386.
11 P. Z. Slack and R. Slack, *Nature*, 1947, **160**, 437.
12 J. F. Corbett and P. F. Holt, *J. Chem. Soc.*, 1960, **3**, 646.
13 A. Etienne and R. Piat, *Bull. Soc. Chim. Fr.*, 1962, 292.
14 J. I. G. Cadogan, M. Cameron-Wood, R. K. Mackie and R. J. G. Searle, *J. Chem. Soc.*, 1965, **4**, 831.
15 J. E. Kmiecik, *J. Org. Chem.*, 1965, **30**, 2014.
16 T. Wohlfahrt, *J. Prakt. Chem.*, 1902, **65**, 295.
17 Y. Shiraishi, Y. Togawa, D. Tsukamoto, S. Tanaka and T. Hirai, *ACS Catal.*, 2012, **2**, 2475.

18 Y. Shiraishi, H. Hirakawa, Y. Togawa, Y. Sugano, S. Ichikawa and T. Hirai, *ACS Catal.*, 2013, **3**, 2318.
19 M. A. Fox, *Nouv. J. Chim.*, 1987, **11**, 129.
20 J. A. Dean, *Handbook of Organic Chemistry*, New York, 1987.
21 R. J. Tayade, R. G. Kulkarni and R. V. Jasra, *Ind. Eng. Chem. Res.*, 2006, **45**, 922.
22 H. Wang, J. Yan, W. Chang and Z. Zhang, *Catal. Commun.*, 2009, **10**, 989.
23 R. J. Tayade and D. L. Key, *Mater. Sci. Forum*, 2010, **657**, 62.
24 Y. Li and L. Wang, *Nanocrystalline Semiconductor Materials*, Elsevier, New York, 1996.
25 B. Pal, T. Torimoto, K. Okazak and B. Ohtani, *Chem. Commun.*, 2007, 483.
26 K. H. Park, H. S. Joo, K. I. Ahn and K. Jun, *Tetrahedron Lett.*, 1995, **36**, 5943.
27 B. Ohtani, S. Tsuru, S. Nishimoto, T. Kagiya and K. Izawa, *J. Org. Chem.*, 1990, **55**, 5551.
28 V. Kambala, S. Rao and M. Subrahmanyam, *Photochem. Photobiol. Sci.*, 2002, **1**, 597.
29 J. Kaur and B. Pal, *Catal. Commun.*, 2014, **53**, 25.
30 R. E. Moore and A. Furst, *J. Org. Chem.*, 1958, **23**, 1504.
31 H. Wang, R. E. Partch and Y. Li, *J. Org. Chem.*, 1997, **62**, 5222.
32 B. Pal, S. Ikeda, H. Kominami, Y. Kera and B. Ohtani, *J. Catal.*, 2003, **217**, 152.

Catalysis Communications 53 (2014) 25–28

Contents lists available at ScienceDirect

Catalysis Communications

journal homepage: www.elsevier.com/locate/catcom

Short Communication

100% selective yield of *m*-nitroaniline by rutile TiO_2 and *m*-phenylenediamine by P25-TiO_2 during *m*-dinitrobenzene photoreduction

Jaspreet Kaur [1], Bonamali Pal *,[1]

School of Chemistry and Biochemistry, Thapar University, Patiala 147004, Punjab, India

ARTICLE INFO

Article history:
Received 20 January 2014
Received in revised form 28 March 2014
Accepted 24 April 2014
Available online 2 May 2014

Keywords:
Rutile-TiO_2 photoactivity
TiO_2 photocatalysis
Nitro to amino reduction
Dinitrobenzene photoreduction

ABSTRACT

Photoreduction of *m*-dinitrobenzene (25 μmol) in the deaerated aqueous iso-propanol exhibits 100% selective yield of *m*-nitroaniline (25 μmol) by rutile TiO_2 (50 mg) or *m*-phenylenediamine (25 μmol) by P25-TiO_2 separately under 8 and 4 h of UV light irradiation (125 W Hg arc, 10.4 mW/cm^2), respectively. It revealed that insertion of a second $-NO_2$ in nitrobenzene ring has an important role in expediting $-NO_2$ reduction to $-NH_2$ as compared to a negligible reduction of nitrobenzene under similar conditions, indicating that electron withdrawing groups lower the electron density on $-NO_2$ present on *meta* position and favor quick reduction of the $-NO_2$ group.

1. Introduction

The selective production of *m*-phenylenediamine (*m*-PDA) and *m*-nitroaniline (*m*-NA) derived from nitroaromatics reduction is very important for their use in pharmaceuticals, food additives, agrochemicals and dye products [1,2]. These are typically synthesized [3–6] by reduction of different nitroaromatics using Fe, Zn, Sn, Au–Ni alloy, Au/Pt-Al_2O_3, Pt/TiO_2, Fe_2O_3 and ZrO_2 etc. catalysts under harsh experimental conditions such as high pressure and temperature, toxic solvents and strong reducing agents like $NaBH_4$, where metal nanoparticles transfer the electron [7] from negatively charged BH_4^- to the nitro compound and thus leading to its reduction. Generally, reduction of *m*-dinitrobenzene (*m*-DNB) to *m*-PDA proceeds via the formation of *m*-NA, and the main challenge lies in the selective production of *m*-NA where the reduction [8,9] of both $-NO_2$ groups favorably produces *m*-PDA. Therefore, finding an effective catalytic process for the synthesis of *m*-NA or *m*-PDA from *m*-DNB under ambient conditions is of great industrial importance. Nitroorganic reduction by TiO_2 photocatalysis [10,11], a greener process is practically viable [12–14] because of the higher conduction band energy of TiO_2 (−0.85 V) relative to −0.5 V vs SCE of the $-NO_2$ group preferably reduced over aceto, cyano, and aldehyde functionality present in the same compound. It has been found that nitrobenzene (NB) generally reduced [15–17] to aniline, azoxybenzene and azobenzene by CdS, WO_3 and P25-TiO_2 under UV irradiation, whereas ZnO particles generate hydroxylamine [18], and core–shell SiO_2@Rh–CdS nanocomposites [19] produced 70% azoxybenzene under 436 nm light exposure. Therefore, activity/selectivity of nitroaromatics can be controlled by the choice of catalyst, its crystal phase, composition and suitable solvent. It revealed that partial reduction of one $-NO_2$ group of *m*-DNB to *m*-NA followed by subsequent reduction of the second $-NO_2$ group to *m*-PDA can limit the selectivity of P25-TiO_2 catalyst. Recently, rutile TiO_2 (R-TiO_2) has attracted much attention because of its superior ability for selective oxidation [20] of benzyl alcohol to benzaldehyde, *m*-nitrotoluene reduction [21] to *m*-aminotoluene, and other nitroorganic reduction [22,23] to aromatic amines. Thus, R-TiO_2 possessing low and slow reactivity could be effective for NA yield over PDA formation. Herein, we report that the photocatalytic reduction of *m*-DNB by R-TiO_2 in iso-propanol suspension led to 100% selective yield of *m*-NA for the first time in comparison to negligible activity for NB reduction, whereas, anatase–rutile mixed P25-TiO_2 produced 100% *m*-PDA yield under the same reaction conditions.

2. Experimental

2.1. Preparation, characterization and photocatalytic study of sintered TiO_2 samples

Commercial Degussa P25-TiO_2 was sintered at 400, 600 and 800 °C for 2 h to get the desired catalyst. Photoreduction was carried out in a test tube containing TiO_2 (50 mg) suspended in 5 ml (50%) of aqueous iso-propanol and NB, or *m*/*p*-DNB (25 μmol) using UV irradiation (125

* Corresponding author at: School of Chemistry and Biochemistry, Thapar University, Patiala-147001, Punjab, India.
E-mail address: bpal@thapar.edu (B. Pal).
[1] Tel.: +91 175 239 3128; fax: +91 175 236 4498.

http://dx.doi.org/10.1016/j.catcom.2014.04.019
1566-7367/

W Hg arc, 10.4 mW/cm^2) under argon atmosphere and magnetic stirring. Reaction samples were analyzed by high performance liquid chromatography (HPLC) and gas chromatography–mass spectroscopy (GC–MS). The details of other characterizations of samples are given in supporting information.

3. Results and discussion

3.1. Structural analysis of catalysts

The rutile phase of sintered P25-TiO_2 was confirmed with XRD spectra as shown in Fig. 1 and the peaks at 2θ = 27.5°, 36.5°, 41°, 54.1°, and 56.5° are assigned to its rutile phase. The fraction of rutile in each sample was calculated by using the Spurr equation [24]

$$\%\text{Rutile} = \frac{1}{1 + 0.8[I_A(101)/I_R(110)]}$$

where I_A is the intensity of the (101) peak and I_R is the intensity of the (110) peak. With the increase in sintering temperature from 400 to 800 °C, rutile content increases in P25-TiO_2 and pure (99.4%) R-TiO_2 sample was obtained at 800 °C. The BET surface area analysis exposed that the surface area decreases from 56 $m^2\ g^{-1}$ of P25-TiO_2 to 18 $m^2\ g^{-1}$ for pure R-TiO_2 with increased rutile content.

3.2. Photocatalytic activity of sintered P25-TiO_2 catalysts

The various solvents *viz*. methanol, ethanol and n-propanol have been tested for the photoreduction of *m*-DNB by R-TiO_2 under 8 h of UV light irradiation (Fig. 2a). Among various solvents, iso-propanol proved to be the best medium for 100% selective yield of *m*-NA, whereas, 46% *m*-PDA formation took place in ethanol solvent. It was reported that iso-propanol can be oxidized to acetone in a photocatalytic reaction, thus effecting the simultaneous reduction of the compound that is dissolved in it. Being a secondary alcohol, iso-propanol has a better hole scavenging capacity [6] than other primary alcohols and exhibits superior electron donating ability for the reduction process.

A comparative HPLC pattern (Fig. A1 in the supporting information) shows a clear separation of *m*-PDA (t_R = 2.9 min), *m*-NA (t_R = 3.6 min) and *m*-DNB (t_R = 4.6 min) peaks in a mixture (5 mM) of authentic samples, and *m*-DNB reduction by R-TiO_2 for 8 h irradiation displayed *m*-NA formation at t_R = 3.6 min and *m*-PDA at t_R = 2.9 min.

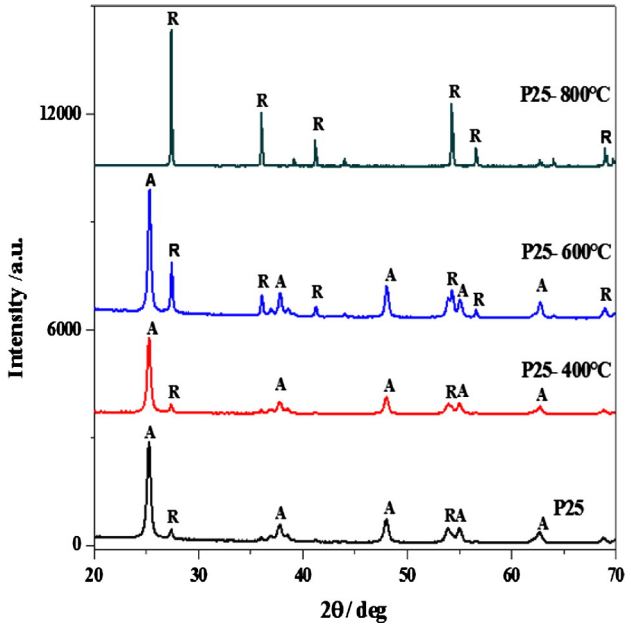

Fig. 1. XRD patterns of sintered P25-TiO_2 for 2 h at different temperatures.

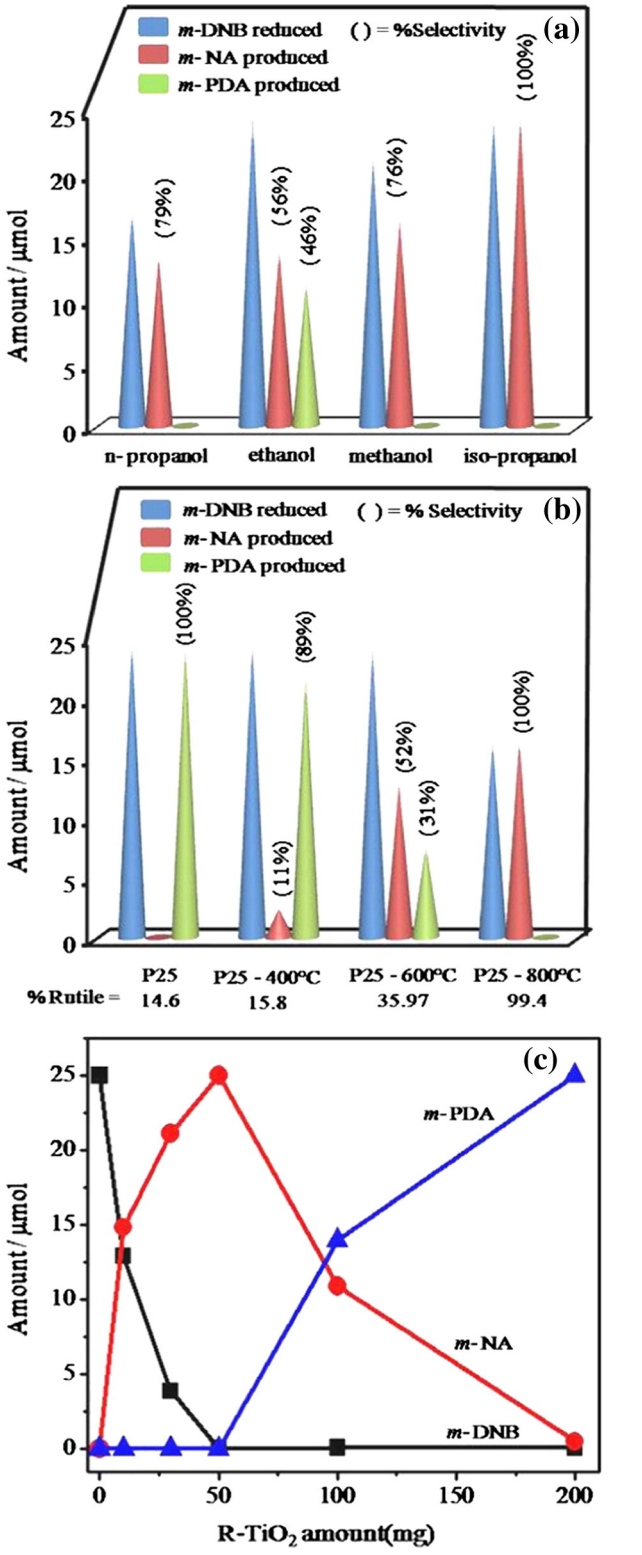

Fig. 2. *m*-DNB photoreduction (25 µmol) by (a) R-TiO_2 in different solvents under 8 h and (b) effect of R-TiO_2 content for 4 h and (c) amount of R-TiO_2 in iso-propanol for 8 h irradiation.

Fig. 2b showed that *m*-DNB (25 µmol) is selectively reduced to 100% *m*-PDA (25 µmol) by anatase–rutile mixed P25-TiO_2 catalyst and thereafter decreases with a gradual increase in *m*-NA yield as a function of

increased rutile content, and reached to 100% *m*-NA yield by pure (99%) R-TiO_2 after 4 h UV irradiation.

The amount of *m*-DNB reduced is also subsequently decreased because of lower photoactivity of R-TiO_2. Fig. 2c demonstrated that *m*-NA yield is highly improved with the increased amount of R-TiO_2, and exhibits maximum *m*-NA yield by 50 mg catalyst, and beyond this amount, the second $-NO_2$ group of *m*-NA starts reducing to give *m*-PDA as a final product. This can be explained on the basis of increased per molecule interactions of *m*-DNB with increasing amount of R-TiO_2 and availability of a higher number of active Ti^{3+} sites that imparted in rapid reduction of both $-NO_2$ groups.

The amount of *m*-DNB is gradually reduced with an increased amount (17.9 μmol) of *m*-NA along with a little amount (3 μmol) of *m*-PDA produced by P25-TiO_2 during 2.5 h UV irradiation and, thereby, *m*-NA gets converted into 100% *m*-PDA (25 μmol) after 4 h light exposure (Fig. 3a). In contrary, complete reduction of *m*-DNB to *m*-NA by R-TiO_2 is clearly observed after 8 h reduction and thereafter irradiation (>8 h) led to less amount of *m*-PDA formation as shown in Fig. 3b. The efficiency of $-NO_2$ reduction to $-NH_2$ group is further verified by simultaneous analysis of acetone formed [11] during oxidation of iso-propanol under photoirradiation. It found that the amount of acetone formed is higher when both the $-NO_2$ groups are reduced to *m*-PDA than one $-NO_2$ reduction to *m*-NA formation as evident in the differences in peak area/height of acetone ($t_R = 1.2$ min) in the GC chromatogram (Fig. A2 in supporting information).

The GC–MS analysis revealed that a single sharp peak at $t_R = 5.5$ min (Fig. 3c) for *m*-PDA and at $t_R = 8.1$ min for *m*-NA (Fig. 3d) production by P25 and R-TiO_2 catalysts, respectively, evidencing cent percent yield and selectivity of the obtained products whose mass (Fig. 3e and f) fragmentation is also matched with the respective authentic samples, confirmed the purity of *m*-NA and *m*-PDA. Thus, it was found that *m*-DNB was efficiently and selectively reduced by the increased percentage of rutile content and reached to the highest rate by pure R-TiO_2 as compared to no appreciable reduction of NB under low intensity of UV light. These findings are little different from the selective reduction [21] of $-NO_2$ to $-NH_2$ group by R-TiO_2 particles (obtained from P25-TiO_2 with HF dissolution) using high power Xe lamp (2 kW, 27.3 W/m^2) illumination. This fact suggests that the substituent and the position of $-NO_2$ group on the NB ring have an important role in the reduction process because the electron withdrawing groups that lower the electron density on a $-NO_2$ group present on *meta* position favor the rapid conversion of the $-NO_2$ into the $-NH_2$ group and hence reduce the nucleophilicity of the resulting *m*-NA as observed in *m*-DNB reduction by P25-TiO_2. As the $-NO_2$ group in the *para* position imparted less electronic induction than the *meta* $-NO_2$ group, the selectivity of *p*-DNB (24 μmol) reduction to *p*-NA (17 μmol, 69%) is notably decreased without any production of *p*-PDA by R-TiO_2. This impact of $-NO_2$ substituent is further supported by the fact that almost no reduction (1–2 μmol) of NB to aniline (1 μmol) occurs by R-TiO_2 even after 8 h irradiation. However, P25-TiO_2 being its mixed anatase–rutile phase has higher catalytic activity; hence, 25 μmol *p*-DNB is reduced to 20 μmol *m*-PDA (82%) and 5 μmol *p*-NA (17%) relative to 14 μmol reduction of NB to 9 μmol aniline (66%) formation only after 4 h UV irradiation. It also observed that reduction of 25 μmol *m*-chloronitrobenzene by P25-TiO_2 gives 100% *m*-chloroaniline (25 μmol), whereas R-TiO_2 gives only 4 μmol of *m*-chloroaniline after 4 and 8 h light irradiation, respectively, probably because of the poor electron withdrawing nature of –Cl as compared to the $-NO_2$ group.

The measured surface area 56 $m^2\ g^{-1}$ of P25 is notably reduced with increased rutile content on increasing sintering temperature i.e., 38, 30 and 18 $m^2\ g^{-1}$ at 400, 600 and 800 °C, respectively. Therefore, although the *m*-DNB reduction rate is decreased from 6.25 to 3.12 μmol/h, the selectivity of *m*-NA yield is considerably improved because of the drastic changes in the surface electronic properties of R-TiO_2 with increased crystallinity [25] where fewer defect sites appeared to promote *m*-NA formation. The low photoreactivity of R-TiO_2 may probably be due to less surface OH concentration leading to poorer O_2 adsorption essentially required for proficient capturing of photoexcited electron [26–28] and hence, exhibits fast recombination of e^-/h^+ pairs relative to P25-TiO_2 catalyst. Many studies [20–29] have revealed that strong oxidation of TiO_2 at elevated temperatures leads to the formation of a metal-deficient oxide and predominant defects are oxygen vacancies that are important reactive agents for enhanced photocatalytic activity. The active sites for $-NO_2$ reduction on R-TiO_2 are the Ti^{3+} atoms [22,29] located at the oxygen vacancies on the R-TiO_2 surface which behave as

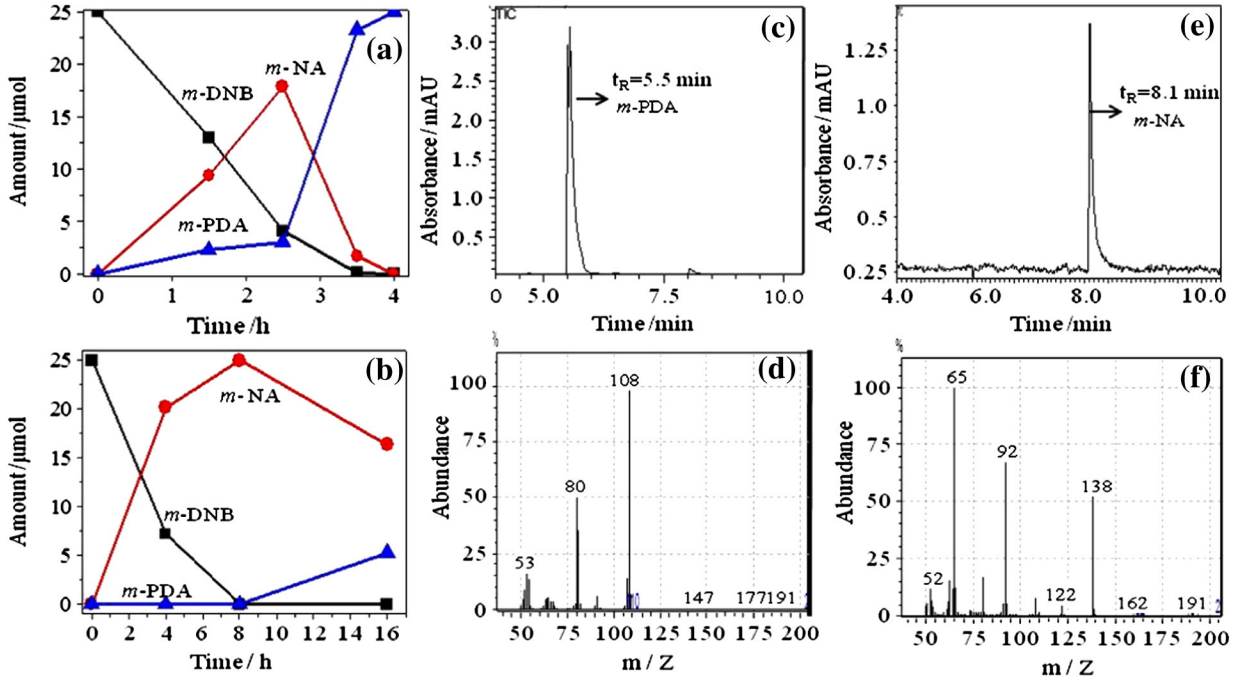

Fig. 3. Time course of *m*-DNB reduction by (a) P25-TiO_2 and (b) R-TiO_2 under UV irradiation, (c–d) and (e–f) chromatograph and mass spectra of *m*-PDA and *m*-NA formation by 4 h and 8 h photoreduction of *m*-DNB by P25-TiO2 and R-TiO_2 catalysts, respectively.

the adsorption site for DNB and the trapping site for conduction band electrons. Experimental results showed that R-TiO_2 particles possess {011} and {110} faces, and the anatase particles are exposed with {001} and {011} crystal faces, where the electronic energy levels of the {110} face are found to be lower than the {011} face helping the quick separation of photoexcited electrons and holes for the rutile [30,31] than anatase particles. This variation in the surface energy of the conduction and valence band of different crystal faces and their atomic arrangements thus affect the TiO_2 photoreactivity; hence facilitating the nitro-to-amine conversion by the surface-trapped electrons, enabling *m*-NA formation.

4. Conclusions

It is demonstrated that both the P25-TiO_2 and R-TiO_2 could be potentially utilized for the selective reduction of nitroaromatics possessing multifunctional reducible groups in *ortho*, *meta* and *para* position without any control of irradiation time. Thus, proper selection of electron donating or withdrawing substituent's in the aromatic moiety would be highly beneficial for several other products to obtain.

Acknowledgments

We are grateful to the Department of Science and Technology, India (SR/NM/NS-40/2008) for partial financial assistance. Special thanks to Dr. Satnam Singh and Inderpreet Singh Grover for surface area analysis.

Appendix A. Supplementary data

Supplementary data to this article can be found online at http://dx.doi.org/10.1016/j.catcom.2014.04.019. These data include MOL files and InChiKeys of the most important compounds described in this article.

References

[1] P.F. Vogt, J.J. Gerulis, Ullmann's Encyclopedia of Industrial Chemistry, Aromatic Amines, , Wiley-VCH, Verlag GmbH & Co. KGaA, Weinheim, 2005. 2.
[2] L. Yingxin, C. Jixiang, Z. Jiyan, Chin. J. Chem. Eng. 15 (2007) 63.
[3] F.C. Lizana, S.G. Quero, N. Perret, M.A. Keane, Catal. Lett. 127 (2009) 25.
[4] H. Rojas, G. Borda, P. Reyes, M. Brijaldo, J. Valencia, J. Chil. Chem. Soc. 56 (2011) 793.
[5] A. Corma, P. Serna, Science 313 (2006) 332.
[6] H. Zhu, X. Ke, X. Yang, S. Sarina, H. Liu, Angew. Chem. 122 (2010) 9851.
[7] S. Kundu, S. Lau, H. Liang, J. Phys. Chem. C 113 (2009) 5150.
[8] M.M. Telkar, J.M. Nadgeri, C.V. Rode, R.V. Chaudhari, Appl. Catal. A Gen. 295 (2005) 23.
[9] Y.X. Liu, J.X. Chen, J.Y. Zhang, Chin. J. Chem. Eng. 15 (2007) 63.
[10] F. Mahdavi, T.C. Bruton, Y. Li, J. Org. Chem. 58 (1993) 744.
[11] K. Imamura, T. Yoshikawa, K. Hashimoto, H. Kominami, Appl. Catal. B Environ. 134–135 (2013) 193.
[12] M.S. Wrighton, Chem. Eng. News 57 (1979) 29.
[13] M.A. Fox, Nouv. J. Chim. 11 (1987) 129.
[14] J.A. Dean, Handbook of Organic Chemistry, McGraw Hill, New York, 1987, (section 8).
[15] R.J. Tayade, R.G. Kulkarni, R.V. Jasra, Ind. Eng. Chem. Res. 45 (2006) 922.
[16] H. Wang, J. Yan, W. Chang, Z. Zhang, Catal. Commun. 10 (2009) 989.
[17] R.J. Tayade, D.L. Key, Mater. Sci. Forum 657 (2010) 62.
[18] Y. Li, L. Wang, in: P. Kamat, D. Meisel (Eds.), Nanocrystalline Semiconductor Materials, Elsevier, New York, 1996.
[19] B. Pal, T. Torimoto, K. Okazak, B. Ohtani, Chem. Commun. 5 (2007) 483.
[20] C.J. Li, G.R. Xua, B. Zhang, J.R. Gonga, Appl. Catal. B Environ. 115 (2012) 201.
[21] A. Hakki, R. Dillert, D.W. Bahnemann, Phys. Chem. Chem. Phys. 15 (2013) 2992.
[22] Y. Shiraishi, Y. Togawa, D. Tsukamoto, S. Tanaka, T. Hirai, ACS Catal. 2 (2012) 2475.
[23] S.C. Li, U. Diebold, J. Am. Chem. Soc. 132 (2010) 64.
[24] R.A. Spurr, H. Myers, Anal. Chem. 29 (1957) 760.
[25] S. Yurdakal, G. Palmisano, V. Loddo, O. Alagoz, V. Augugliaro, L. Palmisano, Green Chem. 11 (2009) 510.
[26] A. Kudo, Y. Miseki, Chem. Soc. Rev. 38 (2009) 253.
[27] K. Kobayatawa, Y. Nakazawa, M. Ikada, Y. Sato, A. Fujshima, Ber. Bunsenges. Phys. Chem. 94 (1990) 1439.
[28] R. Campostrini, G. Carturan, L. Palmisano, M. Schiavello, A. Sclafani, Mater. Chem. Phys. 38 (1994) 277.
[29] S. Yin, H. Hasegawa, D. Maeda, M. Ishitsuka, T. Sato, J. Photochem. Photobiol. A Chem. 163 (2004) 1.
[30] T. Ohno, K. Sarukawa, M. Matsumura, New J. Chem. 26 (2002) 1167.
[31] Y. Aoyama, Y. Oaki, R. Ise, H. Imai, Cryst. Eng. Comm. 14 (2012) 1405.

Journal of Molecular Catalysis A: Chemical 397 (2015) 99–105

Contents lists available at ScienceDirect

Journal of Molecular Catalysis A: Chemical

journal homepage: www.elsevier.com/locate/molcata

Influence of coinage and platinum group metal co-catalysis for the photocatalytic reduction of *m*-dinitrobenzene by P25 and rutile TiO_2

Jaspreet Kaur, Rohit Singh, Bonamali Pal*

School of Chemistry and Biochemistry, Thapar University, Patiala 147 004, Punjab, India

ARTICLE INFO

Article history:
Received 20 June 2014
Received in revised form 4 November 2014
Accepted 9 November 2014
Available online 16 November 2014

Keywords:
Rutile TiO_2
Metal–TiO_2 photoactivity
Photoluminescence
Nitroaromatics reduction
TiO_2 photocatalysis

ABSTRACT

The co-catalytic activity of 1 wt% coinage (Au, Ag and Cu) metals and platinum group (Pt, Pd and Rh) metals deposited P25 and rutile TiO_2 (R-TiO_2) have been relatively investigated for the optical absorption, emission, surface structural morphology and photocatalytic activity for the selective reduction of *m*-dinitrobenzene under UV light irradiation. An average particle size ~122 nm of R-TiO_2 is increased after calcinations of P25-TiO_2 (25–30 nm) at 800 °C and Au and Pt deposits of size ~4.0–6.5 nm were found to be uniformly distributed over TiO_2 surface. Although the optical band gap does not alter much, but intense photoluminescence having several characteristic bands between 400 and 550 nm are significantly quenched depending on the nature of metal loading. Photoirradiation (125 W Hg arc, 10.4 mW cm^{-2}) of bare P25-TiO_2 suspended in isopropanol (50 vol%) containing *m*-dinitrobenzene selectively produces 100% *m*-phenylenediamine, while metal deposited P25-TiO_2 produces *m*-nitroaniline as a major product after 4 h of UV light irradiation. However, bare R-TiO_2 produces 100% *m*-nitroaniline and metal loading does not alter the selectivity except the decrease in reduction efficiency of R-TiO_2. The decrease in active Ti^{3+} sites available on the surface after metal loading might be responsible for the decrease in photocatalytic activity.

1. Introduction

Mixed phase P25-TiO_2 possessing a high surface adsorption affinity, more specific surface area, hydroxylated surface morphology, and better charge separation by rapid electron transfer from rutile (3.0 eV) to anatase (3.2 eV) crystal makes it superior photocatalyst [1–5] for many applications. Whereas, pure rutile TiO_2 (R-TiO_2) phase is generally regarded as less photoactive because of less surface OH concentration and poorer O_2 adsorption essentially required for rapid capturing of photoexcited electrons. Hence, exhibits fast recombination of e^-/h^+ pairs [6–11] that reduced the R-TiO_2 photocatalytic activity (PCA) relative to P25-TiO_2 catalyst. Recently, TiO_2 is utilized for selective reduction of nitroaromatics, benzonitrile to benzylamine, nitrobenzene to aniline and aryl azides to amines etc. and oxidation of alcohols to aldehydes, benzene to phenol [12–17] etc. under UV light irradiation. It revealed that though better PCA was achieved by either pure anatase or mixed P25-TiO_2 crystals generally give a mixture of product distribution, however, desired selectivity in organic conversion is not obtained in many instances. Hence, R-TiO_2 is recently employed [18–21] for the selective oxidation of benzyl alcohol to benzaldehyde, reduction of nitrobenzene to aniline, *m*-nitrotoluene to *m*-aminotoluene and nitroorganics reduction.

As R-TiO_2 is less active and more selective than anatase/P25, it takes longer duration of light irradiation for reduction of nitroaromatics, as also mentioned in our previous [22] report; R-TiO_2 gives 100% selectivity and yield of *m*-nitroaniline (*m*-NA) formation after 8 h irradiation as compared to 3–4 h irradiation in case of P25-TiO_2 which produces *m*-NA and *m*-phenylenediamine (*m*-PDA) during *m*-dinitrobenzene (*m*-DNB) reduction. The PCA for selective reduction can be further improved by Fe, Au, Ag, Cu, Pt, Pd, Ru and Rh etc. deposition onto TiO_2 as evident in photooxidation [23–26] reactions. Generally metal (M) deposition on TiO_2 surface forms a metal-semiconductor Schottky barrier that serves as a trap for photoexcited electrons [27–29], and thereby improved the charge separation efficiency for enhanced oxidation–reduction rate of the surface adsorbed organic substrates. This charge separation and Fermi level equilibration in M/TiO_2 composites are reported to be influenced by the nature, amount, size of distribution, reduction potential, Fermi energy/work function [30] and electronegativity of the deposited metal as depicted in Scheme 1. Metals which have lower reduction potential than the conduction band/Fermi energy

* Corresponding author. Tel.: +91 175 2393443; fax: +91 175 2364498.
E-mail address: bpal@thapar.edu (B. Pal).

http://dx.doi.org/10.1016/j.molcata.2014.11.007
1381-1169/

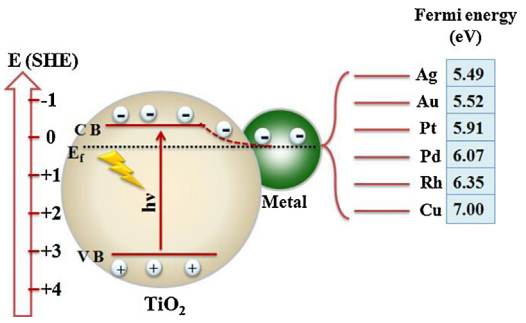

Scheme 1. Schematic illustration of Fermi level equilibration and charge transfer process occur at various metal–TiO_2 interfaces.

of TiO_2 are preferred, as more and more electrons get transfer to the metal and further to the reacting species and alter the reduction efficiency. Although a few reports such as M–TiO_2/CdS composites (M = Pt, Pd, Rh and Fe) were studied for selective conversions [31] of lysine to pipecolinic acid formation, however, the effect of the different nature of metal loading on TiO_2 for selective reduction of nitroaromatics is not reported so far.

Hence, present research highlights the comparative effect of coinage (Au, Ag and Cu) and platinum group (Pt, Pd and Rh) metals co-catalysts deposition onto P25 and R-TiO_2 for improving the PCA for *m*-DNB reduction to optimize the product selectivity and yield upon shorter duration of light illumination.

2. Experimental

2.1. Materials

Degussa P25-TiO_2, hydrogen tetrachloroaurate (III) hydrate ($HAuCl_4{\cdot}3H_2O$), silver nitrate ($AgNO_3$), copper nitrate ($CuNO_3{\cdot}4H_2O$), hexachloroplatinic (IV) acid hexahydrate ($H_2PtCl_6{\cdot}6H_2O$), palladium chloride ($PdCl_2$), rhodium chloride ($RhCl_3$), *m*-DNB ($C_6H_4N_2O_4$), *m*-NA ($C_6H_6N_2O_2$) and *m*-PDA ($C_6H_8N_2$) were purchased from Loba Chemicals and used without further purification. Deionized water was obtained using an ultra filtration system (Milli-Q, Milipore) with a measured conductivity 35 mho cm^{-1} at 25 °C.

2.2. Preparation of R-TiO_2 nanoparticles

R-TiO_2 nanoparticles were prepared by a standard method as reported elsewhere [22]. Briefly, commercial Degussa P25 TiO_2 (1.0 g) powder was placed into a crucible, followed by calcinations at 800 °C in a muffle furnace for 2 h. After the thermal treatment, the powder was allowed to cool down at room temperature and characterized by X-ray diffraction (Fig. S2, Supporting information) to confirm the presence of pure rutile phase.

2.3. Metal photodeposition

As prepared R-TiO_2 or P25 TiO_2 powder (50 mg) was taken in a test tube containing 5 ml of an aqueous isopropanol (50 vol%) solution [32]. An aqueous solution (0.01 M) of metal salts were prepared and subsequently added to above test tube corresponding to its 1 wt% i.e., 256 μl of $HAuCl_4{\cdot}3H_2O$, 468 μl of $AgNO_3$, 787 μl of $Cu(NO_3)_2{\cdot}4H_2O$, 256 μl of $H_2PtCl_6{\cdot}6H_2O$, 465 μl of $PdCl_2$ and 495 μl of $RhCl_3$ (details of calculations are given in Supporting information). The test tube was capped with a septum, purged with argon gas for 15–20 min and irradiated by UV light (125 W Hg arc, 10.4 mW/cm^2) under constant magnetic stirring for 2 h in a photochemical reactor. Finally, the solution was centrifuged, washed repeatedly with distilled water and ethanol followed by drying in oven at 50 °C for 30 min.

2.4. Characterization techniques

The optical absorption spectra of M/TiO_2 samples were recorded with a diffuse reflectance spectrophotometer by Avantes using $BaSO_4$ as reflectance standard. Photoluminescence (PL) spectra were recorded by using a spectrofluorimeter by Perkin-Elmer LS55 at room temperature on excitation with xenon lamp (λ_{ext}) at 320 nm in ethanol suspension. Transmission electron microscope (TEM) photographs were taken on the Hitachi 7500 model with resolution 2 Å operating at voltage 120 kV. The crystallographic studies have been carried out by using X-ray diffractometer by PANalytical X'Pert PRO with Cu-Kα (k = 1.54060 Å) radiation operated at 45 kV. The specific surface area was determined by N_2 adsorption method using a Smart Sorb 92/93 instrument after preheating 100 mg of samples at 150 °C for 1 h.

2.5. Photocatalytic activity for m-DNB reduction

The photoreduction was carried out in a test tube containing 50 mg of bare or M/TiO_2 powder suspended in 5 ml isopropanol (50 vol%) and 5 mM of *m*-DNB (25 μmol) in argon atmosphere under

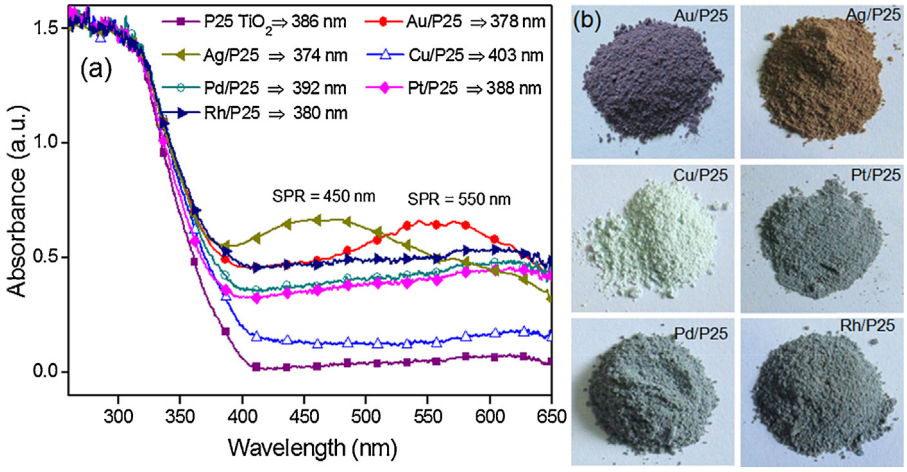

Fig. 1. Absorption spectra of different (a) metal (1 wt%) deposited P25-TiO_2 powders and (b) their colours.

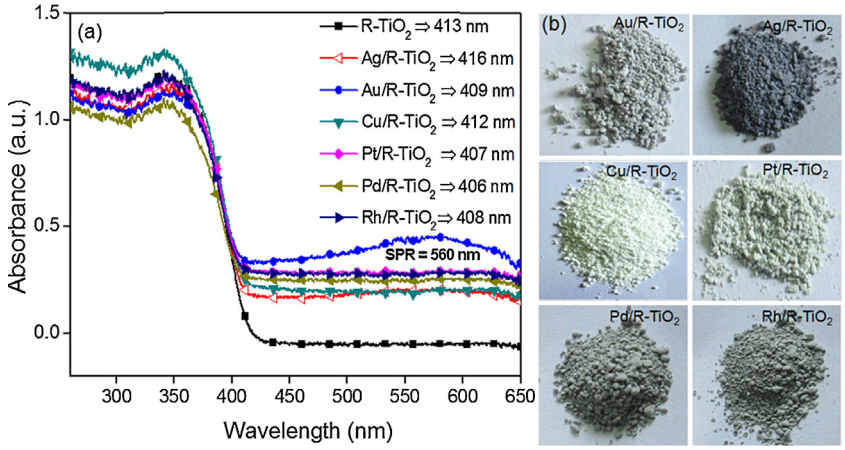

Fig. 2. Absorption spectra of (a) 1 wt% metal deposited rutile titania, and (b) their corresponding colours.

continuous magnetic stirring and UV light irradiation. The reaction solution after *m*-DNB photoreduction was centrifuged, filtered through cellulose filter (0.22 μm) and the product was analyzed by HPLC [Agilent 1120 Compact LC equipped with a Qualisil BDS C-18 column (250 mm × 4.6 mm, 5 μm)] at λ = 254 nm with a flow rate of 1 ml/min using MeOH:H_2O (70:30) as mobile phase and by Gas chromatography–mass spectroscopy (GC-MS-QP 2010 plus) using RTX-5Sil-MS column (15 m × 0.25 mm × 0.25 μm).

3. Results and discussion

3.1. Optical absorption of M/TiO_2 composites

Fig. 1a shows the absorption spectra of different metals (1 wt%) photodeposited P25-TiO_2 powder samples. The bare P25-TiO_2 sample exhibited a strong peak at 386 nm, which is attributed to the electronic transition from oxygen 2p orbital's in the valence band

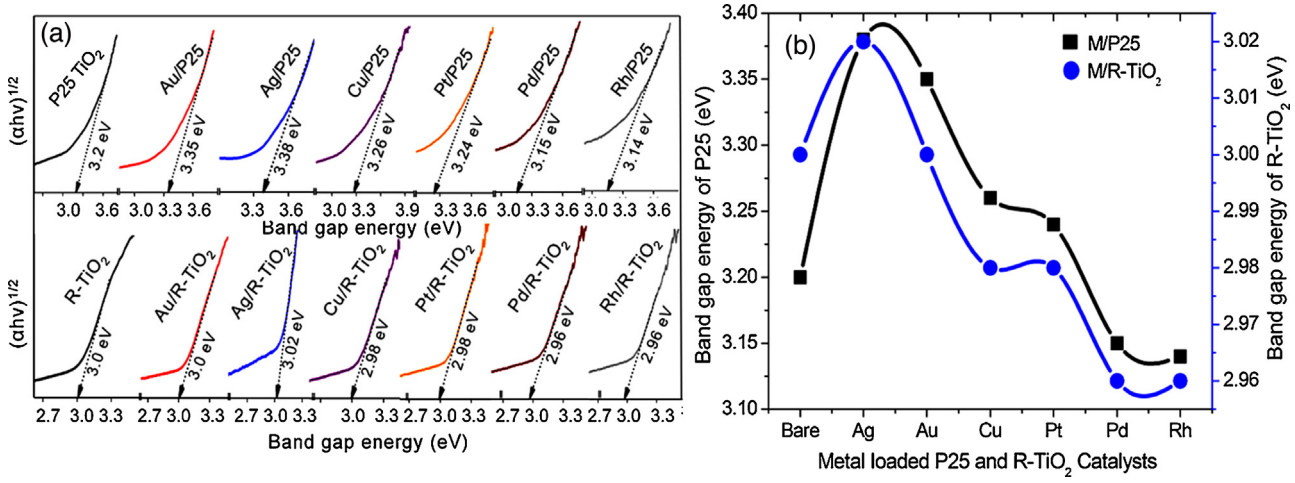

Fig. 3. (a) The plot of $(\alpha h\nu)^{1/2}$ function versus the band gap energy of various pure and deposited samples. (b) Variation in the band gap energy of pure and metal deposited samples.

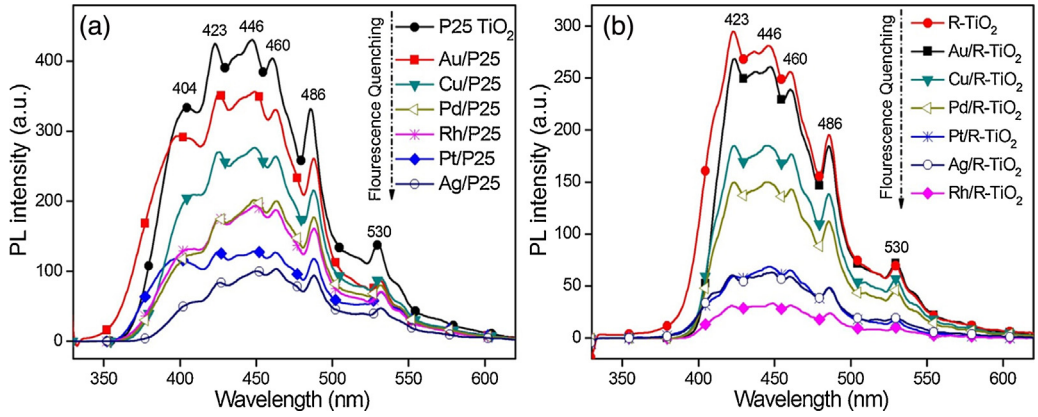

Fig. 4. Change in photoluminescence spectra of (a) P25 and (b) rutile after 1 wt% loading of different metals.

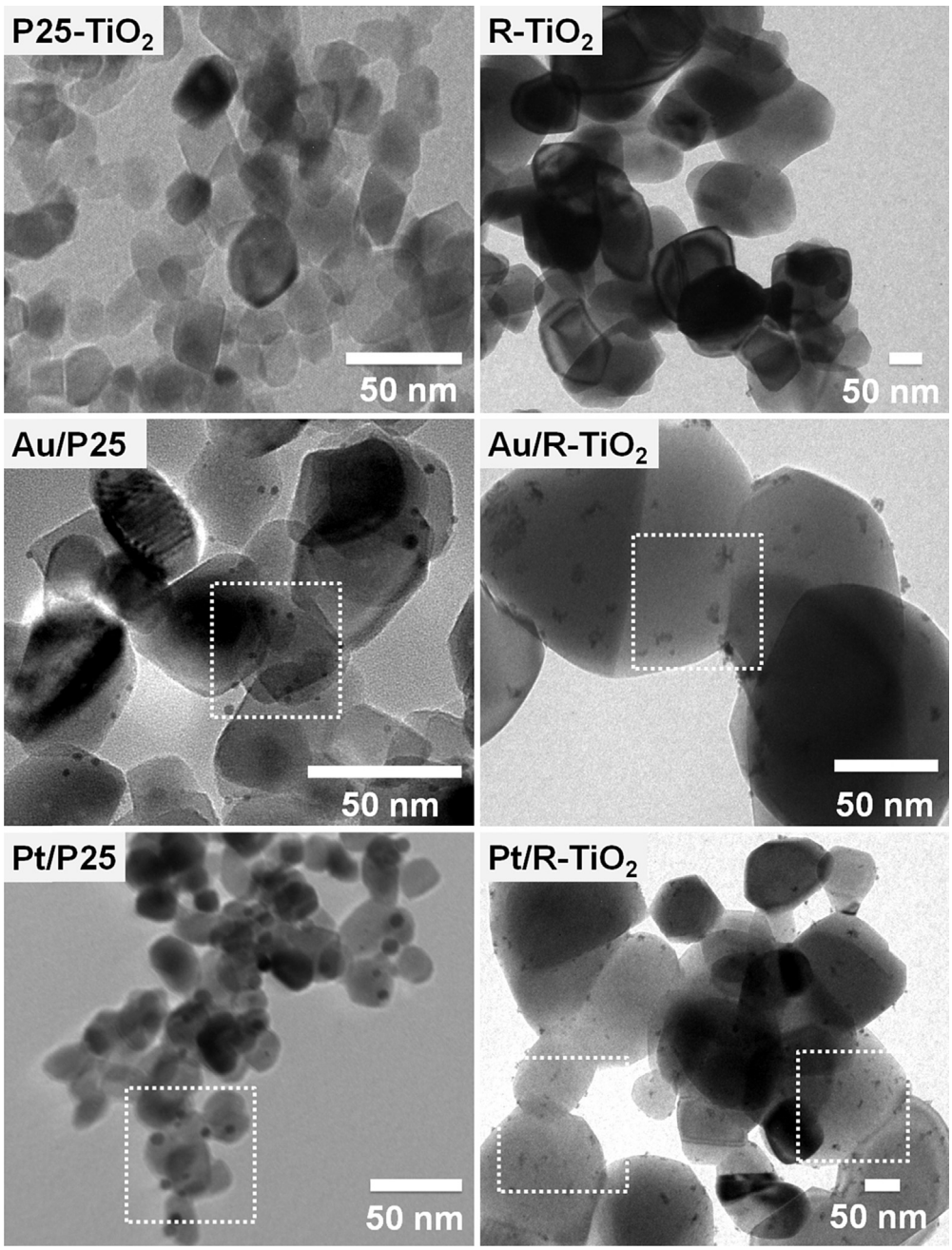

Fig. 5. TEM images of (a) P25-TiO_2, (b) rutile TiO_2, (c) 1 wt% Au/TiO_2, (d) 1 wt% Au/R-TiO_2, (e) 1 wt% Pt/TiO_2 and (f) 1 wt% Pt/R-TiO_2 composites.

to the titanium 3d orbital's in the conduction band. In comparison to P25-TiO_2, the absorption onset in slightly red-shifted to 403 nm in Cu/TiO_2 and thereby varied to a little extent due to charge transfer transitions between the metal ion electrons and the TiO_2 conduction, depending upon the nature of M deposits over TiO_2 surface. However, Au and Ag loading displayed a characteristic surface plasmon resonance (SPR) band at 450 and 550 nm, respectively.

During UV light irradiation, the adsorbed metal ions on TiO_2 are reduced by the photoexcited electrons in conduction band as $M^{n+} + ne^- \rightarrow M^0$, and randomly deposited over the surface. It is well reported [33–35] that Au^{3+}, Ag^+, Cu^{2+}, Pt^{4+}, Pd^{2+} and Rh^{3+} ions are generally reduced to their metallic state because of their suitable reduction potential/work function that lies below the conduction band position of TiO_2. Hence, photoreduction of metal ions onto the respective titania nanoparticles led to a significant change in their colours, as shown in Fig. 1b.

As shown in Fig. 2a, the absorbance onset at 413 nm for bare R-TiO_2 does not induce any notable shift even after metal deposition, which is confirmed by the limit in colour variation from light grey to dark grey (Fig. 2b). The decrease in intensity of absorption edge at 340 nm of R-TiO_2 relative to P25-TiO_2 is due to enhanced scattering of light by larger crystallites [36] formed by the calcination of P25-TiO_2, owing to the difference in surface morphologies, crystallite size, phase structure, and compositions.

The band gaps of bare and various metals deposited samples were calculated by using Tauc relation [37], which is given by $\alpha h\nu = A(h\nu - E_g)^n$, where α is the absorption coefficient, $h\nu$ is the photon energy, A is a constant and E_g is the bandgap of the material, exponent n is the type of the transition ($n = 1/2$ for direct, 2 for indirect band gap). The exact value of the bandgap is determined by extrapolating the straight-line portion of $\alpha h\nu$ versus E_g graph to the x-axis. It can be seen from Fig. 3a that Au/P25 exhibits band

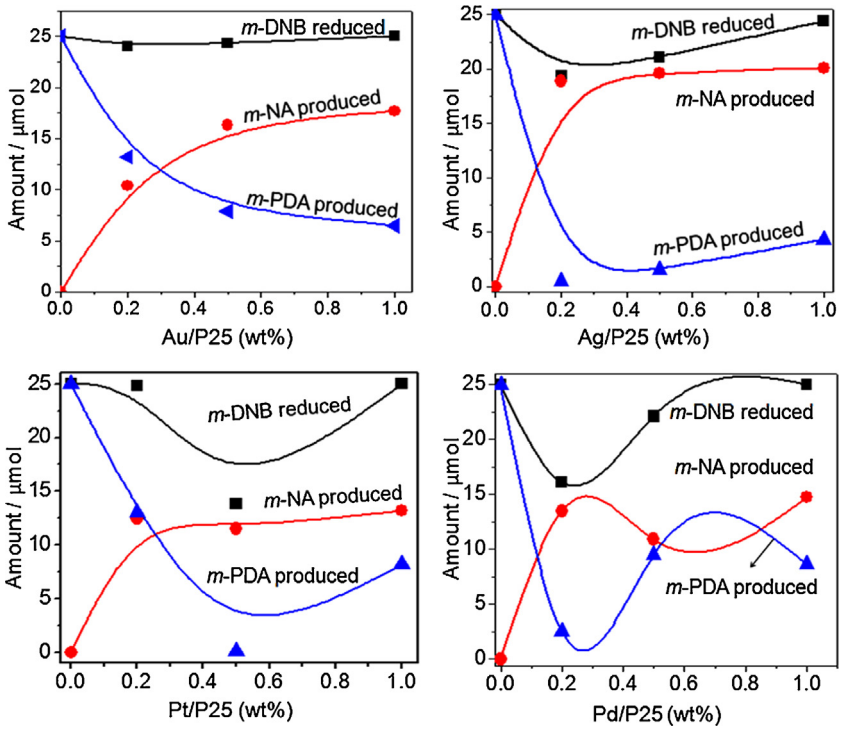

Fig. 6. *m*-DNB photoreduction products with different amounts of Au, Ag, Pt and Pd deposited P25-TiO_2 catalysts.

gap energy 3.38 eV and Pt/P25 possess band gap of 3.24 eV relative to 3.2 eV for pure P25-TiO_2 sample. While metals loading did not modify the band energy relative to 3.0 eV of pure R-TiO_2, and comparative changes in band gap energy between different M/P25 and M/R-TiO_2 did not demonstrate any significant difference except Ag, Au and Cu loading which increased the band gap energy in a small extent relative to bare TiO_2 as observed in Fig. 3b.

The photoluminescence (PL) spectra in Fig. 4a showed that P25-TiO_2 exhibited a set of the emission bands in the range of 400–550 nm indicated that commercial available P25 material is not much crystalline due to the presence of many surface defect sites. The band at 404 nm is attributed to band edge emission; originate from the recombination of photoexcited electron–hole pair's and the emission bands at 423 nm, 446 nm, 460 nm is assigned to shallow-trap state near absorption band edge emission, correspond to the presence of oxygen vacancies [38], whereas, bands at 486 nm and 530 nm are corresponds to the deep-trap states far below the band edge emissions and collectively called surface state emissions. These charge carriers are generally trapped by oxygen vacancies and surface hydroxyl groups, which contribute in their visible luminescence [39]. After deposition of 1 wt% M onto the TiO_2 surface always quench the PL intensity depending on the kind of M deposits, where Ag and Pt loading led to a maximum reduction in PL intensity as compared to Au deposition and bare P25 catalysts. While Rh, Pt and Ag deposition displayed higher PL quenching relative to bare and Au loaded R-TiO_2. This could be attributed to effective shuttling of photogenerated charge carriers from TiO_2 surface to deposited M islands that prevent the recombination and hence quench the PL emission. Similar defects have been observed in case of R-TiO_2 except the band at 404 nm as shown in Fig. 4b and the intensity of emission peak at 423 nm is higher than that of 400 nm indicates that the M/TiO_2 nanoparticles having more surface states dominate the excitonic emission.

TEM photographs in Fig. 5 revealed that pure P25 and R-TiO_2 having size around 25 nm and 122 nm. This large difference in the size distribution of P25 and R-TiO_2 was probably due to the induced growth of crystallite size after high temperature calcination at 800 °C. Many smaller Au nanoparticles of average size ~4 nm and ~5 nm were found to be uniformly deposited over P25-TiO_2 and R-TiO_2 surface, respectively, while Pt nanoparticles of size ~6 nm were found to be homogeneously distributed on both the TiO_2 (evaluated by considering 20 particles) follows Gaussian curve fitting (Fig. S1, Supporting information). It can be seen from the XRD pattern (Fig. S2, Supporting information) that the characteristic mixed anatase-rutile P25-TiO_2 and rutile TiO_2 phase has been observed with a good degree of crystallinity. Notably, 1 wt% M loading did not show any characteristic diffraction peak because of their low concentration in the sample.

3.2. Photocatalytic study

Fig. 6 shows the reduction of *m*-DNB to *m*-PDA and *m*-NA formation (GC-MS pattern in Fig. S3, Supporting information) after 4 h UV irradiation and their distribution with 0.2–1 wt% metals (Au, Ag, Pt and Pd) loaded P25-TiO_2 catalysts. It found that always *m*-DNB (25 μmol) is selectively reduced to 100% *m*-PDA by bare P25-TiO_2 and thereby *m*-NA formation started increased upto 80% (20 μmol) with decreasing *m*-PDA yield (5 μmol) with increased amount (0.2–1 wt%) of Au and Ag loading as in Fig. 6. Notably, the same trend is also observed in case of Pt and Pd loaded P25-TiO_2 with relatively low yield (<12 μmol) of *m*-PDA and (59%) *m*-NA (~14.7 μmol) during *m*-DNB photoreduction, evidencing higher co-catalytic activity of Au and Ag than Pt and Pd metal imparted to TiO_2 photocatalysts. Fig. 7a showed comparative products distribution, where *m*-NA selectivity and yield is significantly enhanced by coinage metal loading relative to 100% *m*-PDA yield by bare P25-TiO_2 during 4 h irradiation. Whereas, bare R-TiO_2 always exhibited the highest photoactivity for 100% selective reduction of *m*-DNB to *m*-NA formation, and 1 wt% metals loading significantly reduced the photoreactivity even after 8 h light irradiation as shown in Fig. 8.

The selectivity of the photocatalytic reduction is ascribed [40–42] to the presence of face specific reactive sites on rutile crystals which is predominantly terminated by {110}, {100} and {011} faces, whereas the anatase particles exposed with {001}

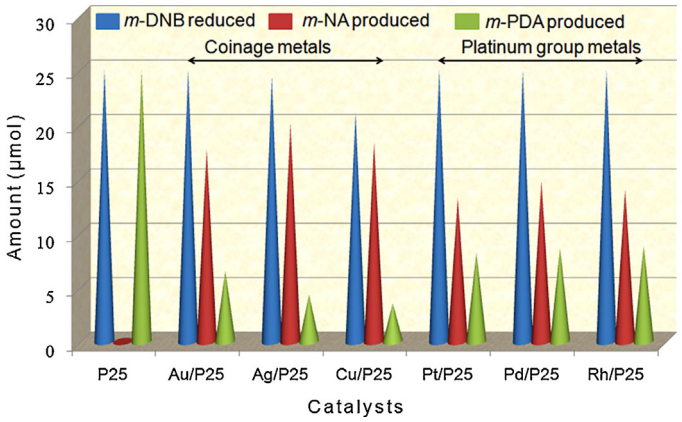

Fig. 7. *m*-DNB reduction by 1 wt% coinage metal and platinum group metals loaded P25-TiO_2 under 4 h UV light irradiation.

and {011} faces. It is reported [43,44] that reduction plane associated with anatase {011} face contains a rich array of defects compared to reduction plane of R-TiO_2 {110}. These defect sites are identified as Ti^{3+} which behave as an active site [20] on the TiO_2 surface and are necessary for adsorption and the conversion of nitro group to amine. Further, the improved crystallinity [45] of R-TiO_2 may also contribute to the product selectivity obtained during the photoreduction. It found that surface area (Table S1, Supporting information) 56 $m^2\,g^{-1}$ of P25 is reduced to 18 $m^2\,g^{-1}$ for R-TiO_2 due to increased particle size after high temperature treatment and 1 wt% M deposition always decreased the surface area of P25 and R-TiO_2 to 45–35 $m^2\,g^{-1}$ and 4–8 $m^2\,g^{-1}$, respectively, does not seem to have any beneficial effects to PCA. This decreased surface area of TiO_2 by M loading probably because of the surface coverage [23] of smaller metal nanoparticles on the porous surface of TiO_2.

The fluctuation in the co-catalytic activity of coinage and platinum group metals could be attributed [46,47] to the differences in the Fermi energy, work function, electron affinity and redox potential etc. which usually facilitate electron accumulation in the metal nanodeposits depending upon the extent of Fermi level equilibration between conduction band electrons of TiO_2 and loaded metals (Scheme 1). It is evident that owing to lower work function 4.2 eV of Pt than 5.5 eV of Au, the conduction band electrons of TiO_2 may be easily transferred to Pt deposits. It is also reported [48] that metals like Pt quickly discharge electrons to the substrate, unlike Au and Ag, which store a fraction of electrons captured from conduction band of TiO_2 and thus exhibiting higher co-catalytic activity of

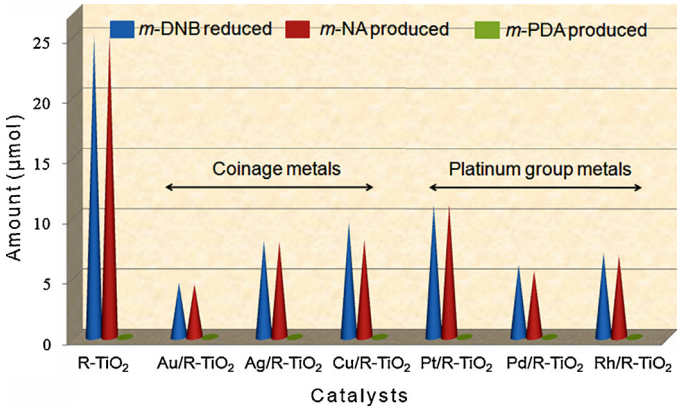

Fig. 8. *m*-DNB reduction by 1 wt% coinage and precious metal loaded R-TiO_2 under 8 h UV light irradiation.

1 wt% Pt/TiO_2 that simultaneously reduced two NO_2 groups of *m*-DNB to selective formation of *m*-PDA relative to one $-NO_2$ group reduction to *m*-NA formation by 1 wt% Au/TiO_2 after 4 h UV irradiation. Moreover, plasmonic interaction of platinum group metals having characteristics absorption bands in the UV-region could impart crucial effects on the charge transfer kinetics and energetic for superior co-catalytic activity of M–TiO_2 photocatalysis under UV light irradiations.

4. Conclusion

In summary, 1 wt% metal loading on P25 and R-TiO_2 does not seem to improve the PCA except the improved selectivity by M/P25 which is opposite to high PCA for oxidation reactions by M/TiO_2 catalysts generally observed. Coinage metals e.g., Ag/P25 exhibit higher selectivity (80%) and yield for *m*-NA formation. Irrespective of the nature of metal loading, the *m*-DNB photoreduction is always notably reduced as compared to the highest photoreactivity of bare R-TiO_2 that produces 100% *m*-NA. This decrease in PCA for the nitro group reduction by all M/TiO_2 could thus be attributed to the decrease in active Ti^{3+} sites available on the surface after metal nanodeposits loading that might also act as a recombination centre for photoexcited charge species.

Acknowledgements

We are grateful to the University Grants Commission, India (grant no. 41-209/2012 (SR)) for partial financial assistance. We are thankful to Dr. Satnam Singh and Inderpreet Singh Grover of School of Chemistry and Biochemistry, Thapar University, Patiala for their timely help in surface area measurement.

Appendix A. Supplementary data

Supplementary data associated with this article can be found, in the online version, at http://dx.doi.org/10.1016/j.molcata.2014.11.007.

References

[1] H. Yuzawa, T. Mori, H. Itoh, H. Yoshida, J. Phys. Chem. C 116 (2012) 4126.
[2] D. Friedmann, C. Mendive, D. Bahnemann, Appl. Catal. B: Environ. 99 (2010) 398.
[3] C.N.R. Rao, A. Govindaraj, Adv. Mater. 21 (2009) 4208.
[4] S. Sarina, H.Y. Zhu, Z.F. Zheng, S.E. Bottle, J. Chang, Chem. Sci. 3 (2012) 2138.
[5] K. Fuku, T. Kamegawa, K. Mori, H. Yamashita, Chem. Asian J. 7 (2012) 1366.
[6] Y. Yang, H. Zhong, C. Tian, Res. Chem. Intermed. 37 (2011) 91.
[7] H. Kawaguchi, T. Wejima, Kagaku Kogaku Ronbun 9 (1983) 107.
[8] H. Kawaguchi, Environ. Technol. Lett. 5 (1984) 471.
[9] V. Augugliaro, L. Palmisano, A. Sclafani, C. Minero, E. Pelizzetti, Toxicol. Environ. Chem. 16 (1988) 89.
[10] M. Addamo, V. Augugliaro, A. Di Paola, E. Garcıa Lopez, V. Loddo, G. Marci, R. Molinari, L. Palmisano, M. Schiavello, J. Phys. Chem. B 108 (2004) 3303.
[11] S. Bakardjieva, J. Šubrt, V. Štengl, M.J. Dianez, M.J. Sayagues, Appl. Catal. B: Environ. 58 (2005) 193.
[12] A. Maldotti, L. Andreotti, A. Molinari, S. Tollari, A. Penoni, S. Cenini, J. Photochem. Photobiol. A: Chem. 133 (2000) 129.
[13] T. Zhang, L. You, Y. Zhang, Dyes Pigm. 68 (2006) 95.
[14] K. Imamura, T. Yoshikawa, K. Nakanishi, K. Hashimoto, H. Kominami, Chem. Commun. 49 (2013) 10911.
[15] H. Huanga, J. Zhoua, H. Liu, Y. Zhou, Y. Fenga, J. Hazard. Mater. 178 (2010) 994.
[16] V. Augugliaro, H. Kisch, V. Loddo, M.J. López-Muñoz, C. Márquez-Alvárez, G. Palmisano, L. Palmisano, F. Parrino, S. Yurdakal, Appl. Catal. A: Gen. 349 (2008) 189.
[17] Y. Shiraishi, N. Saito, T. Hirai, J. Am. Chem. Soc. 127 (2005) 12820.
[18] C.J. Li, G.R. Xua, B. Zhang, J.R. Gonga, Appl. Catal. B: Environ. 115 (2012) 201.
[19] A. Hakki, R. Dillert, D.W. Bahnemann, Phys. Chem. Chem. Phys. 15 (2013) 2992.
[20] Y. Shiraishi, Y. Togawa, D. Tsukamoto, S. Tanaka, T. Hirai, ACS Catal. 2 (2012) 2475.
[21] S.C. Li, U. Diebold, J. Am. Chem. Soc. 132 (2010) 64.
[22] J. Kaur, B. Pal, Catal. Commun. 53 (2014) 25–28.
[23] C.G. Silva, R. Juarez, T. Marino, R. Molinari, H. Garicia, J. Am. Chem. Soc. 133 (2011) 595.

[24] S. Sakthivel, M.V. Shankar, M. Palanichamy, B. Arabindoo, D.W. Bahnemann, V. Murugesan, Water Res. 38 (2004) 3001.
[25] N. Zhang, S. Liu, X. Fu, Y.J. Xu, J. Phys. Chem. C 115 (2011) 9136.
[26] R. Wang, K. Hashimoto, A. Fujishima, M. Chikumi, E. Kojima, A. Kitamura, M. Shimohigoshi, T. Watanabe, Nature 388 (1997) 431.
[27] K. Li, B. Chai, T. Peng, J. Mao, L. Zan, ACS Catal. 3 (2013) 170.
[28] Y. Ma, Q. Xu, X. Zong, D. Wang, G. Wu, X. Wang, C. Li, Energy Environ. Sci. 5 (2012) 6345.
[29] A. Tanaka, S. Sakaguchi, K. Hashimoto, H. Kominami, ACS Catal. 3 (2013) 79.
[30] V. Subramannian, E.E. Wolf, P.V. Kamat, J. Am. Chem. Soc. 126 (2004) 4943.
[31] B. Ohtani, B. Pal, S. Ikeda, Catal. Surv. Asia 7 (2003) 165.
[32] U. Diebold, Surf. Sci. Rep. 48 (2003) 53.
[33] M.I. Litter, Appl. Catal. B: Environ. 23 (1999) 89.
[34] H. Reiche, W.W. Dunn, A.J. Bard, J. Phys. Chem. 83 (1979) 2248.
[35] M.D. Ward, A.J. Bard, J. Phys. Chem. 86 (1982) 3599.
[36] J.G. Yu, H.G. Yu, B. Cheng, X.J. Zhao, J.C. Yu, W.K. Ho, J. Phys. Chem. B 107 (2003) 13871.
[37] R. Singh, B. Pal, Mater. Res. Bull. 48 (2013) 1403.
[38] N.D. Abazovic, L. Mirenghi, I.A. Jankovic, N. Bibic, D.V. Sojic, B.F. Abramovic, M.I. Comor, Nanoscale Res. Lett. 4 (2009) 518.
[39] S. Mathew, A.K. Prasad, T. Benoy, P.P. Rakesh, M. Hari, T.M. Libish, P. Radhakrishnan, V.P.N. Nampoori, C.P.G. Vallabhan, J. Fluoresc. 22 (2012) 1563.
[40] M.A. Behnajady, N. Modirsha, H.M. Shokri, B. Rad, Global NEST J. 10 (2008) 1.
[41] S. Wendt, R. Schaub, J. Matthiesen, E.K. Vestergaard, E. Wahlstrom, M.D. Rasmussen, P. Thostrup, L.M. Molina, E. Lagsgaard, I. Stensgaard, B. Hammer, F. Besenbacher, Surf Sci. 598 (2005) 226.
[42] O. Bikondoa, C.L. Pang, R. Ithnin, C.A. Muryn, H. Onishi, G. Thornton, Nat. Mater. 5 (2006) 189.
[43] S. Wendt, J. Matthiesen, R. Schaub, E.K. Vestergaard, E. Lagsgaard, F. Besenbacher, B. Hammer, Phys. Rev. Lett. 96 (2006) 066107.
[44] Z. Zhang, O. Bondarchuk, J.M. White, B.D. Kay, Z. Dohnalek, J. Am. Chem. Soc. 128 (2006) 4198.
[45] S. Yurdakal, G. Palmisano, V. Loddo, V. Augugliaro, L. Palmisano, J. Am. Chem. Soc. 130 (2008) 1568.
[46] P.V. Kamat, Pure Appl. Chem. 74 (2002) 1693.
[47] K.T. Ranjit, T.K. Varadarajan, B. Viswanathan, J. Mater. Sci. Lett. 96 (1996) 181.
[48] H. Choi, W.T. Chen, P.V. Kamat, ACS Nano 6 (2012) 4418.